

POLITECNICO DI TORINO
Department of Energy - DENERG



Master of Science Thesis in
Electrical Engineering

**Implementation of an urban
distribution system digital twin
in real-time**

Candidate

Andrea Michele Aleo

Supervisor

Prof. Enrico Pons

Advisors

Prof. Ettore F. Bompard

Dott. Andrea Mazza

March 2021

Abstract

All countries must ensure sustainability and strengthen resilience while improving people's health and welfare. For this reason, one of the needs remains for an accelerated path to meet global climate goals through the decarbonisation of our societies. Recently, the energy trends have confirmed the need to accelerate a reduction in CO₂ emissions and Renewable Energy Sources (RES) are an enabling technology both to reach the goals and limit the rise in average global temperatures to 1.5°C. As IRENA has estimated, RES, together with demand reduction and energy efficiency, could account for over 80% of the CO₂ emission reductions needed. Despite this, RES-based solutions have not been explored to date with the rigor and urgency that is needed.

However, the large penetration of RES involves some issues: for example, the presence of Distributed Energy Resources (DER) may cause overvoltages in some nodes of the electrical grid that are impossible to control with traditional voltage control strategies that are centralised in HV/MV substations, like on-load tap changer, without negatively impacting the other feeders connected on the same bus. Moreover, short-circuit currents could increase at the distribution system nodes with respect to the normal levels (without DER) due to the contribution of the Distribution Generation (DG) and, in worst case, they could exceed the short-circuit capability declared, affecting the protection devices sizing inside the MV/LV substations.

For these reasons, nowadays it is of utmost importance be able to predict the consequences that the penetration of RES would have in the electrical grid. To do that, digital twin is one of the most promising methods. The purpose of this thesis is to implement a digital twin of a portion of the electrical grid of Turin for emulating the real behaviour of the network.

A RTDS[®] Simulator, made by RTDS Technologies Inc., was used for the implementation. It is a real-time simulator that runs electromagnetic transients and load flow analysis, especially for electrical power systems.

The electrical grid analysed in this thesis is the model of a portion of the real urban distribution system of Turin after Stura HV/MV substation in which

there are three power transformers, one per each MV busbar. However, only five MV feeders were implemented. For the LV level, two MV/LV substations were included. All the parameters relating to the structure of the system, the characteristics of the components and the loads connected are based on the data provided by the DSO that manages the electrical grid in the city of Turin.

Regarding the protection system, the control logic of the relays associated to the various circuit breakers was implemented by building block schemes made up of components from *Controls* library. The settings of the various thresholds are based on the data provided by the Italian TSO and the above-mentioned DSO.

The accuracy of the digital twin implemented was proved by simulating some fault conditions and by comparing the results with both fault theory and the ones obtained with OPARL-RT[®] Simulator, made by *OPAL-RT TECHNOLOGIES, Inc.* With these tests, also the functionality of the protection system and its control logic, was verified.

Starting from this model, other components, like photovoltaic panels or wind turbine generators, can be added in order both to highlight potential failures in the network due to RES and to modify the protection system for considering the power generation at MV and LV level. Moreover, also Power Hardware-In-the-Loop simulations can be done by interfacing real component with the digital twin that simulates the main grid.

Contents

1	Introduction	1
1.1	Overview of the current situation and possible future scenarios	1
1.2	What is a <i>Smart Grid</i> ?	5
1.3	What is a <i>Micro Grid</i> ?	6
1.4	Energy Communities	8
1.5	The evolution of the Ancillary Services market and the new roles of the system operators	10
1.6	Ancillary services processes	12
1.7	Distribution grid constraints	16
1.8	Drawbacks of RES penetration	18
1.9	Thesis aim and organization	20
2	Digital twin and simulation	22
2.1	Network structure	22
2.2	Network model	26
2.2.1	HV grid	26
2.2.2	HV/MV Transformers	27
2.2.3	On Load Tap Changer (OLTC) Control	28
2.2.4	MV/LV transformer	29
2.2.5	Distribution lines	31
2.2.6	Loads	35
2.2.7	Load Flow data	40
2.3	RTDS [®] Simulator	41
2.3.1	Hardware	41
2.3.2	Software	43
2.3.3	Simulation parameters	43
3	Comparison of results	44
3.1	Tests for comparison	44
3.1.1	Normal operating conditions	44
3.1.2	Fault conditions	45

4	Automated protection system	52
4.1	Primary substation protection systems	52
4.1.1	HV Breaker	54
4.1.2	MV Breaker	55
4.1.3	Magra and Brenta breaker	57
4.2	Secondary substation protection systems	60
4.2.1	MV Switch Disconnecter and Fuses	61
4.2.2	Breaker 3A, 3D and 3E	63
4.3	Low voltage cable protection system	67
4.4	Protection devices models	68
4.4.1	Circuit breaker, switch disconnecter and LV fuses	68
4.4.2	MV Fuses	69
4.5	Control logic of the relays	71
4.5.1	HV breaker relays	71
4.5.2	MV breaker relays	73
4.5.3	Magra and Brenta breaker relays	76
4.5.4	Breaker 3A, 3D and 3E	80
4.5.5	LV fuses	82
4.6	Manual control of the circuit breakers	84
5	Simulation results	85
5.1	Multiphase faults	85
5.2	Phase-to-earth faults with compensated neutral	88
5.3	Conclusion	89
A	Block schemes of the relays	90
A.1	HV breaker	91
A.2	MV breaker	92
A.3	Magra and Brenta breaker relays	95
A.4	Breaker 3A, 3D and 3E	98
A.5	LV fuses	99
	References	100

List of Figures

1.1	Energy-related CO_2 emissions, energy demand and fossil-fuel outlook [1]	2
1.2	Worldwide economic overview about RES solutions	4
1.3	Types of Micro Grids based on level of service provided and main grid connection [10]	8
1.4	Benefits obtained with the diffusion of RES-based micro grids [11]	9
1.5	Standard structure of balancing services provision [15]	14
1.6	Standard structure of balancing services provision [14]	16
1.7	Benefits and risks across scenarios regarding DSO grid constraints [14]	17
1.8	Overvoltages caused by DG unit [16]	19
1.9	Ineffectiveness of the centralized voltage control [16]	19
2.1	Single-line diagram of the MV network	24
2.2	Single-line diagram of the LV network	25
2.3	HV network equivalent model	26
2.4	Γ equivalent circuit of the transformers	27
2.5	HV/MV transformer component	27
2.6	OLTC control component	29
2.7	MV/LV transformer component	30
2.8	Π equivalent circuit for 3-phase lines [20]	31
2.9	MV lines component	32
2.10	LV lines component	34
2.11	Load components	36
2.12	Block scheme for P and Q set point computation for an industrial load	37
2.13	RTDS [®] Simulator hardware components [27]	42
3.1	Three-phase fault comparison	48
3.2	Comparison of <i>b-phase</i> transient	49

3.3	Phase-to-phase fault comparison	50
3.4	Phase-to-phase fault comparison	51
4.1	Protection devices implemented in Stura primary substation for Magra-Brenta transformer and feeders	53
4.2	Time-Current 50/51T HV relays characteristic	54
4.3	Time-Current 51T MV relay characteristic	56
4.4	Time-Current 50/51 MV relay characteristic	58
4.5	Time-Current characteristics of 51T and 50/51 MV relays and 50/51T HV relays	58
4.6	Protection devices implemented in secondary substation 203845	60
4.7	Total clearing time-current characteristic of the MV fuses with $I_n = 10A$	61
4.8	Selectivity among secondary substation protections and MV feeders breakers	62
4.9	Inrush current phenomenon of MV/LV transformer	63
4.10	<i>Ekip Touch</i> relay set up ranges [37]	65
4.11	Time-current characteristic of LV feeders relays	66
4.12	<i>NH2GG40V200-1</i> time-current characteristic	67
4.13	Circuit breakers, switch disconnectors and LV fuses component	68
4.14	MV fuses component	69
4.15	Total clearing time-current characteristics of the MV fuses models	70
4.16	Flow chart of the <i>a-phase</i> control logic of relays 50/51T	72
4.17	Block scheme implemented of the <i>a-phase</i> control logic of re- lays 50/51T	73
4.18	Flow chart of the <i>a-phase</i> control logic of relays 51T	74
4.19	Flow chart of the <i>a-phase</i> control logic of relays 59	75
4.20	Flow chart of the control logic of relays 59N	75
4.21	Flow chart of the <i>a-phase</i> control logic of relays 50/51	78
4.22	Flow chart of the first threshold control logic of relays 67N	79
4.23	Flow chart of the fifth threshold control logic of relays 67N	80
4.24	Flow chart of the <i>a-phase</i> control logic of LV electronic relay	81
4.25	Flow chart of the control logic of the LV fuse	82
4.26	Control logic for both relays deactivation and manual reclosing of circuit breakers	84
5.1	Operating time of MV feeder circuit breaker for multiphase faults at MV level	86
5.2	Operating time of transformer circuit breakers for multiphase faults at MV level with failure of MV feeder breaker	87

5.3	Operating time of circuit breakers for phase-to-earth faults at MV level	88
5.4	Operating time of circuit breakers for phase-to-earth faults at MV level with failure of MV feeder breaker	89
A.1	Block scheme of the <i>a-phase</i> control logic of relays 50/51T in HV breaker	91
A.2	Block scheme of the <i>a-phase</i> control logic of relays 51T in MV breaker	92
A.3	Block scheme of the <i>a-phase</i> control logic of relays 59 in MV breaker	93
A.4	Block scheme of the <i>a-phase</i> control logic of relays 59N in MV breaker	94
A.5	Block scheme of the <i>a-phase</i> control logic of relays 50/51 in MV feeder breaker	95
A.6	Block scheme of the <i>a-phase</i> control logic of relays 67N.S1 in MV feeder breaker	96
A.7	Block scheme of the <i>a-phase</i> control logic of relays 67N.S4 in MV feeder breaker	97
A.8	Block scheme of the <i>a-phase</i> control logic of relays 49/50/51 with $I_n = 160A$ in LV feeder breaker	98
A.9	Block scheme of emulating the time-current characteristic of the LV fuses	99

List of Tables

1.1	Overview of RES in Italy [3]	5
1.2	INECP targets for Italy [3]	5
1.3	Types of Energy Communities [12]	10
1.4	Overview of the roles of the market parties in the ancillary services market [14]	12
1.5	Coordination schemes proposed for Ancillary Services (AS) market models [14]	13
2.1	Parameters of Magra-Brenta and Chieri transformers	26
2.2	Parameters of Magra-Brenta and Chieri transformers	28
2.3	Parameters of Fiat-Grosso transformer	28
2.4	Parameters of OLTC of Fiat-Grosso transformer	29
2.5	Parameters of 203845 transformer	30
2.6	Parameters of 203844 transformer	30
2.7	MV lines parameters	32
2.8	LV lines parameters	34
2.9	Coefficients of exponential load model [22]	36
2.10	Parameters of load components	36
2.11	MV loads parameters	37
2.12	LV loads parameters	39
2.13	Average values of the utilization factor per each load type [24]	40
3.1	Comparison of current values in normal operating condition	45
3.2	Three-phase fault values obtained with RTDS [®]	46
3.3	Peak values of <i>b-phase</i> component of voltage and current after the three-phase fault	46
3.4	Phase-to-phase fault values obtained with RTDS [®]	47
3.5	Peak values of <i>b-phase</i> and <i>c-phase</i> components of voltage and current after the phase-to-phase fault	47
4.1	50/51T HV relays setting	55

4.2	51T MV relay setting	55
4.3	59 MV relay setting	56
4.4	59N MV relay setting	57
4.5	50/51 MV relay settings [34]	57
4.6	67N MV relay settings [34]	59
4.7	Parameters for inrush current computation [36]	63
4.8	Cross-sectional area and current carrying capacity of LV lines after secondary substation 203845, data from [38]	64
4.9	Nominal current of LV feeders circuit breakers	64
4.10	Formalism for <i>Ekip Touch</i> relay settings [37]	64
4.11	Settings of 49/50/51 LV relays with $I_n = 160A$	65
4.12	Settings of 49/50/51 LV relays with $I_n = 250A$	65
4.13	Cross-sectional area and current carrying capacity of the sec- ond segment of LV lines after secondary substation 203845, data from [38]	67
4.14	Parameters circuit breakers, switch disconnectors and LV fuses component	69
4.15	Parameters of MV fuses for MV/LV transformer protection . .	69
4.16	<i>Lookup table</i> for simulating LV fuses time-current characteristic	83

Chapter 1

Introduction

In this introductory chapter, an overview of the current world situation and future scenarios about energy transition will be given. After that, some definitions about smart grid, micro grid and Renewable Energy Sources (RES) are provided, in order to better understand the next sections of the thesis. Then, a more technical analysis of the micro grid components, functionality and ancillary services provided to the main electrical grid on Dispatching Services Market (MSD) is carried out. Moreover, some drawbacks of the RES will be presented. In conclusion, the structure of this thesis will be illustrated and the contributor of the candidate is highlighted.

1.1 Overview of the current situation and possible future scenarios

The health, humanitarian, social and economic crises set off by the COVID-19 pandemic requires a decisive and large-scale response guided by appropriate social and economic measures. All countries must to ensure sustainability and strengthening resilience while improving people's health and welfare. For this reason, one of the need remains for an accelerated path to meet global climate goals through the decarbonisation of our societies.

In [1], the International Renewable Energy Agency (IRENA) provides an ambitious, yet technically and economically feasible, pathway for deploying low-carbon technologies to create a more clean and sustainable energy future. This roadmap, presents several scenarios with related socio-economic outcomes:

- **Baseline Energy Scenario (BES)**: it is based on polices that were in place just after the Paris Agreement of 2015;

- **Planned Energy Scenario (PES):** it provides a perspective about energy systems development based on governments' current plans;
- **Transforming Energy Scenario (TES):** it describes a pathway, largely based on RES, to improve energy efficiency and to keep the rise of global temperature well below $2^{\circ}C$;
- **Deeper Decarbonisation Perspective (DDP):** it suggests additional options beyond the TES in order to reduce CO_2 emissions to zero in 2050 - 2060.

Recently, the energy trends confirm the need to accelerate a reduction in CO_2 emissions and RES are an enabling technology to reach the goals [1]. In fact, fossil-fuels continue producing negative effects such as pollution and energy-dependence from abroad. In Fig.1.1, the above-mentioned trends and future ones are reported.

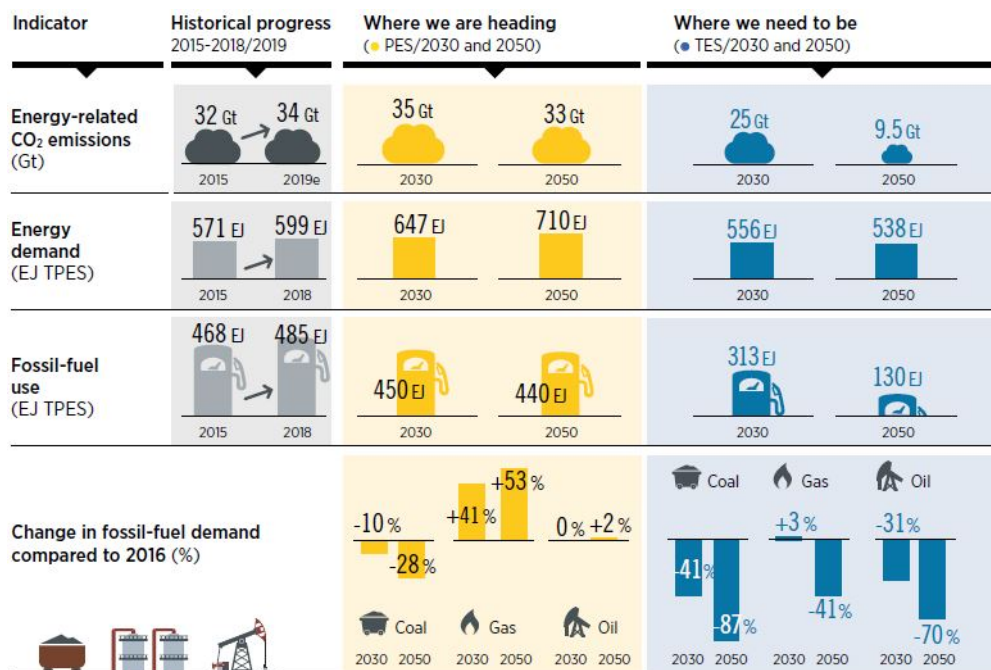


Figure 1.1: Energy-related CO_2 emissions, energy demand and fossil-fuel outlook [1]

Limiting the rise in average global temperatures to $1.5^{\circ}C$ requires all sectors of the economy to reach zero carbon dioxide emissions early in the second half of this century [2]. Doing so presents significant technical and

economic challenges, particularly in seven highly energy-intensive sectors of industry and transport:

- **Energy-intensive industrial sectors**
 - Iron and steel;
 - Chemicals and petrochemicals;
 - Cement and lime;
 - Aluminium.
- **Freight and long-haul transport sectors**
 - Road freight;
 - Aviation;
 - Shipping.

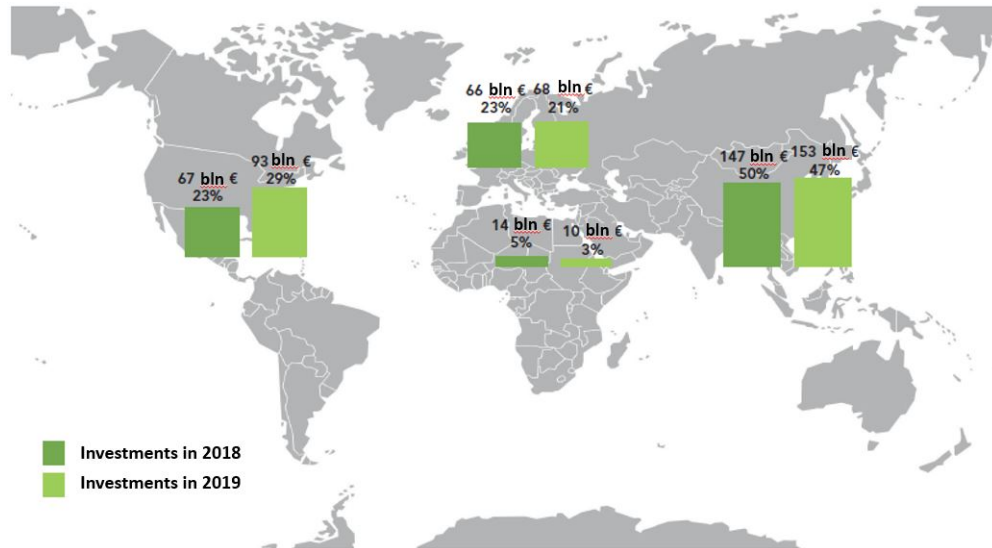
Together, those seven sectors could account for 38% of the energy and process emissions and 43% of the final energy use by 2050 unless major policy changes are pursued now [2]. IRENA has identified five *emission reduction measures* that could, if applied at scale, reduce industry and transport CO_2 emissions to zero. They are:

- Direct use of clean, predominantly renewable, electricity;
- Reduced demand and improved energy efficiency;
- Direct use of renewable heat and biomass;
- Indirect use of clean electricity via synthetic fuels and feedstocks;
- Use of carbon dioxide removal measures;

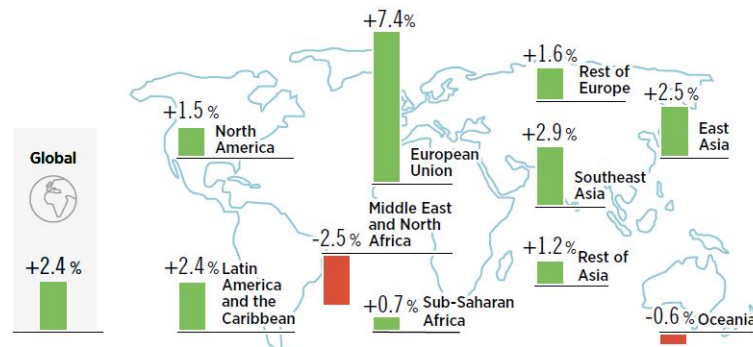
The rapid decline in the costs of renewables over the past decade, and the future potential for further cost reductions and scaling, opens up options for the use of RES energy that were previously dismissed. As IRENA has estimated, RES together with demand reduction and energy efficiency could account for over 80% of the CO_2 emission reductions needed. Despite this, RES-based solutions have not been explored to date with the rigor and urgency that is needed.

In Fig.1.2a, the investments on RES-based solutions of each geographic area are shown. As it can be seen, the amount of investments grew up from 2018 to 2019 in all countries except African area [3]. Moreover, the regional

distribution of the differences in Gross domestic Product (GDP), taken as economic index, between the TES and the PES in 2050 is shown in Fig.1.2b and confirm the benefits of a bigger penetration of renewables, also in economic terms [1].



(a) Worldwide investments on RES in 2018 and 2019 [3]



(b) Percentage difference in countries' GDP between the PES and the TES in 2050 [1].

Figure 1.2: Worldwide economic overview about RES solutions

Finally, in 2019 almost 2.3 millions of electric and plug-in electric cars and light-duty vehicles were registered. Consequently, the number of electric charging points grew up 59% with respect to the previous year [4]. In Italy the situation is in agreement with respect to the worldwide one. The commitment is to obtain a gradual reduction of dependence on fossil fuels, reaching a share of 30% of the gross final consumption of energy by 2030

from renewable sources [3]. In Tab.1.1 all the objectives are resumed.

Table 1.1: Overview of RES in Italy [3]

Sectors	2017	2030	Δ 2030-2017
<i>RES gross electricity production</i>	9729tep	16060tep	+65%
<i>RES gross final consumption for heating and cooling</i>	11211tep	15031tep	+34%
<i>RES final consumption for transport</i>	1060tep	2337tep	+120%
<i>Total gross final consumption</i>	120435tep	111359tep	-7.5%
<i>RES share</i>	18.3%	30%	

In December, 2019 in Italy *Integrated National Energy and Climate Plan* (INECP) was declared. The process aimed at establishing the mix of solutions and instruments that is most compatible with the objectives of the 2030 Energy and Climate Plan and other requirements, including those relating to environmental impacts [5]. The INECP is intended to contribute to a wide-ranging transformation of the economy. For instance, the combination of decarbonisation, circular economy, efficiency and the rational and fair use of natural resources represents the objectives and the instruments needed for an economy to be respectful towards people and the environment. In conclusion, in the four sectors reported in Tab.1.2 substantial investments will be required to achieve the objectives [3]. Until now there is a gap, in terms of installed power, to be bridged over the next 10 years.

Table 1.2: INECP targets for Italy [3]

Sectors	Target INECP 2025	Target INECP 2030
<i>Solar photovoltaic</i>	+7.8GW	+31.2GW
<i>Eolic</i>	+5.3GW	+8.6GW
<i>Heat Pump</i>	+1564ktep	+3103ktep
<i>Storage System</i>	+3GW(<i>centralised</i>)	+4.4GW(<i>distributed</i>)

1.2 What is a *Smart Grid*?

The “classical” electrical grids are designed for an unidirectional power flow from the plants, in which electricity is produced, to the loads served, where electricity is used. However, in the last few years, due to the great penetration of RES, some users are converting from *consumers* to *prosumers*, that are users that not only consume, but also produce energy. Therefore, also at Medium and Low voltage levels, there could be production of electricity and

power flow has become bidirectional. In this way, the management of the grid is becoming more difficult due to both the lack of sensors and communication and the technical issues explained in Chap.1.8. For these reasons, digital technologies are needed to improve transparency and to increase reliability as well as efficiency. Thanks to the employment of Information and Communication Technologie (ICT) devices, especially sensors, the traditional grid are turning into *smart grid* [6].

This term was used for the first time in 1997 in [7] as acronym for *Self-Managing And Reliable Transmission Grid* (SMARTGrid). It was defined as an automated system that utilized information technology to improve grid reliability and capability. However, defining the smart grid in a concise way is very difficult still today.

In [6], some definitions about what is a smart grid in different authors and organisations opinions are provided. To sum up, we can briefly conclude that a smart grid is an “intelligent” electrical grid, whose operations are based on ICTs and whose “intelligence” resides within the digital information infrastructure itself that allows to understand the state of the grid and helps to maintain safe, secure, efficient and reliable the whole power system. This modernisation, based on grid automation, enables modern strategies and technologies like Demand-Side Management, Distributed Generation (DG), Real-Time Pricing of electricity and so on.

1.3 What is a *Micro Grid*?

Starting from the more general concept of Smart Grid, *Micro Grid* can be defined. From a more technical point of view, the U.S. Department of Energy defines it as “a group of interconnected loads and Distributed Energy Resources (DERs) with clearly defined electrical boundaries that acts as a single controllable entity with respect to the grid and can connect and disconnect from the grid to enable it to operate in both grid-connected or island mode” [8]. This concept was born in 1882 when Thomas Edison built his first Direct Current (DC) power plant. To date, the main components of modern micro grid RES-based are:

- **Optional grid connection:** the switch at the Point of Common Coupling (PCC) performs micro grid islanding by disconnecting it from the main grid;
- **Loads:** categorised in fixed and flexible with Demand Management System (DMS);

- **Distributed Energy Resources (DERs):** Distributed Generation (DG) units, distributed Energy Storage System (ESS) and Demand Response (DR) programs including DMS;
- **Smart switches and protective devices:** manage the connections between DERs and loads by connecting/disconnecting lines based on the operational conditions;
- **Master controller:** determines the micro grid interaction with the main grid, the decision to switch between interconnected and islanded mode and optimal operation of local resources;
- **Communication, control and automation system:** used to implement control actions and to ensure constant, effective and reliable interaction among micro grid components.

Thanks to micro grid, sometimes also called *mini grid*, electricity can be provided to both just a few customers in a remote settlement and hundreds of thousand of customers in a town/city. In fact, micro grid has not been defined in terms of size even if the vast majority of the micro grids analysed in [9] ranged from a few of kilowatts to several megawatts.

Micro grids can be categorised according to:

- **generation** to which they belong [9];
- **level of service** provided and **connection** to the main grid [10];

Basing on [9], there are three generations of micro grids:

- **1st generation:** almost all current centralized electricity grid systems started with isolated micro grids, which gradually interconnected themselves. These first micro grids were pivotal to the early development and industrialization of most modern economies. These systems were introduced in the late 19th and early 20th centuries;
- **2nd generation:** they are widespread in many low-income and developing countries today. These systems are typically small and isolated, powered by diesel or hydro, and built to provide access to electricity primarily in rural areas that have not already been reached by the main grid. Tens of thousands of these systems were built, starting in the 1980s and ramping up through the 1990s and early 2000s and provided important lessons to the development of the last generation;

- **3rd generation:** these are the more modern systems, mostly solar photovoltaic (PV) hybrid, grid-interconnection ready and use remote management systems and other ICTs technologies.

Basing on [10], a RES-based micro grid can be *interconnected* to the main grid or independent from neighbouring grids, in this case it is considered *autonomous*. Renewable micro grids can provide different levels of service, from *basic* services, such as lighting, to *higher* levels of services, such as satisfying commercial energy demand. In Fig.1.3 this concept is summarised.

	Lower Tier of Service	Higher Tier of Service
Autonomous	<p>Autonomous Basic (AB mini-grids) Generation Sources: PV, hydro and biomass Tier of service: Less than 24-hour power End-users: Remote community without major commercial or industrial activity Added value:</p> <ul style="list-style-type: none"> • Enable enhanced energy access • Alternative to grid-extension • Improve quality of life • Cost savings 	<p>Autonomous Full (AF mini-grids) Generation Sources: PV, hydro and wind Tier of service: 24/7 power End-users: Remote communities with major commercial or industrial requirements; industrial sites disconnected from grid Added value:</p> <ul style="list-style-type: none"> • Alternative to expensive polluting imported fuels • Diversification and flexibility of supply • Cost savings
Interconnected	<p>Interconnected Community (IC mini-grids) Generation Sources: PV, wind and biomass/biogas Tier of service: High critical/interruptible End-users: Medium to large grid-connected community, such as university campus Added value:</p> <ul style="list-style-type: none"> • Community control • Improved reliability • Response to catastrophic events • Cost savings 	<p>Interconnected Large Industrial (ILI mini-grids) Generation Sources: PV, wind and biomass/biogas Tier of service: Very high: Critical/uninterruptible End-users: Data centres, industrial processing or other critical uses Added value:</p> <ul style="list-style-type: none"> • High reliability for critical loads • Enhance environmental performance • Resiliency

Figure 1.3: Types of Micro Grids based on level of service provided and main grid connection [10]

1.4 Energy Communities

An *Energy Community* can be defined as a set of energy users who decide to make common choices from the point of view of meeting their energy needs, in order to maximize the benefits deriving from this “collegial” approach, which can be implemented through distributed generation and intelligent

management of energy flows. Energy communities represent one of the main constituent elements of the new micro grid architecture [11].

However, micro grid and energy communities need to be differentiated. In fact, only RES-based micro grids are debated in this thesis while an energy community could be formed by portions of “traditional” system, without prosumers but only consumers. Moreover, more than one micro grids can be grouped for forming a unique energy community.

Nowadays, finding the financial resources necessary for the creation of an energy community is the most significant criticality for end users. In [11] a market model is proposed. In particular, in a *Micro grid-as-a-service* model there is an *Energy Community Provider* that finances all the needed investments and provides Operations and Maintenance (O&M) services to the micro grid. The remuneration for this third-part subject is guaranteed by stipulation of multi-years contracts with the end-users of the micro grid.

In conclusion, in Fig.1.4 the benefits obtained by the spread of RES-based micro grids and energy communities are summarized [11].

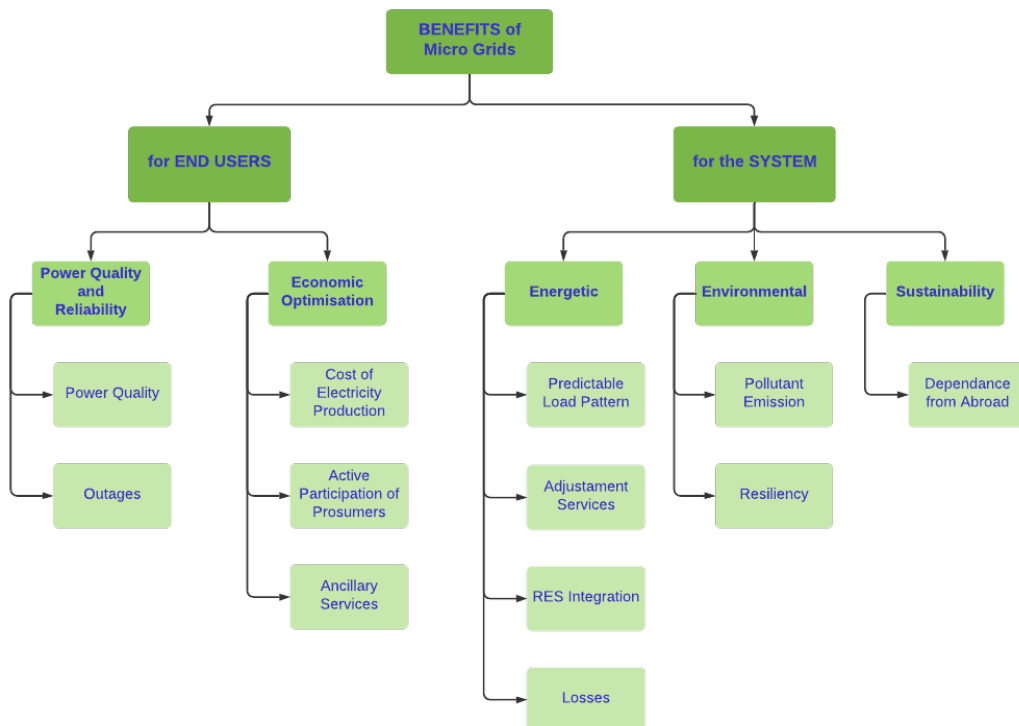


Figure 1.4: Benefits obtained with the diffusion of RES-based micro grids [11]

The concept of Energy Community was introduced by the European Com-

mission in two directives of the *Clean Energy for all Europeans Package* [12]:

- **Renewable Energy Directive 2018/2001 (RED II):** it defines the “Renewable Energy Community” (REC) and jointly-acting renewable self-consumers. Its aim is to encourage the spread of renewable energy sources for electricity production and increase public acceptance of projects for new renewable plants;
- **Directive on common rules for the internal market for electricity 2019/944 (IEM):** it defines the “Citizen Energy Community” (CEC) and jointly-acting active customer. Its main purpose is to adapt the EU electricity market to the technological and structural changes taking place.

The main characteristics of REC and CEC are summarised in Tab.1.3.

Table 1.3: Types of Energy Communities [12]

	REC	CEC
<i>Members</i>	Residential, Tertiary, Public Administration, SME	Residential, Tertiary, Public Administration, Small enterprise
<i>Type of Energy</i>	Electric and Thermal, only from RES	Electrical, from RES and conventional sources
<i>Limits</i>	Closeness	None
<i>Enabled activities</i>	Production, Sale, Self-consumption, Storage, Sharing, Market access	Production, Sale, Self-consumption, Storage, Sharing, Distribution, Supplying, Energy Efficiency services, EV charging, Market access

1.5 The evolution of the Ancillary Services market and the new roles of the system operators

Ancillary services are all the services necessary to ensure the safety of the whole power electricity system. Among these services, the most relevant

concern frequency and voltage regulation [13]. At transmission level, they are used for both balancing the system and limiting the energy fluctuations. While, at distribution level can be used to manage small local systems [14]. The ancillary services market is used by the System Operator (SO) to restock sources that will be “turn-on” when needed.

To date, frequency regulation is carried out exclusively through programmable generation units with an installed power greater than 10MVA . Furthermore, the presence of rotating generators guarantees the inertia of the network in the moments immediately following a disturbance. With the spread of RES plants, a growing replacement of thermoelectric plants (programmable) with non-programmable (RES) ones is in place. The result is a reduction of the adequacy margin, especially in the hours in which production from RES plants is lower, which in any case cannot guarantee a contribution equal to that provided from conventional generation [12].

However, the increase of DER connected at the distribution grid provides an additional opportunity for system operators to use these resources for services such as frequency control, voltage control and congestion management, both at the distribution and transmission grid. For this reason, resources from the distribution grid are starting to participate to the Transmission System Operator (TSO) Ancillary Services (AS) market. This trend needs an increase in cooperation between system operators, in particular Distribution System Operator (DSO) and TSO. In [14], five coordination schemes are proposed that present different ways of organizing the coordination between system operators. Each coordination scheme is characterized by a specific set of roles, taken up by system operators, and a detailed market design. The differences between the coordination schemes have mainly an impact on the procurement phase of the AS or local system services. The schemes above-mentioned and their characteristics are resumed in Tab.1.5. Until now, there is not a unique regulation for participation of DER to AS market and there are specifications that differs from country to country. In Italy, for example, DER can not participate to AS for the main grid, except for some pilot project that began after the approval of Deliberation 300/2017 (and successive modifications). Thanks to it, UVAM (“mixed virtual enabled units”), that are in compliance with some technical requirements, are enabled to participate to the following AS services in rise/drop mode [12]:

- Congestion management;
- Rotating tertiary reserve and tertiary replacement reserve;
- Balancing.

In ancillary services market, each market party has a role. In Tab.1.4, the different roles needed are described [14]. The coordination schemes proposed in [14] for market organization and their characteristics are explained in Tab.1.5

Table 1.4: Overview of the roles of the market parties in the ancillary services market [14]

Domain	Role	Explanation	Adopted by
Grid Operation	<i>System Operator (SO)</i>	Operates and manages the physical system in question	TSO; DSO
	<i>System Balance Responsible (SBR)</i>	Ensures the balance of the grid and reduces deviations for a system or certain area by the activation of reserves	TSO; DSO
	<i>Data Manager (DM)</i>	Handles grid data (incl. formatting, storage and provision), separately for each network level	TSO; DSO; IMO
Prequalification	<i>Flexibility Feasibility Checker (FFC)</i>	Responsible for assessing potential impact at distribution grid level (system prequalification) caused by the provision of flexibility-based services from a DER unit requesting participation to the AS flexibility market (central or local)	DSO
Procurement	<i>Reserve Allocator (RA)</i>	Determines the amount of flexibility-based services (e.g. reserves) to be procured	TSO; DSO
	<i>Buyer</i>	Acquirer of flexibility-based services in a market setting	TSO;DSO;CMP
	<i>Seller</i>	Provider of flexibility-based services in a market setting	TSO;DSO;CMP
	<i>Market Operator (MO)</i>	Responsible for setting up the market platform and operating the market	TSO;DSO;IMO
	<i>Aggregator</i>	Collector of DER flexibility for its offering in a market setting	DSO;CMP
Activation	<i>Flexibility Dispatcher (FD)</i>	Activates DER units providing flexibility by sending operational signals	TSO;DSO;IMO; CMP
Settlement	<i>Metered Data Responsible (MDR)</i>	Responsible for measuring activated energy and for providing relevant related data to the party calculating the settlement	TSO;DSO;CMP

1.6 Ancillary services processes

System operators use different processes and products in order to balance the system and restore the frequency. In [14], the ancillary services considered are:

Table 1.5: Coordination schemes proposed for Ancillary Services (AS) market models [14]

MODEL	MARKET design	TSO role	DSO role
<i>Centralised AS</i>	One common market, operated by TSO	Responsible for the operation of its own market for AS. The TSO does not take DSO constraints actively into account	Is not involved in the procurement and activation process of AS
<i>Local AS</i>	Separate local market managed by the DSO. The DSO aggregates and transfers bids to the AS market, operated by the TSO	Responsible for the operation of its own market for AS	Clears the market, selects the necessary bids for local use, aggregates and transfers the remaining bids to the TSO-market
<i>Shared balancing responsibility</i>	Two market: one, managed by TSO, for the resources connected to the TSO-grid; one, managed by DSO, for the ones connected to the DSO-grid	Responsible for the operation of its own market and for the balancing of the transmission grid	Responsible for the operation of its own market and for both local congestion management and balancing of the distribution grid
<i>Common TSO-DSO AS</i>	Common market for both resources connected at TSO-grid and DSO-grid. TSO and DSO are both responsible for the organization and operation of the market	It is contracting AS services from both transmission and distribution	It uses flexible resources from the distribution grid in cooperation and interaction with the TSO. DSO constraints are integrated in the market clearing process
<i>Integrated flexibility</i>	No priority for TSO, DSO or CMP ^a . Resources are allocated to the party with the highest willingness to pay	It is contracting AS services in a common market	It is contracting flexibilities in a common market. DSO constraints are integrated in the market clearing process

^aCMP: Commercial Market Party

- Frequency control;
- Frequency restoration/balancing and congestion management;
- Voltage control.

The European Commission Regulation (EU) 2017/2195 of 23 November 2017 sets up the requirements for the technical parameters of standard products in order to facilitate the exchange of balancing energy across borders [15]. In Fig.1.5, the structure of balancing services provision is shown.

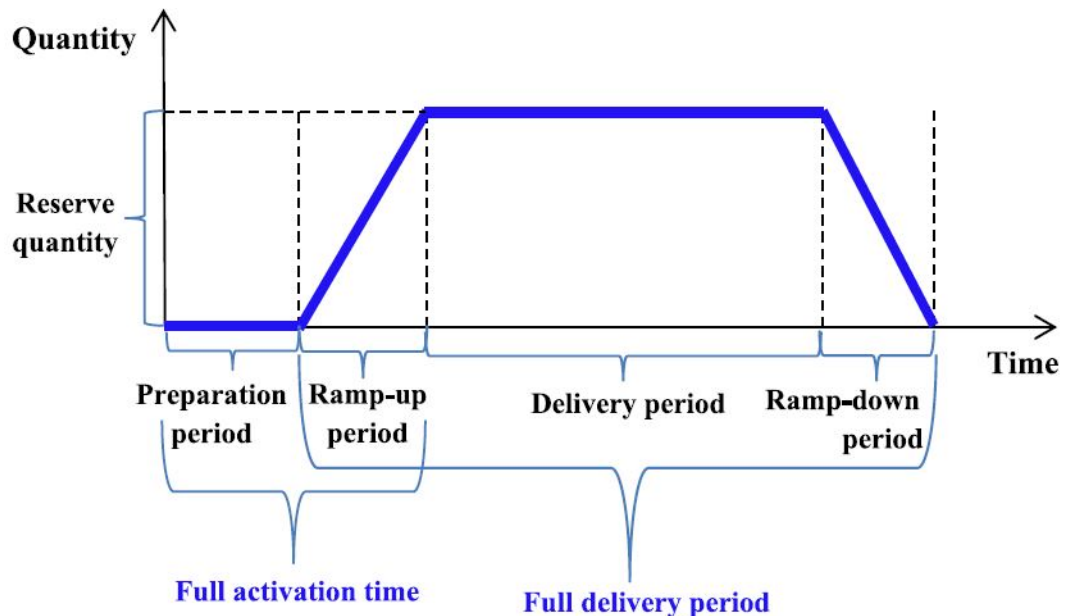


Figure 1.5: Standard structure of balancing services provision [15]

About frequency regulation (control and restoration/balancing), the following processes are taken into account [15]:

- **Frequency Containment Reserve (FCR):** the active power reserves available to contain system frequency deviation after the occurrence of an imbalance. During the ramp-up period, it requires the delivery of 50% of the reserve within 15s, and 100% within 30s. The FCR rules also specify that this delivery should be sustained for 15 min. In addition, the FCR must have automatic activation (primary regulation);

- **Frequency Restoration Reserve (FRR):** the active power reserves available to restore system frequency to the set point and, for a synchronous area consisting of more than one load-frequency control area, to restore power balance to the scheduled value. The standard FRR can be activated automatically (aFRR, secondary regulation) or manually (mFRR, tertiary regulation). The full activation time for the first one shall be $5min$, while for the second is $12.5min$;

- **Replacement Reserve (RR):** the active power reserves available to restore or support the required level of FRR to be prepared for possible additional system imbalances. The full activation time of the RR service is $30min$, considering the preparation and the rampup periods from 0 to $30min$. Moreover, the duration of the delivery period is between $15min$ and $60min$, while the activation of the service is scheduled with manual activation

The decision if a coordination scheme is applicable to a certain ancillary service is based on the question if the characteristics of the ancillary service are serving the needs of certain market parties [14]. In fact, due to the type, not every coordination scheme is feasible or relevant. In Fig.1.6, a mapping between ancillary services and relevant coordination schemes is shown.

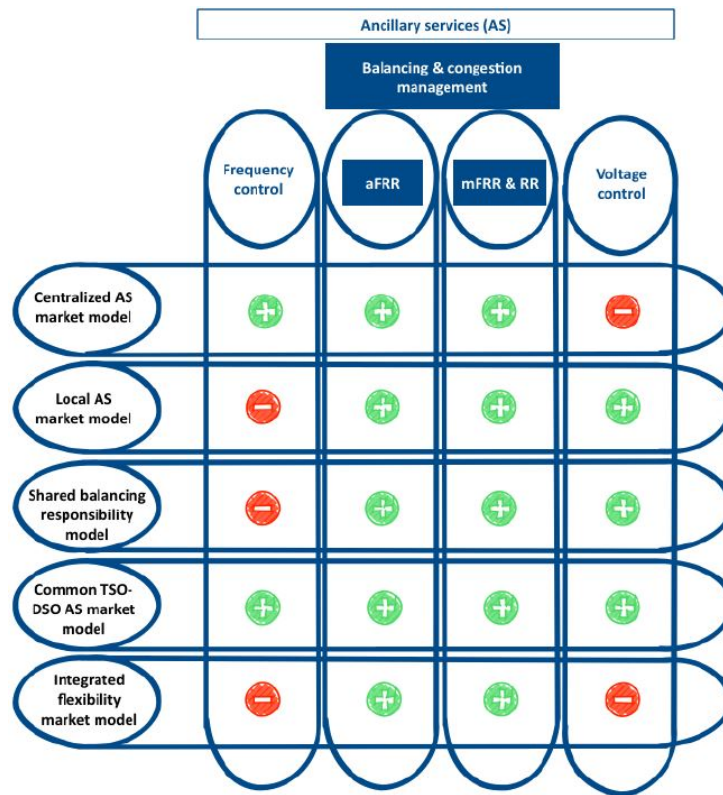


Figure 1.6: Standard structure of balancing services provision [14]

As is known, frequency control is the unique responsibility of the TSO. Therefore, only the coordination schemes where the TSO is directly involved in the operation of the market are relevant, i.e. the Centralized AS market model and the Common TSO-DSO AS market model. On the other hand, voltage issues and their control are specific for each location, so the involvement of the DSO is needed. Hence, the Central AS market model is not applicable in the context of voltage control.

1.7 Distribution grid constraints

The use of flexibility from DER connected at the DSO grid may have an impact by imposing constraints to grid operation. For instance, the activation of DER might violate voltage limits and/or overload distribution lines and transformers, leading to an increase in losses [14]. Therefore, it is important to assess how DSO grid constraints should be integrated in the processes of procurement and activation of ancillary services in order to safeguard security of supply and quality of service. Four scenarios are possible and their benefits

and risks are resumed in Fig.1.7.

	Benefits	Risks
Scenario 1 (distribution constraints not considered)	<ul style="list-style-type: none"> No additional cost 	<ul style="list-style-type: none"> Constraints might not be respected
Scenario 2 (DSO involved in system prequalification)	<ul style="list-style-type: none"> Implementation costs might be low DSO grid constraints are taken into account Provides more information to the DSO (enhancing grid observability) 	<ul style="list-style-type: none"> Constraints might not be respected Need for accurate forecasts of future grid load In order to secure the grid, safety margins taken by the DSO might be very conservative
Scenario 3 (DSO also involved after market clearing)	<ul style="list-style-type: none"> DSO grid constraints are always respected Provides more information to the DSO (enhancing grid observability) Mathematically not difficult to implement 	<ul style="list-style-type: none"> Heavy operational process (manual and iterative) Deadline of finishing the market clearing process might be endangered by this process Could create uncertainty in the market as it is unclear on which base DSOs might block activations Issues with transparency
Scenario 4 (Constraints integrated in market clearing)	<ul style="list-style-type: none"> DSO grid constraints are always respected Provides more information to the DSO (enhancing grid observability) Operational process is relatively light No issues related to 'neutrality' of the DSO 	<ul style="list-style-type: none"> Heavy mathematical process to integrate all constraints in the clearing Need for sharing data between DSO and market operator (discussions on security and privacy of data)

Figure 1.7: Benefits and risks across scenarios regarding DSO grid constraints [14]

The *Scenario 1* is currently the case in most European countries. However, it is easy to understand that this choice can be acceptable in case the share of DERs connected from the distribution grid is below a certain threshold.

In *Scenario 2*, during the system prequalification process, DSO analyzes DER assets and gives or not its approval to participate to the flexibility market. This process is not a technical prequalification process in which DSO assesses the technical requirements of a certain DER, but it assesses the impact of the delivery of a specific service by a certain DER on the grid.

In *Scenario 3*, DSO is involved during system prequalification and also after clearing of the market. In this way, it has the possibility to block the activation of a DER with a manual and iterative process in case distribution grid constraints might be violated.

In *Scenario 4*, the DSO is not only involved during prequalification (before

procurement), but grid constraints are also integrated in the market clearing algorithm. The advantage of this scenario with respect to Scenario 3 is that it is operationally much easier, as no manual actions from the DSO are required after market clearing and no iterations are needed. Nevertheless, integrating physical grid constraints in the market algorithm might be heavy from a mathematical point of view.

1.8 Drawbacks of RES penetration

In the previous sections, the benefits of RES and micro grids were well explained. However, as revealed in advance in Chap.1.2, the large penetration of RES involves some technical issues. More specifically, the problems are related to the operations of DERs connected to the grid. The most relevant issues concerning:

- **Short-circuit currents:** with DG penetration, the short-circuit currents could increase due to the contribution of generation units that can not be controlled by the DSO. In the worst cases, the value of these currents becomes bigger than the short-circuit capability declared at each node of the distribution grid and, consequently, the sizing of the protection devices installed in secondary substations becomes inadequate [16];
- **Frequency:** RES-based DG are interfaced to the main grid through power electronic converters. So there are not mechanical rotating masses that can provide inertia and damping to the power system. An under analysis solution are the Virtual Synchronous Generators (VSG): they are generation units interfaced with the main grid through inverters that are controlled by a logic that emulate the behaviour of the synchronous generators [17];
- **Voltage control:** the voltage profile can be modified by the presence of DER. It means that could be overvoltages in the nodes at which DG are connected caused by the power supplied by the units [16]. To better clarify this aspect, an example is shown in Fig.1.8. As it can be seen, at the beginning of the feeder the voltage is equal to the nominal one V_0 . Without DG, the voltage along the feeder decreased as much as the distance d increases, due to the voltage drop caused by the load currents I_1 , I_2 and I_3 . If there is a DG unit, instead, the voltage profile is modified since the currents flowing in the feeder are different from the previous case, due to DG contribution.

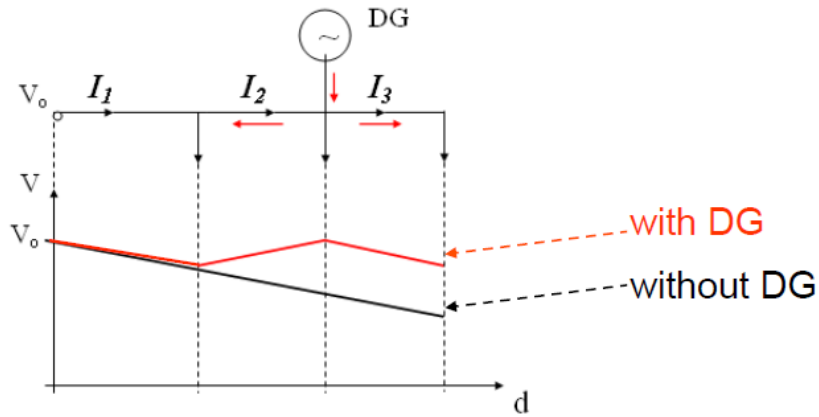


Figure 1.8: Overvoltages caused by DG unit [16]

In the worst cases, this overvoltage exceeded the voltage upper limit and this issue can not be solved with On Load Tap Changer (OLTC) in primary substation. An evidence of ineffectiveness of the centralized voltage control is shown in Fig.1.9. After the HV/MV station there are both DG and passive feeders. It means that the eventual tap operation for decreasing the voltage on MV busbar V_{MV} and insure that DG feeder is in the allowed voltage range, could involve the excessive decreasing of passive feeder voltage that will pass the lower limit [16].

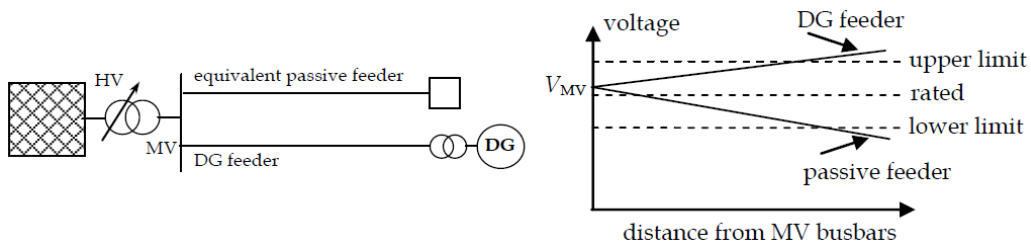


Figure 1.9: Ineffectiveness of the centralized voltage control [16]

Due to the above-mentioned issues, it is important to be able to evaluate the degree of DER penetration. To do that, the *Stiffness ratio* can be computed [16]:

$$R = \frac{S_{ccR} + S_{ccDER}}{S_{ccDER}} \quad (1.1)$$

where:

- S_{ccR} : is the short-circuit power of the network;
- S_{ccDER} : is the short-circuit power of the DER to be connected.

The ratio R is evaluated at the Point of Common Coupling (PCC), except when there is a transformer dedicated to a single user (in this case, the ratio is computed at the High Voltage side of the dedicated transformer) and gives information about the stiffness of the main grid. In particular [16]:

- If $R > 200$, the main grid is stiff enough and the problems related to DER penetration will be limited;
- If $R < 50$, the main grid is weak and some rules must be established in order to limit the installation of new DER.

However, this ratio provide only an overview of DER penetration because it does give information neither about their locations nor about their time-availability [16].

1.9 Thesis aim and organization

Basing on the above-mentioned drawbacks, it is quite clear the importance to be able to predict the consequences that the large penetration of RES will have on the main grid. In order to do that, simulation studies are the most promising methods. For this reason, the aim of this thesis is to implement a digital twin of a portion of urban distribution system in Turin. The Real-Time Digital Simulator made by *RTDS Technologies Inc.* was used for the implementation. Thanks to the real-time execution, also Hardware-In-the-Loop (HIL) simulations will be carry out by using the digital twin of the power system.

In Chapter 2, the simulated electrical grid is presented. It is a portion of the distribution network after Stura primary substation, in Turin. After the description of the network structure, basing on the parameters provided by the Turin DSO to the *Politecnico di Torino*, all the components models used for the implementation and their configuration are described in detailed way. At the end of the chapter, the characteristics of both the RTDS[®] Simulator in the *Energy Center Lab* and the simulator software package RSCAD[®] are provided together with the simulation parameters set.

In Chapter 3, there is a comparison between the results obtained with RTDS[®] Simulator and the ones obtained with OPAL-RT[®] Simulator, made by *OPAL-RT TECHNOLOGIES, Inc.* In fact, in the thesis [18] the author developed

a digital twin of the same distribution system in *Simulink* environment for interfacing with OPAL-RT[®] Simulator.

In Chapter 4, the protection devices implemented in the simulation are described. In particular, in order to simulate their real behaviour, the time-current characteristics of both the circuit breakers and the fuses are produced by using the blocks in the *Controls* library of RSCAD[®]. A specific control logic was implemented by building a block scheme based on the correct settings. For comprehension facilitating, the flow charts on which these control logics are based are shown. Finally, for completeness, also the manual deactivation of each relay was implemented in order both to give the users the possibility to simulate fault electromagnetic transients and to test selectivity among the protection devices.

In Chapter 5, the control logic of the relays implemented is proved. Firstly, a multiphase fault and a single-phase fault are simulated in order to test the accuracy of the operating time of, respectively, the overcurrent protections and the earth-directional protections. Once verified the correct functionality, the same faults are simulated after disabling the above-mentioned relays for testing the accuracy of the other relays and the selectivity among them.

It can be concluded that the model developed in this thesis works properly. RES components can be added in the digital twin in order to evaluate the technical issues and their possible solutions. Moreover, other electromagnetic transients concerning the power system can be evaluated. Finally, thanks to real-time implementation, a real component can be added in the simulation loop by interfacing with the digital twin, that works as main grid, for Power Hardware-In-the-Loop (PHIL) simulations.

Chapter 2

Digital twin and simulation

In this chapter, the digital twin of a portion of the urban distribution system of Turin will be presented. At the beginning, the structure of the electrical grid will be analysed. After that, a description of the components used to “build” the model in the simulation software package RSCAD[®] will be shown. In conclusion, the main parameters of the real time simulation and hardware characteristics will be provided.

2.1 Network structure

The electrical system analysed is a portion of the electrical distribution grid after Stura HV/MV substation in Turin. In particular, the network analysed consist of three parts:

- **High Voltage (HV) grid:** it is the Transmission Network before the Distribution Network. It is meshed with a nominal voltage of $220kV$. In the digital twin, transmission lines that supply the primary substation were replaced by their Thévenin Equivalent Circuit composed by an ideal three-phase voltage generator with an equivalent three-phase RRL impedance that outlines the impedance of the transmission grid, so there is only one bus at HV level;
- **Medium Voltage (MV) grid:** it is part of the Distribution Network. It is weakly meshed but radial-managed with a nominal voltage of $22kV$ and made up of underground cables. In Stura primary substation there are three three-phase power transformers from which depart more MV feeders. However, only five of ones were implemented: MARGRA, BRENTA, GROSSO, FIAT and CHERI. The neutral point of the secondary winding of the HV/MV transformers is insulated. With

few modifications of the transformers configuration, also the compensated neutral could be simulated. However, neutral point connection is relevant only for phase-to-ground faults evaluation. The single-line diagram of the MV network is shown in Fig.2.1. As it can be seen, there are 53 nodes at MV level;

- **Low Voltage (LV) grid:** in this thesis, the LV network after the *Node 5* and *6* of Magra MV feeder is analysed. Low voltage grid is radial with a nominal voltage of 400V and made up of underground and overhead cables lines. The secondary substations implemented are the 203845 (after *Node 5*) and the 203844 (after *Node 6*). In every substation there is a MV/LV three-phase power transformer whose neutral point of the secondary winding is directly grounded (for safety reasons). The single-line diagram of the LV network is shown in Fig.2.2. As in can be seen, there are 27 nodes at LV level.

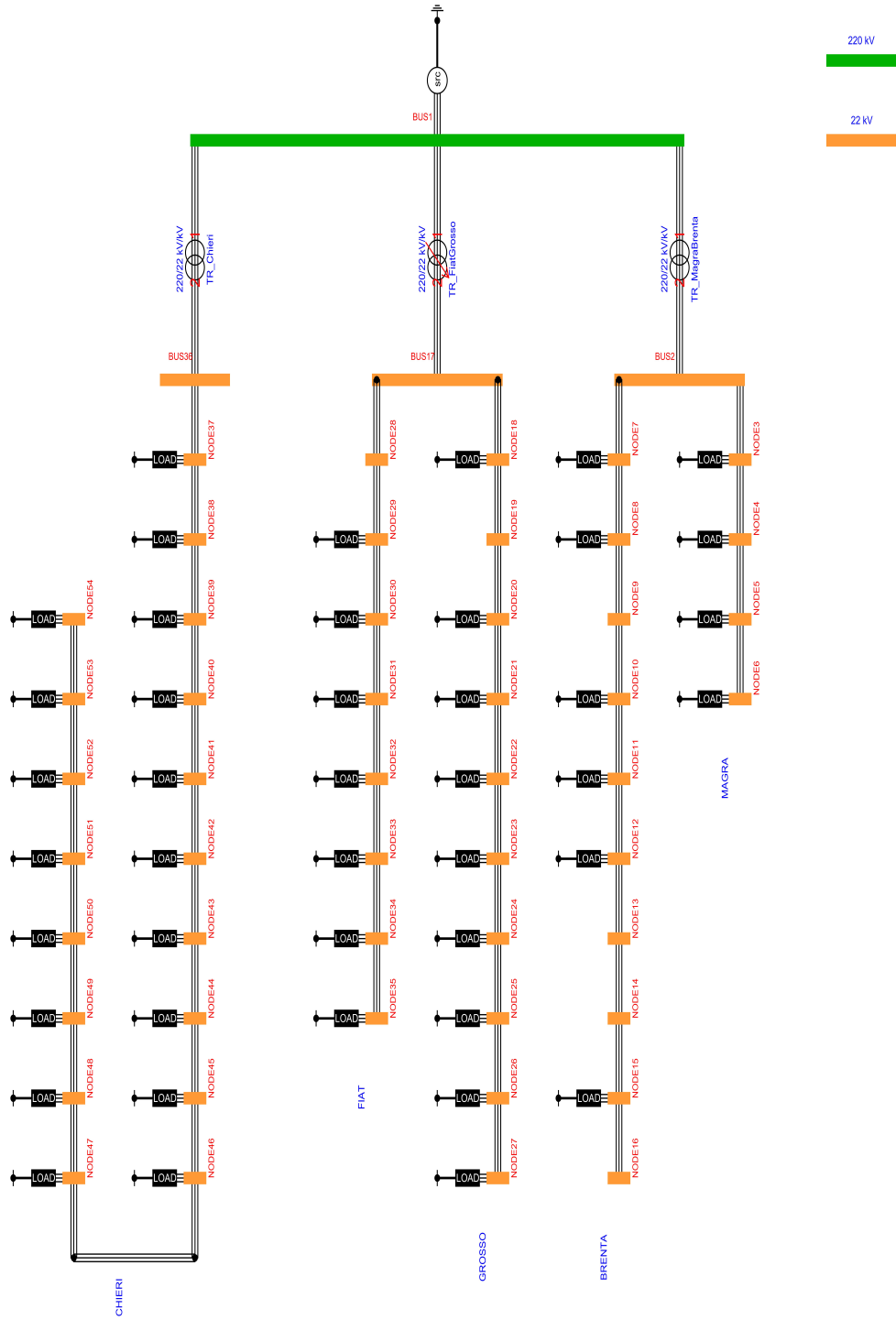


Figure 2.1: Single-line diagram of the MV network

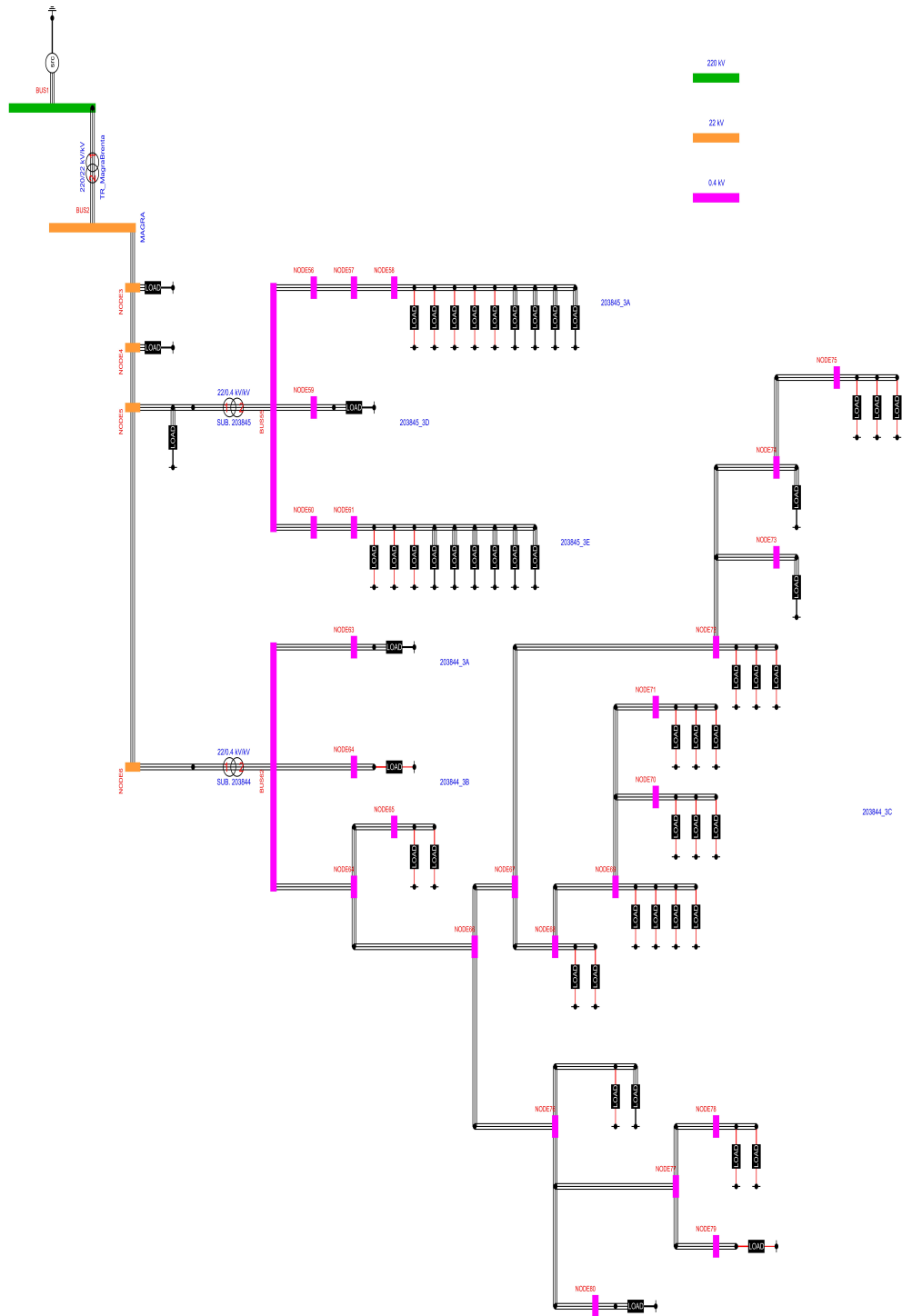


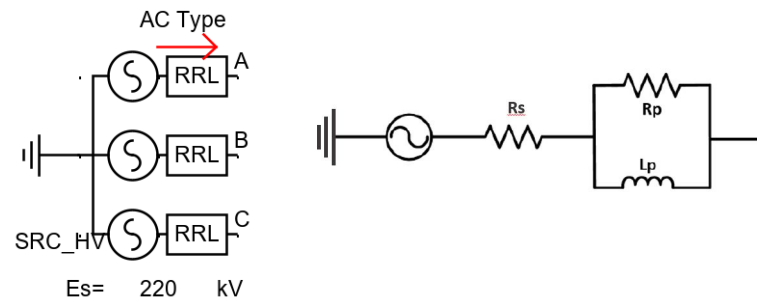
Figure 2.2: Single-line diagram of the LV network

2.2 Network model

In this section, the model of the various components used to implement the digital twin in simulation software package RSCAD[®] will be described.

2.2.1 HV grid

The HV transmission network, as above-mentioned, is replaced with its Thévenin equivalent circuit. This model includes an ideal 3-phase voltage generator, with a nominal Root Means Square (RMS) line-to-line (l-l) voltage of $220kV$ and a nominal frequency of $50Hz$, and a series impedance. The component used is shown in Fig.2.3.



(a) *Thévenin equivalent circuit of HV transmission network.* (b) *Single-phase circuit model of series impedance.*

Figure 2.3: HV network equivalent model

The values of the components of the series impedance, provided by the Turin DSO, are shown in Fig.2.1.

Table 2.1: Parameters of Magra-Brenta and Chieri transformers

Parameter	Symbol	Value	Meas. unit
Series resistance	R_s	1.445	Ω
Parallel resistance	R_p	≈ 0	Ω
Parallel inductance	L_p	0.046	H

2.2.2 HV/MV Transformers

The 3-phase power transformers in the primary substation have two windings. The primary winding is Δ -connected, while the secondary one is Y-connected. The neutral point of the secondary winding can be insulated or compensated. The “ Γ ” equivalent circuit model shown in Fig.2.4 was used to compute the parameters.

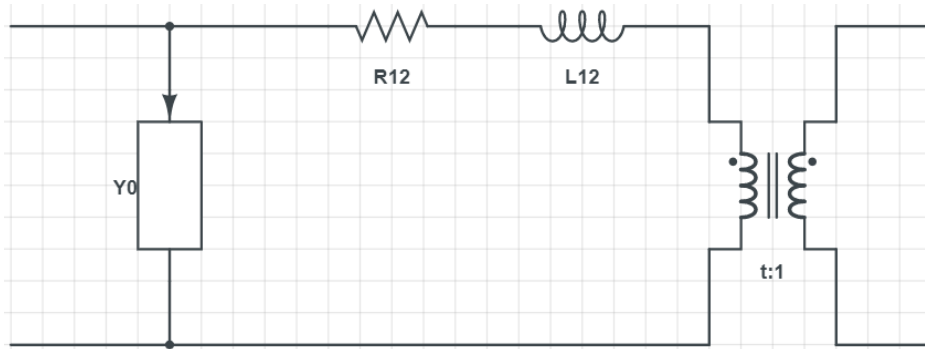


Figure 2.4: Γ equivalent circuit of the transformers

The component used for modeling the HV/MV transformers is shown in Fig.2.5.

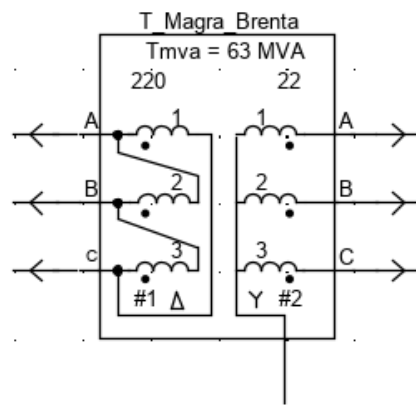


Figure 2.5: HV/MV transformer component

The parameters, required by RSCAD[®], of the HV/MV transformers were provided by Turin DSO and are shown in Tab.2.2 and 2.3.

Table 2.2: Parameters of Magra-Brenta and Chieri transformers

Parameter	Value	Meas. unit
Transformer rating	63	<i>MVA</i>
Primary winding base voltage	220	<i>kV</i>
Secondary winding base voltage	22	<i>kV</i>
Base frequency	50	<i>Hz</i>
Leakage reactance	0.1593	<i>p.u.</i>
No load losses	$6.619 \cdot 10^{-4}$	<i>p.u.</i>
Copper losses	0.0022	<i>p.u.</i>

Table 2.3: Parameters of Fiat-Grosso transformer

Parameter	Value	Meas. unit
Transformer rating	55	<i>MVA</i>
Primary winding base voltage	220	<i>kV</i>
Secondary winding base voltage	22	<i>kV</i>
Base frequency	50	<i>Hz</i>
Leakage reactance	0.1146	<i>p.u.</i>
No load losses	$6.617 \cdot 10^{-4}$	<i>p.u.</i>
Copper losses	0.0033	<i>p.u.</i>

In particular, for Fiat-Grosso transformer the On Load Tap Changer (OLTC), whose control model is described in Chap.2.2.3, was simulated.

2.2.3 On Load Tap Changer (OLTC) Control

This component is used as a step-voltage regulator to automatically adjust the tap position of the OLTC to keep the voltage at the specified set point. The measured voltage is compared to the rated one and deviation must be greater than the parameter dv for a tap operation to be considered [19]. The voltage to be compared is measured at the secondary side of the transformer by using a voltage transformer (VT). In RSCAD[®], OLTC is implemented on the primary side of the transformer. For example, when the measured voltage goes down the control system commands for a tap up operation. In order to increase the voltage on the secondary side, the voltage on primary winding is increased, while the turns ratio remains unchanged. In other words, differently than the real behaviour, in RSCAD[®] the OLTC does not modify the

turns ratio of the transformer but operates by adjusting the primary winding voltage. The change in leakage reactance due to tap setting is neglected because it is too small [20]. By selecting the *Step/Limit* mode, the step size and the upper/lower limit for the tap operations can be set. Finally, also the manual mode is included with which a tap operation can be forced through a pushbutton in *Runtime* environment. The component implemented in the digital twin for the OLTC control is shown in Fig.2.6.

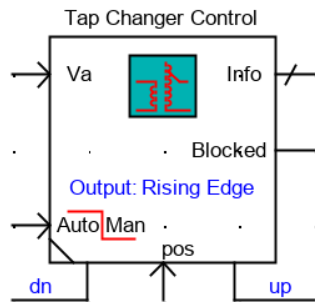


Figure 2.6: OLTC control component

The parameters, required by RSCAD[®], of the OLTC were provided by Turin DSO and are shown in Tab.2.4:

Table 2.4: Parameters of OLTC of Fiat-Grosso transformer

Parameter	Value	Meas. unit
Rated voltage	22	<i>kV</i>
Step size	0.0125	<i>p.u.</i>
Upper limit	1.1	<i>p.u.</i>
Lower limit	0.9	<i>p.u.</i>
Starting position	1	<i>p.u.</i>

It means that the OLTC has 17 positions with a regulation range of $\pm 10\%$.

2.2.4 MV/LV transformer

In the two secondary substation of the network analysed there is a MV/LV two-winding 3-phase power transformer. The primary winding of each transformer is Δ -connected, while the secondary one is Y-connected. The neutral point of the secondary winding is directly grounded. The “T” equivalent

circuit model is shown in Fig.2.4. The component used for the MV/LV transformers is shown in Fig.2.7.

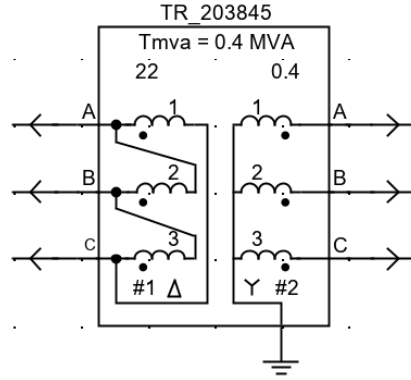


Figure 2.7: MV/LV transformer component

The parameters, required by RSCAD[®], of the MV/LV transformers were provided by Turin DSO and are shown in Tab.2.5 and 2.6.

Table 2.5: Parameters of 203845 transformer

Parameter	Value	Meas. unit
Transformer rating	400	<i>kVA</i>
Primary winding base voltage	22	<i>kV</i>
Secondary winding base voltage	0.4	<i>kV</i>
Base frequency	50	<i>Hz</i>
Leakage reactance	$3.83 \cdot 10^{-2}$	<i>p.u.</i>
No load losses	$2.3 \cdot 10^{-3}$	<i>p.u.</i>
Copper losses	$1.15 \cdot 10^{-2}$	<i>p.u.</i>

Table 2.6: Parameters of 203844 transformer

Parameter	Value	Meas. unit
Transformer rating	400	<i>kVA</i>
Primary winding base voltage	22	<i>kV</i>
Secondary winding base voltage	0.4	<i>kV</i>
Base frequency	50	<i>Hz</i>
Leakage reactance	$3.88 \cdot 10^{-2}$	<i>p.u.</i>
No load losses	$1.6 \cdot 10^{-3}$	<i>p.u.</i>
Copper losses	$9.6 \cdot 10^{-3}$	<i>p.u.</i>

2.2.5 Distribution lines

For simulating distribution lines the Π equivalent circuit was used. The most complete Π equivalent circuit for 3-phase lines is shown in Fig.2.8.

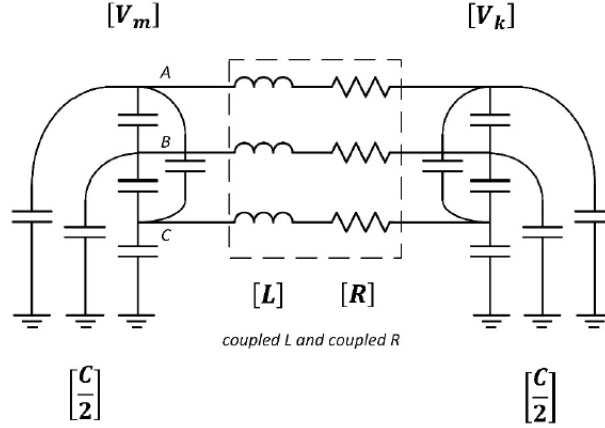


Figure 2.8: Π equivalent circuit for 3-phase lines [20]

In the figure above, V_m and V_k are the voltages of two general nodes of the electrical grid linked together by a distribution line whose electrical parameters, in matrix form, are mutual and self-resistances R , mutual and self-inductances $[L]$ and mutual and self-capacitances $[\frac{C}{2}]$ defined as follow

$$R = \begin{bmatrix} R_s & R_m & R_m \\ R_m & R_s & R_m \\ R_m & R_m & R_s \end{bmatrix} \quad L = \begin{bmatrix} L_s & L_m & L_m \\ L_m & L_s & L_m \\ L_m & L_m & L_s \end{bmatrix} \quad C = \begin{bmatrix} C_s & C_m & C_m \\ C_m & C_s & C_m \\ C_m & C_m & C_s \end{bmatrix}$$

Supposing that all the three phases of the circuit are balanced, all mutual and self-impedances are the same. So, instead of specifying the mutual and self-impedances, the input parameters required by RSCAD[®] are the zero-sequence impedance and positive-sequence one. They are linked to the self and mutual impedances according to the following relations [20]:

$$R_s = \frac{R_0 + 2R_+}{3} \quad L_s = \frac{L_0 + 2L_+}{3} \quad C_s = \frac{C_0 + 2C_+}{3}$$

$$R_m = \frac{R_0 - R_+}{3} \quad L_m = \frac{L_0 - L_+}{3} \quad C_m = \frac{C_0 - C_+}{3}$$

The components used for MV lines and LV lines are different each other, as well as their equivalent circuit. In fact, LV lines are usually very short so their shunt capacitances can be neglected.

MV lines

The component used to simulate the Π -section model of MV lines is shown in Fig.2.9.

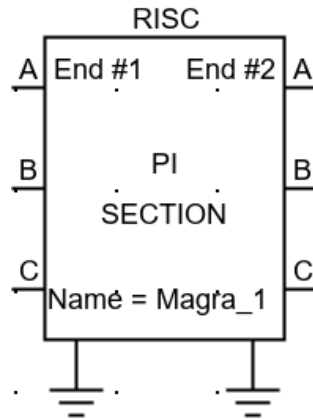


Figure 2.9: MV lines component

The parameters of all the MV lines, provided by Turin DSO, are listed in Tab.2.7.

Table 2.7: MV lines parameters

Line	$R_+ [\Omega]$	$X_{L+} [\Omega]$	$X_{C+} [M\Omega]$	$R_0 [\Omega]$	$X_{L0} [\Omega]$	$X_{C0} [M\Omega]$
Magra 1	0.0189	0.0116	0.1480	0.0284	0.0174	0.1480
Magra 2	0.5157	0.3770	0.0043	0.7736	0.5655	0.0043
Magra 3	0.1889	0.0649	0.0365	0.2833	0.0973	0.0365
Magra 4	0.4105	0.1383	0.0168	0.6157	0.2074	0.0168
Brenta 1	0.3149	0.2199	0.0070	0.4724	0.3456	0.0070
Brenta 2	0.0902	0.0428	0.0483	0.1352	0.0642	0.0483
Brenta 3	0.0404	0.0192	0.1079	0.0605	0.0287	0.1079
Brenta 4	0.0256	0.0131	0.1742	0.0385	0.0197	0.1742
Brenta 5	0.0240	0.0128	0.1686	0.0360	0.0192	0.1686
Brenta 6	0.0404	0.0192	0.1079	0.0605	0.0287	0.1079
Brenta 7	0.5296	0.2827	0.0075	0.7945	0.4398	0.0075
Brenta 8	0.0902	0.0428	0.0483	0.1352	0.0642	0.0483
Brenta 9	0.0085	0.0048	0.3763	0.0127	0.0072	0.3763
Brenta 10	0.0322	0.0159	0.1445	0.0482	0.0238	0.1445
Grosso 1	0.1440	0.1030	0.0153	0.2160	0.1545	0.0153
Grosso 2	0.1660	0.1188	0.0132	0.2490	0.1781	0.0132
Grosso 3	0.1440	0.1030	0.0153	0.2160	0.1545	0.0153

Grosso 4	0.0457	0.0324	0.0488	0.0686	0.0486	0.0488
Grosso 5	0.0364	0.0257	0.0616	0.0546	0.0385	0.0616
Grosso 6	0.0623	0.0376	0.0459	0.0934	0.0564	0.0459
Grosso 7	0.0314	0.0149	0.1388	0.0471	0.0223	0.1388
Grosso 8	0.0445	0.0216	0.0937	0.0667	0.0324	0.0937
Grosso 9	0.0217	0.0156	0.1011	0.0326	0.0233	0.1011
Grosso 10	0.0295	0.0211	0.0745	0.0443	0.0317	0.0745
Fiat 1	0.4033	0.2885	0.0055	0.6050	0.4328	0.0055
Fiat 2	0.0336	0.0240	0.0655	0.0503	0.0360	0.0655
Fiat 3	0.0514	0.0368	0.0428	0.0771	0.0552	0.0428
Fiat 4	0.0824	0.0443	0.0424	0.1235	0.0665	0.0424
Fiat 5	0.0838	0.0451	0.0417	0.1257	0.1676	0.0417
Fiat 6	0.0540	0.0307	0.0590	0.0809	0.0461	0.0590
Fiat 7	0.0526	0.0300	0.0606	0.0790	0.0449	0.0606
Fiat 8	0.0596	0.0432	0.0413	0.0894	0.0648	0.0413
Chieri 1	0.2048	0.1294	0.0130	0.6050	0.4328	0.0130
Chieri 2	0.2058	0.0977	0.0212	0.3087	0.1465	0.0212
Chieri 3	0.2968	0.2615	0.0319	0.4452	0.3923	0.0319
Chieri 4	0.0729	0.0399	0.0456	0.1094	0.0599	0.0456
Chieri 5	0.0736	0.0349	0.0592	0.1104	0.0524	0.0592
Chieri 6	0.2780	0.1319	0.0157	0.4170	0.1979	0.0157
Chieri 7	0.2074	0.0984	0.0210	0.3112	0.1477	0.0210
Chieri 8	0.2386	0.1132	0.0183	0.3579	0.1698	0.0183
Chieri 9	0.0533	0.0253	0.0816	0.0800	0.0380	0.0816
Chieri 10	0.0729	0.0399	0.0465	0.1094	0.0599	0.0465
Chieri 11	0.2058	0.0977	0.0212	0.3087	0.1465	0.0212
Chieri 12	0.2393	0.1136	0.0182	0.3590	0.1704	0.0182
Chieri 13	0.0723	0.0385	0.0492	0.1085	0.0577	0.0492
Chieri 14	0.1004	0.0365	0.0492	0.1085	0.0577	0.0492
Chieri 15	0.3776	0.2089	0.0085	0.5664	0.3133	0.0085
Chieri 16	0.3776	0.2089	0.0085	0.5664	0.3133	0.0085
Chieri 17	0.2393	0.1136	0.0182	0.3590	0.1704	0.0182
Chieri 18	0.3059	0.1777	0.0096	0.4588	0.2666	0.0096

LV lines

The component used to simulate the Π -section model of LV lines is shown in Fig.2.10. Conversely to the one shown in Fig.2.9, this component allows the user to disable capacitive shunts and to use only longitudinal parameters (resistance and inductive reactance). In fact, due to their length, shunt capacitances of the LV lines is negligible.

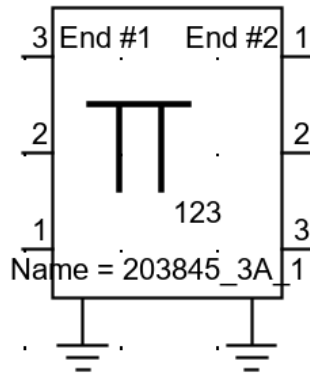


Figure 2.10: LV lines component

Basing on both the length and the cross-sectional of the lines, provided by Turin DSO, and by using cables parameters in [21], the parameters of the LV lines were retrieved and they are listed in Tab.2.8. For the cross-sectional data not available in the reference, an exponential interpolation was done.

Table 2.8: LV lines parameters

Line	R_+ [Ω]	X_{L+} [Ω]	R_0 [Ω]	X_{L0} [Ω]
203845_3A_1	0.0210	0.0124	0.0367	0.3062
203845_3A_2	0.0010	0.0004	0.0016	0.0093
203845_3A_3	0.0200	0.0079	0.0325	0.1931
203845_3D_1	0.0107	0.0042	0.0173	0.1028
203845_3E_1	0.0084	0.0033	0.0136	0.0806
203845_3E_2	0.0126	0.0050	0.0205	0.1214
203844_3A_1	0.0439	0.0172	0.0712	0.4226
203844_3B_1	0.0358	0.0140	0.0580	0.3443
203844_3C_1	0.0435	0.0171	0.0706	0.4189
203844_3C_2	0.0150	0.0011	0.0167	0.0261
203844_3C_3	0.0067	0.0026	0.0109	0.0646
203844_3C_4	0.0136	0.0053	0.0220	0.1308

203844_3C_5	0.0432	0.0031	0.0483	0.0755
203844_3C_6	0.0109	0.0022	0.0146	0.0537
203844_3C_7	0.0317	0.0063	0.0426	0.1563
203844_3C_8	0.0080	0.0031	0.0130	0.0769
203844_3C_9	0.0124	0.0025	0.0167	0.0614
203844_3C_10	0.1139	0.0257	0.1519	0.4960
203844_3C_11	0.1099	0.0248	0.1466	0.4788
203844_3C_12	0.0287	0.0057	0.0386	0.1416
203844_3C_13	0.0506	0.0036	0.0566	0.0884
203844_3C_14	0.1122	0.0253	0.1497	0.4889
203844_3C_15	0.0103	0.0011	0.0128	0.0279
203844_3C_16	0.0462	0.0051	0.0571	0.1247
203844_3C_17	0.0290	0.0032	0.0358	0.0782

2.2.6 Loads

In the simulated electrical grid there are both single-phase and three-phase loads. Per each load, the values of the active and reactive power installed were provided by the Turin DSO. However, power absorption varies according to the real value of the node voltage at which the load is connected. In order to implement a load model voltage-dependent, in this thesis the *exponential load* model was chosen. According to this, the instantaneous value of active and reactive power component is expressed by the algebraic functions below:

$$P_{set} = P_0 \cdot \left(\frac{V}{V_0}\right)^\alpha \quad (2.1)$$

$$Q_{set} = Q_0 \cdot \left(\frac{V}{V_0}\right)^\beta \quad (2.2)$$

where:

- V_0 is the rated voltage of the load;
- P_0 is the active power absorbed/supplied by the load at rated voltage;
- Q_0 is the reactive power absorbed/supplied by the load at rated voltage;
- V is the instantaneous rms value of the voltage applied to the load;
- α and β are the coefficients set based on the type of the load aggregate or individual load.

In Tab.2.9, the coefficients used for better modeling the real behaviour of the loads are provided [22].

Table 2.9: Coefficients of exponential load model [22]

Aggregate/Type	α	β
<i>Residential</i>	0.92	4.04
<i>Commercial</i>	1.51	3.4
<i>Industrial</i>	0.18	6

The components used for implementing MV and LV loads are shown in Fig.2.11.

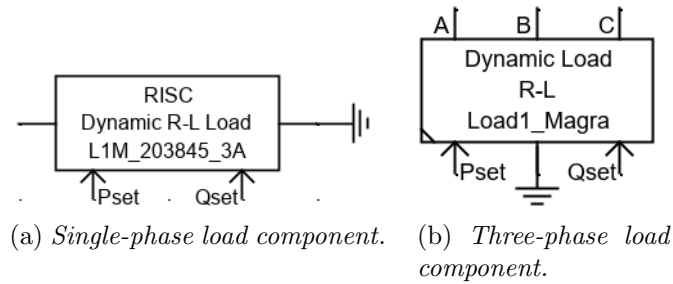


Figure 2.11: Load components

The main parameters, required by RSCAD[®], for the loads are shown in Tab.2.10:

Table 2.10: Parameters of load components

Parameter	Value	Meas. unit
Type of load	<i>RL</i>	-
Connection type	<i>Y – connection</i>	-
Rated voltage (l-l, rms, 3-ph loads)	22 or 0.4	<i>kV</i>
Rated voltage (l-g, rms, 1-ph loads)	0.23	<i>kV</i>
Base frequency	50	<i>Hz</i>
Control	<i>CC</i>	-

The last above-mentioned parameter set in *CC* mode allows to control the active and reactive power absorbed/supplied. In fact, P and Q set points of each load can be provided to the P_{set} and Q_{set} input wires and can be retrieved by using a control block scheme [20]. In order to compute the set point of active and reactive power, the control scheme in [23] was implemented in RSCAD[®] and it is shown in Fig.2.12 for an industrial load. However, differently from the reference, the section concerning the frequency dependence was not implemented.

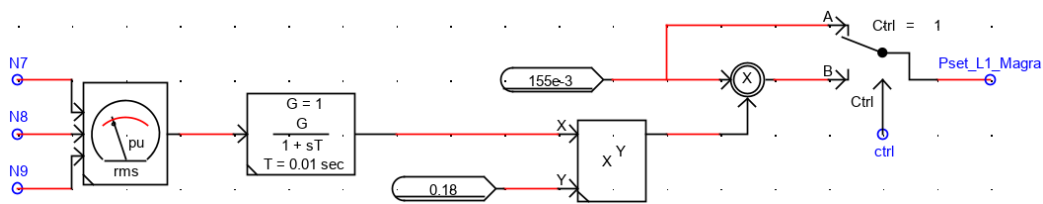


Figure 2.12: Block scheme for P and Q set point computation for an industrial load

In Tab.2.11, all the loads connected at the MV level are listed together with their main characteristics provided by the Turin DSO (load aggregates types were supposed). For all these loads, $V_0 = 22kV$. In this case, the coefficients α and β are related with the type of load aggregate.

Table 2.11: MV loads parameters

Load	P_0 [kW]	Q_0 [kvar]	Aggregate
Magra 1	310	113.6	Industrial
Magra 2	310	113.6	Industrial
Magra 3	Secondary substation 203845		
Magra 4	Secondary substation 203844		
203845_8A	501	165	Industrial
Brenta 1	1347	427	Residential
Brenta 2	638	225	Commercial
Brenta 3	256	48	Commercial
Brenta 4	181	-223.2	Residential
Brenta 5	182	111	Commercial
Brenta 6	256	48	Residential
Grosso 1	41	51	Industrial
Grosso 2	1347	427	Commercial
Grosso 3	182	111	Industrial

Grosso 4	638	225	Commercial
Grosso 5	78	7	Commercial
Grosso 6	638	225	Residential
Grosso 7	256	48	Commercial
Grosso 8	571	289	Residential
Grosso 9	638	225	Residential
Fiat 1	1347	427	Industrial
Fiat 2	1347	427	Commercial
Fiat 3	256	48	Commercial
Fiat 4	698	382	Industrial
Fiat 5	698	382	Residential
Fiat 6	638	225	Commercial
Fiat 7	78	-7	Commercial
Chieri 1	155	57	Industrial
Chieri 2	110	44	Industrial
Chieri 3	638	225	Commercial
Chieri 4	571	389	Commercial
Chieri 5	182	111	Commercial
Chieri 6	227	125	Residential
Chieri 7	155	57	Residential
Chieri 8	110	44	Residential
Chieri 9	256	48	Residential
Chieri 10	256	48	Commercial
Chieri 11	571	388	Commercial
Chieri 12	571	388	Residential
Chieri 13	181	-223	Residential
Chieri 14	256	48	Residential
Chieri 15	256	48	Residential

In Tab.2.12, all the loads connected at the LV level are listed together with their main characteristics provided by Turin DSO (load types were supposed). For single-phase loads $V_0 = 0.23kV$, while for three-phase ones $V_0 = 0.4kV$. The number of phases of the loads can be deduced by the third letter of the load name. In particular:

- **M** is for single-phase loads;
- **T** is for three-phase loads.

In this case, the coefficients α and β are related with the type of individual load.

Table 2.12: LV loads parameters

Load	P_0 [kW]	Q_0 [kvar]	Type
L1M_203845_3A	4.5	2.2	Residential
L2T_203845_3A	100	32.9	Industrial
L3T_203845_3A	35	11.5	Commercial
L4T_203845_3A	3	1.5	Residential
L5M_203845_3A	3	1.5	Residential
L6M_203845_3A	6	2.9	Residential
L7M_203845_3A	1.5	0.7	Residential
L8M_203845_3A	1.5	0.7	Residential
L9T_203845_3A	62	20.4	Industrial
L1T_203845_3D	150	49.3	Industrial
L1T_203845_3E	20	6.6	Commercial
L2T_203845_3E	53	17.4	Commercial
L3T_203845_3E	100	32.9	Industrial
L4M_203845_3E	3	1.5	Residential
L5T_203845_3E	76	25	Industrial
L6M_203845_3E	10	4.8	Residential
L7T_203845_3E	20	6.68	Commercial
L8M_203845_3E	6	2.9	Residential
L1T_203844_3A	63	20.7	Industrial
L1M_203844_3B	3	1.5	Residential
L1M_203844_3C	3	1.5	Residential
L2M_203844_3C	3	1.5	Residential
L3M_203844_3C	3	1.5	Residential
L4T_203844_3C	15	4.9	Commercial
L5M_203844_3C	3	1.5	Residential
L6T_203844_3C	6	2	Commercial
L7T_203844_3C	62.5	20.5	Industrial
L8M_203844_3C	4.5	2.2	Residential
L9M_203844_3C	3	1.5	Residential
L10M_203844_3C	3	1.5	Residential
L11M_203844_3C	1	0.5	Residential
L12M_203844_3C	3	1.5	Residential
L13M_203844_3C	3	1.5	Residential
L14M_203844_3C	3	1.5	Residential
L15M_203844_3C	3	1.5	Residential
L16M_203844_3C	3	1.5	Residential
L17M_203844_3C	3	1.5	Residential

L18M_203844_3C	1.5	0.7	Residential
L19T_203844_3C	54	17.7	Commercial
L20T_203844_3C	3	1.5	Residential
L21M_203844_3C	3	1.5	Residential
L22M_203844_3C	3	1.5	Residential
L23M_203844_3C	3	1.5	Residential
L24M_203844_3C	3	1.5	Residential
L25M_203844_3C	3	1.5	Residential
L26M_203844_3C	3	1.5	Residential
L27M_203844_3C	3	1.5	Residential
L28M_203844_3C	3	1.5	Residential

The values of power listed in Tab.2.12 are the installed power ones, that are the maximum values of power that each load can absorb. However, every load does not absorb always the maximum power. The ratio between the average power and the maximum one is called *utilization factor* [24]. Furthermore, in a LV distribution grid the various loads does not absorb the maximum power at the same time or, even more important, they are not always turned on. Consequently, a *coincidence factor* can be used to take into account the power absorbed by a group of loads [24]. In conclusion, the P_{set} and Q_{set} values computed with the exponential load model, only for the LV loads, are first multiplied by the F_u , basing on the type of load, provided in Tab.2.13 and then set as the inputs of the components shown in Fig.2.11.

Table 2.13: Average values of the utilization factor per each load type [24]

Type	F_u
<i>Residential</i>	0.35
<i>Commercial</i>	0.4
<i>Industrial</i>	0.45

2.2.7 Load Flow data

The real-time simulation software RSCAD[®] includes the possibility to run the load flow analysis. In a general bus/node k of the grid, there are four unknown variables:

- P_k : active power;
- Q_k : reactive power;

- V_k : voltage amplitude;
- δ_k : voltage angle.

At the beginning, all buses and nodes have to be characterized basing on the following classification:

- **PQ node:** P_k and Q_k assigned, V_k and δ_k to be computed;
- **PV node:** P_k and V_k assigned, Q_k and δ_k to be computed;
- **V δ or Slack node:** V_k and δ_k assigned, P_k and Q_k to be computed.

In the grid shown in Fig.2.1 the Slack node is the *BUS1*, while all other nodes are characterized as PQ node. Finally, the nominal frequency at which load flow is executed is $50Hz$, while the user-specified tolerance is $1kVA$.

2.3 RTDS[®] Simulator

In this section, the characteristics of the hardware and software used for the digital twin implementation are provided. The RealTime Digital Simulator (RTDS) is a special purpose computer designed to study electromagnetic transient phenomena in real-time [20]. RTDS[®] Simulator, by *RTDS Technologies Inc.*, is a combination of custom hardware and software that are used together to achieve real-time power system simulation, also for hardware-in-the-loop (HIL) testing of protection, control and power equipment [25] in order to validate the performance of power system devices and de-risk deployment [26].

2.3.1 Hardware

RTDS[®] hardware uses advanced parallel processing techniques in order to achieve the computation speeds required to maintain continuous realtime operation [20]. The Simulator used for this thesis is in the *Energy Center Lab* of the *Politecnico di Torino*. In the frontal part of the rack, there is the GUI of the *NovaCor* processor. In this processor, only 4 out of 10 cores were activated. In the rear part of the rack, there are 24 ports for connecting the multicore processor cards with the I/O cards through optical fiber. The ones installed in the rack in the *Energy Center Lab* are [27]:

- **GTAI/GTAO:** they are used for analog connection with external components directly at $\pm 10 V_{pk}$ or can be interfaced via power amplifiers;

- **GTDI/GTDO:** they are used for digital connection with external components directly at $5 \div 30 V_{dc}$;
- **GTFPIV2:** is used to read and write signals between the front panel and the RTDS Simulator [28];
- **GTNETx2:** it is used as interface to external equipment by using various Ethernet-based communication protocols.

The simulation software package used for digital twin implementation is installed in a server in the *Energy Center Lab* and it is remotely accessible. In Fig.2.13, the hardware components of the simulator are shown.

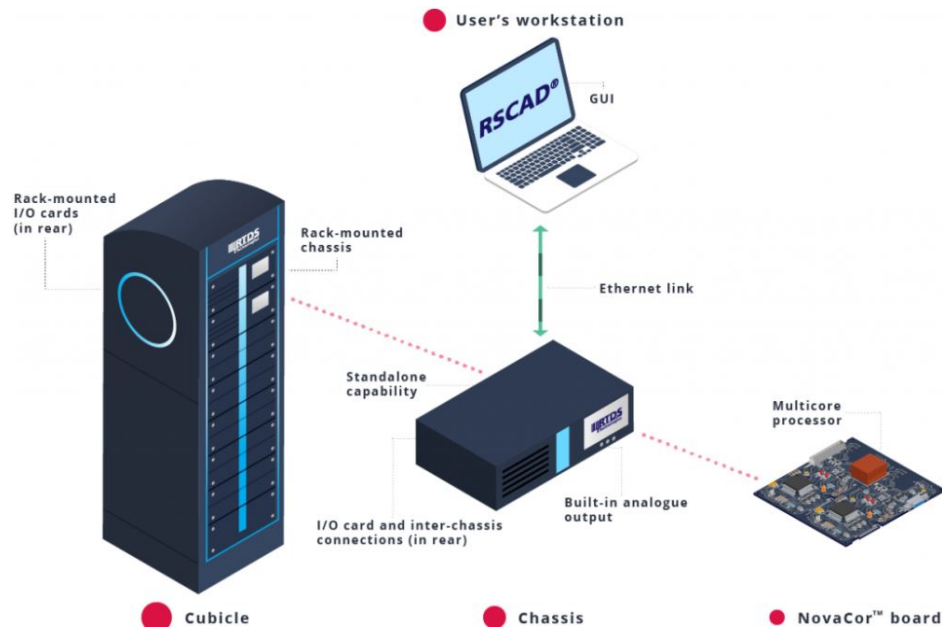


Figure 2.13: RTDS[®] Simulator hardware components [27]

Moreover, the simulator is equipped with 12-bit DAC that can be used for HIL simulation. This type of simulation involves interfacing RTDS with external devices such as motors, inverters, transformers or protection equipment. HIL simulations are normally closed-loop where the Device-Under-Test (DUT) receives signals from the simulation and provides signals back to the simulation. Basing on the type of DUT, HIL simulations can be divided into two classes [29]:

- **Control HIL (CHIL):** for physical control or protection relays testing;

- **Power HIL (PHIL):** for power devices testing.

The difference between CHIL and PHIL is in the power of the DUT and, consequently, in the interface equipment required for connection between simulator and DUT itself (amplifiers, filters and so on).

2.3.2 Software

RSCAD[®] is the proprietary simulation software package that is used to configure the simulations that are then possibly run on parallel processing hardware [25]. It runs on the user's PC and allows the implementation, the execution and the analysis of real-time simulations. It was in-house developed by *RTDS Technologies Inc.* and requires no third-party modules [30]. The power system simulated for this thesis was built by choosing the components already included in *Power System* and *Controls* libraries. The overall network solution technique employed in the RTDS[®] is based on nodal analysis. The Graphical User Interface (GUI) is included in the RSCAD[®] software package: the electrical grid is built in the *Draft* environment, while simulation results are displayed in *Runtime* one.

2.3.3 Simulation parameters

The power system simulated was built in *Distribution Mode*: even if this mode does not include the complete library of components, it allows to implement electrical grid with several hundred to over a thousand nodes [31]. In this way, the model used for the aim of this thesis will be able to be enlarged by adding new nodes and other components without computational problems. In fact, digital simulators compute the state of the networks at discrete time instants. During the time between these discrete instants, the so called "simulation time-step" (Δt), the simulator computes the power system solution. By definition, in order to operate in real time, all computations for the system solution must be completed in less than Δt . The minimum time-step allowed depends on the frequency of interest. For example, power electronic applications require very small time-steps since switching of the converters occurs at very high frequencies. Quite the opposite, in distribution network, for which it is interesting power flow due to penetration of renewable energy sources, a too small time-step is not required [20]. In *Distribution Mode*, the time-step is in the range $150 \div 200 \mu s$ [31]. In this model, the simulation time-step was fixed to $\Delta t = 150 \mu s$. In this way, being the system a radial network, the computational burden for network solution is relatively low.

Chapter 3

Comparison of results

In this chapter, the results obtained with RTDS[®] Simulator are compared with the ones obtained with OPARL-RT[®] Simulator, by *OPAL-RT TECHNOLOGIES, Inc.*. In [18], the same power system was implemented in *Simulink* environment for interfacing with OPARL-RT[®] for real-time simulation. In the following sections, the tests carried out for comparing the results are described.

3.1 Tests for comparison

For the comparison the power system in Fig.2.1 was used. In that model the secondary substation after the *Node 5* and *6* of Magra feeder was replaced by two three-phase loads with the same characteristics of load *Magra 1* in Tab.2.11. The network implemented in OPARL-RT[®] Simulator is identical. After the implementation, the comparison was done by considering two conditions:

- Normal operating conditions;
- Fault conditions.

3.1.1 Normal operating conditions

In order to compare the results obtained with the two above-mentioned Simulators, some current were taken into account. In Tab.3.1, peak values of the sinusoidal currents flowing in the branches identified by the sending and receiving buses/nodes listed below are compared.

Table 3.1: Comparison of current values in normal operating condition

Branch	I_RTDS [A]	I_OPAL-RT [A]
SRC - BUS 1	70	70
TR_MagraBrenta - BUS 2	154	158
TR_FiatGrosso - BUS 17	368	369
TR_Chieri - BUS 36	172	173
BUS 2 - NODE 3	46	47
BUS 2 - NODE 7	108	111
BUS 17 - NODE 18	172	172
BUS 17 - NODE 28	198	198

As it can be seen in the table above, the values computed with the two Simulator are almost the same.

3.1.2 Fault conditions

In order to compare the electromagnetic transients computed by the two Simulator, two types of fault in MV network are implemented. In particular:

- Three-phase fault;
- Phase-to-phase fault.

The faults are simulated in *Node 6*, at the end of Magra feeder (see Fig.2.1). The phase-to-phase fault resistance is fixed to 0.001Ω .

Three-phase fault

It is a symmetrical fault. The following variables are evaluated (see Fig.2.1):

- RMS value of line-to-line voltages in *BUS 2*;
- RMS value of line-to-line voltages in *Node 6*;
- Peak value of current in the branch between *BUS 2* and *Node 3*.

In Tab.3.2, the value of the above-mentioned variables is provided by comparing pre-fault and fault conditions results obtained with RTDS[®] Simulator.

Table 3.2: Three-phase fault values obtained with RTDS[®]

Condition	I_{23} [kA]	V_2 [kV]	V_6 [kV]
Pre-fault	0.047	21.94	21.91
Fault	8.31	13.01	≈ 0

In Fig.3.1, the electromagnetic transients for three-phase fault computed with RTDS[®] and OPARL-RT[®] are compared by plotting the phase voltages on *BUS 2* and the phase currents between *BUS 2* and *Node 3*.

The *b-phase* component of the above-mentioned variables are plotted in Fig.3.2 by putting on the same graph the results obtained with both RTDS[®] and OPARL-RT[®].

In Tab.3.3, the peak values of the variables plotted in Fig.3.2 are compared after fault instant ($t = 0.15s$).

Table 3.3: Peak values of *b-phase* component of voltage and current after the three-phase fault

Simulator	\hat{V}_b [kV]	\hat{I}_b [kA]
RTDS [®]	11.5	8.3
OPARL-RT [®]	12.4	9.5

Phase-to-phase fault

It is an asymmetric fault. A fault between *b-phase* and *c-phase* is simulated. The following variables are evaluated:

- RMS value of phase voltages in *BUS 2*;
- RMS value of line-to-line voltages in *Node 6*;
- Peak value of current in the branch between *BUS 2* and *Node 3*.

Since fault asymmetry, in Tab.3.4 the value of the above-mentioned variables is provided per each phase by comparing pre-fault and fault conditions results obtained with RTDS[®] Simulator.

Table 3.4: Phase-to-phase fault values obtained with RTDS[®]

Condition	I_{23a} [kA]	I_{23b} [kA]	I_{23c} [kA]	V_{2a} [kV]	V_{2b} [kV]	V_{2c} [kV]	V_{6a} [kV]	V_{6b} [kV]	V_{6c} [kV]
Pre-fault	0.046	0.046	0.046	12.67	12.67	12.67	12.65	12.65	12.65
Fault	0.056	7.21	7.21	12.70	11.09	6.48	12.68	6.34	6.34

As can be demonstrated by using the *method of symmetrical components*, the absolute value of the ratio between three-phase fault current and phase-to-phase one is equal to:

$$\left| \frac{\bar{I}_{2ph}}{\bar{I}_{3ph}} \right| = \frac{\sqrt{3}}{2} \approx 0.866 \quad (3.1)$$

Analysing the results obtained with RTDS[®] Simulator, it can be computed:

$$\left| \frac{\bar{I}_{2ph}}{\bar{I}_{3ph}} \right| = \frac{7.21}{8.31} \approx 0.868 \quad (3.2)$$

This is a way to verify the accuracy of the results.

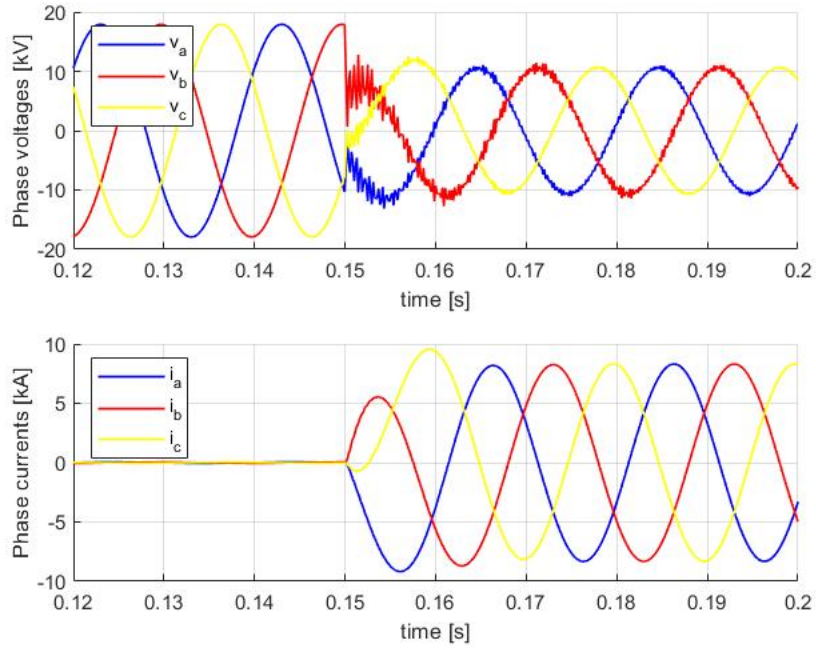
In conclusion, in Fig.3.3, the electromagnetic transient for phase-to-phase fault computed with RTDS[®] and OPARL-RT[®] are compared.

The *b-phase* and *c-phase* components of the above-mentioned variables are plotted in Fig.3.4 by putting on the same graph the results obtained with both RTDS[®] and OPARL-RT[®].

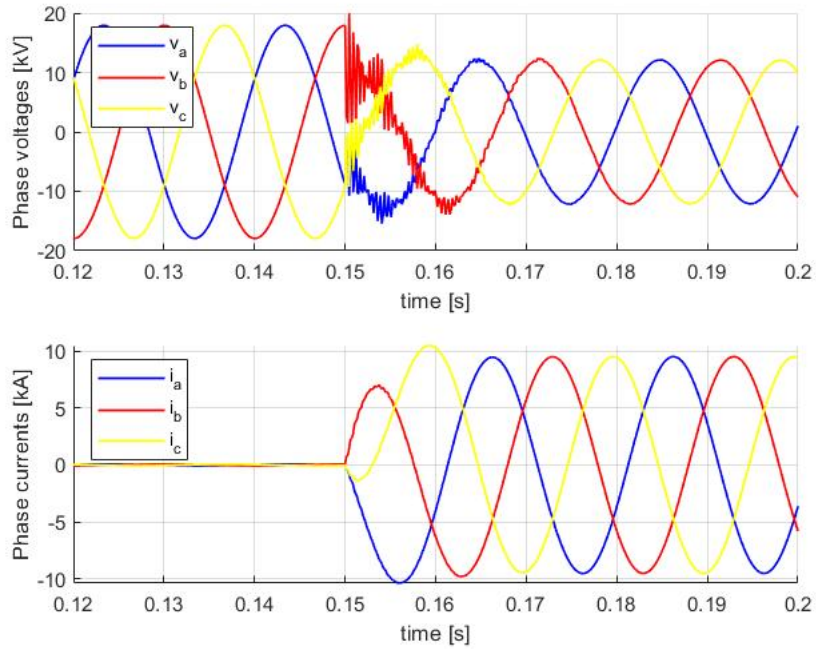
In Tab.3.5, the peak values of the variables plotted in Fig.3.4 are compared after fault instant.

Table 3.5: Peak values of *b-phase* and *c-phase* components of voltage and current after the phase-to-phase fault

Simulator	\hat{V}_b [kV]	\hat{I}_b [kA]	\hat{V}_c [kV]	\hat{I}_c [kA]
RTDS [®]	16	7.2	9.5	7.9
OPARL-RT [®]	16.4	8.3	10.6	8.8

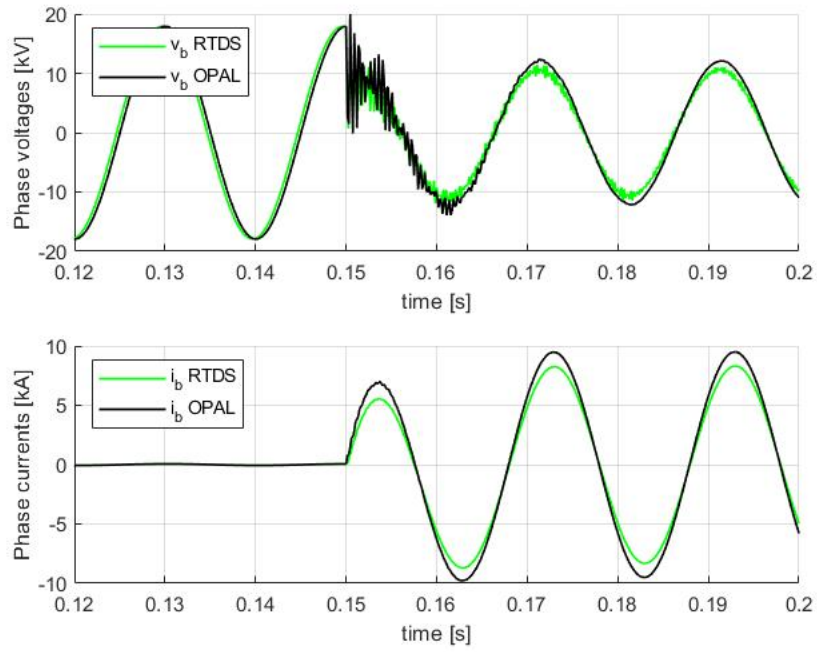


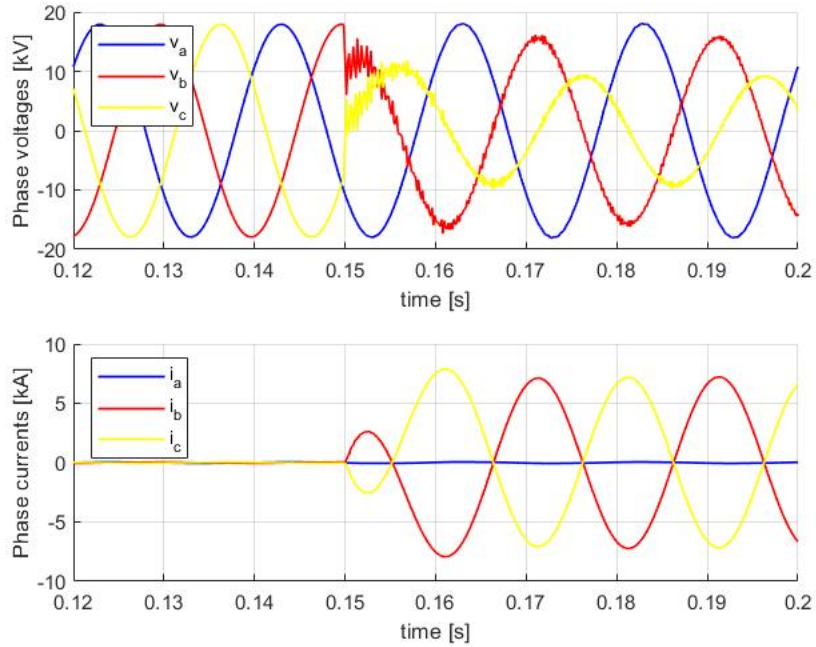
(a) Three-phase fault transient by RTDS[®]



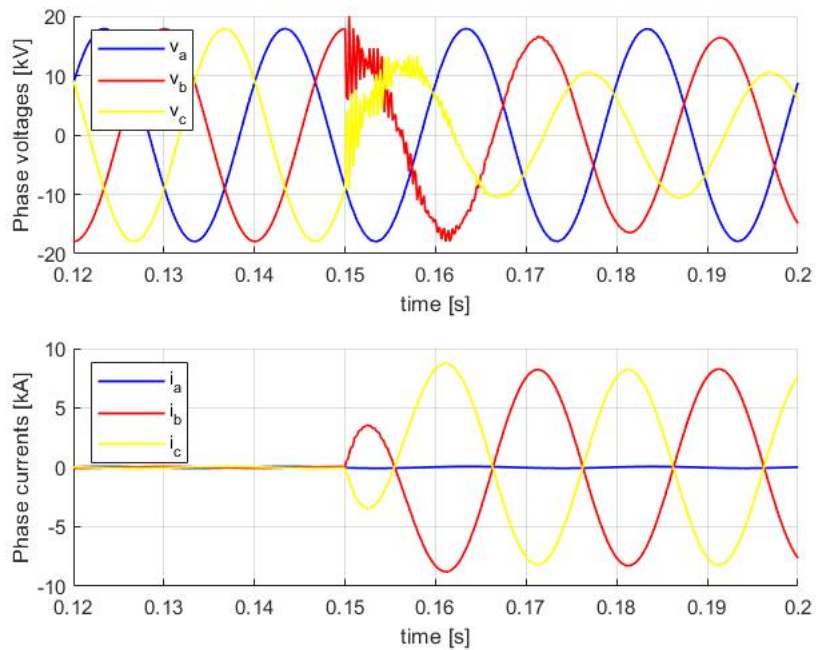
(b) Three-phase fault transient by OPAL-RT[®]

Figure 3.1: Three-phase fault comparison

Figure 3.2: Comparison of *b-phase* transient

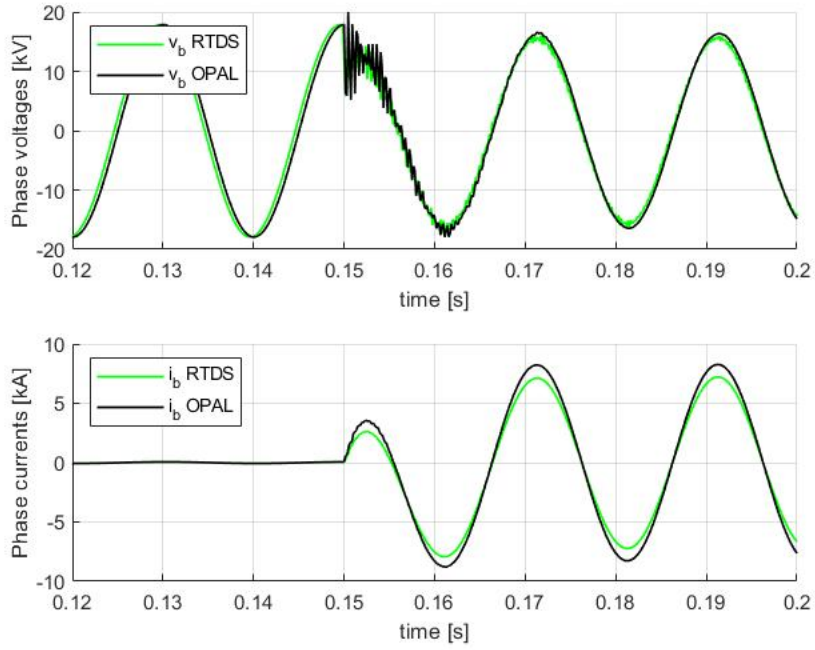


(a) Phase-to-phase fault transient by RTDS®

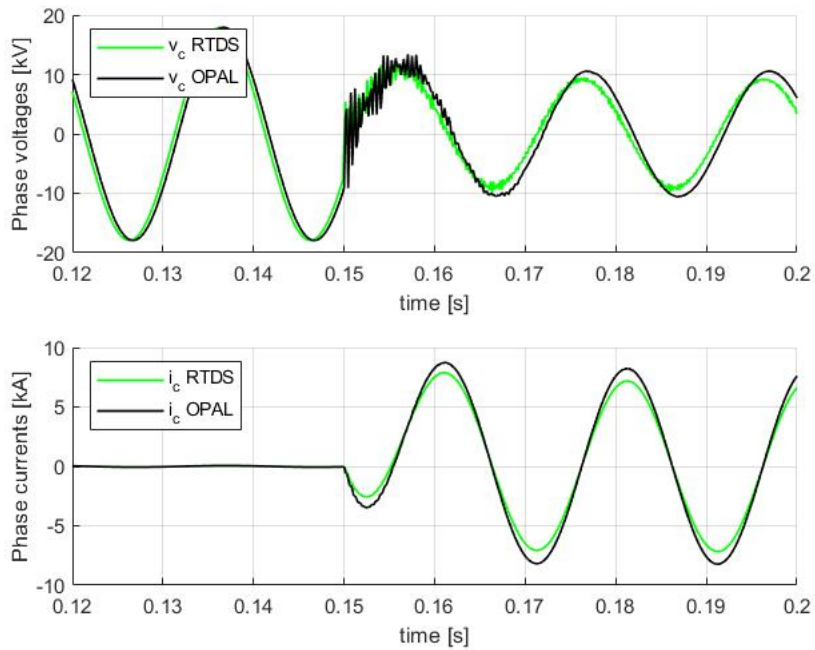


(b) Phase-to-phase fault transient by OPAL-RT®

Figure 3.3: Phase-to-phase fault comparison



(a) Comparison of b-phase transient



(b) Comparison of c-phase transient

Figure 3.4: Phase-to-phase fault comparison

Chapter 4

Automated protection system

In this chapter, all the components and the control systems used to simulate the behaviour of the protection systems will be described. Firstly, a brief theoretical reminder about the protection system in primary and secondary substation will be done, including the settings of the relays. After that, the models used to implement both the circuit breakers and the fuses will be described. Finally, the block schemes built for emulating the electronic relays functionalities will be explained by using the flow chart of the control logic.

4.1 Primary substation protection systems

Stura primary substation is owned by the DSO that manages the electrical distribution grid in Turin. In this case, the protection of the transformers is carried out by means of both maximum phase current relays, installed in the HV and MV stalls of the machines, and homopolar maximum voltage relays installed on the MV busbars [32]. Moreover, each MV feeder is equipped with both maximum phase current and earth-directional relays. The protection system was implemented only for Magra-Brenta Transformer and its MV feeders of the digital twin. The circuit breakers simulated in HV/MV substation are shown in Fig.4.1. As it can be seen, there is not a circuit breaker for HV lines that supply Stura primary substation because they were replaced by their Thévenin equivalent circuit.

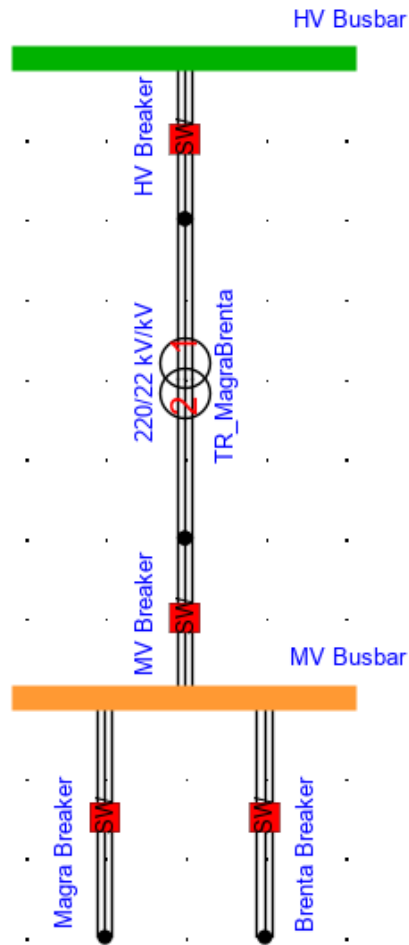


Figure 4.1: Protection devices implemented in Stura primary substation for Magra-Brenta transformer and feeders

In order to compute the values of the thresholds of both HV and MV breakers, according to the guidelines provided in [32], the following HV/MV transformer parameters were first computed:

- Primary winding nominal current:

$$I_{1n} = \frac{S_n}{\sqrt{3} \cdot V_{1n}} = \frac{63 \cdot 10^6}{\sqrt{3} \cdot 220000} = 165A; \quad (4.1)$$

- Secondary winding nominal current:

$$I_{2n} = \frac{S_n}{\sqrt{3} \cdot V_{2n}} = \frac{63 \cdot 10^6}{\sqrt{3} \cdot 22000} = 1653A; \quad (4.2)$$

- Secondary side nominal rms phase-to-earth voltage:

$$V_{2n,ph} = \frac{V_{2n}}{\sqrt{3}} = \frac{22000}{\sqrt{3}} = 12.7kV; \quad (4.3)$$

- Three times the maximum homopolar voltage due to a phase-to-earth fault:

$$3V_{0,max} = |v_a + v_b + v_c|_{max} = 53.9kV. \quad (4.4)$$

In the following sections, the various relays installed in the circuit breakers will be presented.

4.1.1 HV Breaker

For the HV circuit breaker, an overcurrent protection with two independent time tripping thresholds is required [33]. It is against short circuits of any type on the HV side of the transformers. As it can be seen in Fig.4.2, this protection function is operated by relays 50/51T: the first thresholds is delayed while the second one is instantaneous. The setting are better specified in Tab.4.1.

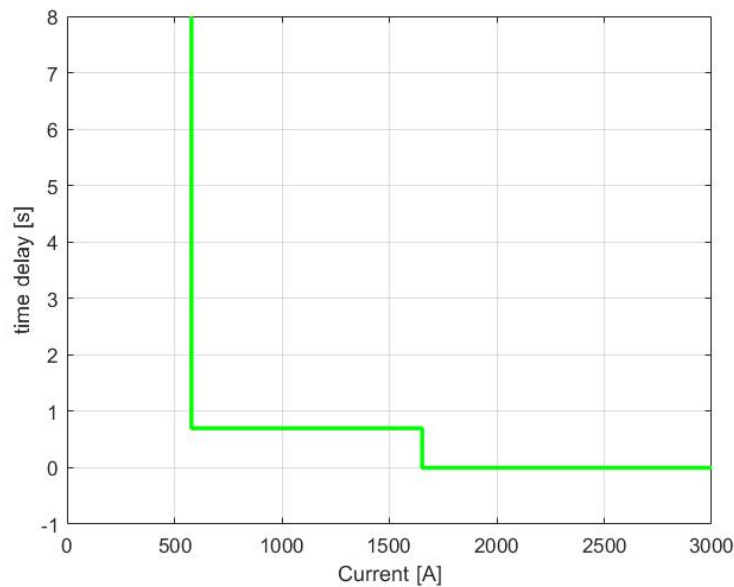


Figure 4.2: Time-Current 50/51T HV relays characteristic

Table 4.1: 50/51T HV relays setting

Threshold	Current [A]	Delay [s]	Tripping
51T	$3.5I_{1n} = 579$	0.7	HV & MV breaker
50T	$10I_{1n} = 1653$	0	HV & MV breaker

4.1.2 MV Breaker

For the MV circuit breaker, the following protections are required:

- Overcurrent protection: **51T**;
- Overvoltage protection on MV busbars: **59**;
- Homopolar overvoltage protection on MV busbars: **59N**.

The relays used are described in the following sections.

Overcurrent protection

For the MV circuit breaker, an overcurrent protection with one independent time tripping threshold is required [33]. It is against multiphase short circuits on both the MV side of the transformers and the MV busbars. Furthermore, these relays perform the backup protection function for multiphase short circuits on MV feeders. As suggested in [32], two thresholds can be also implemented. As it can be seen in Fig.4.3, this protection function is operated by relay 51T with two delayed thresholds. The settings are better specified in Tab.4.2.

Table 4.2: 51T MV relay setting

Threshold	Current [A]	Delay [s]	Tripping
51T.S1	$1.4I_{2n} = 2315$	1.5	HV & MV breaker
51T.S2	$3I_{2n} = 4960$	0.5	HV & MV breaker

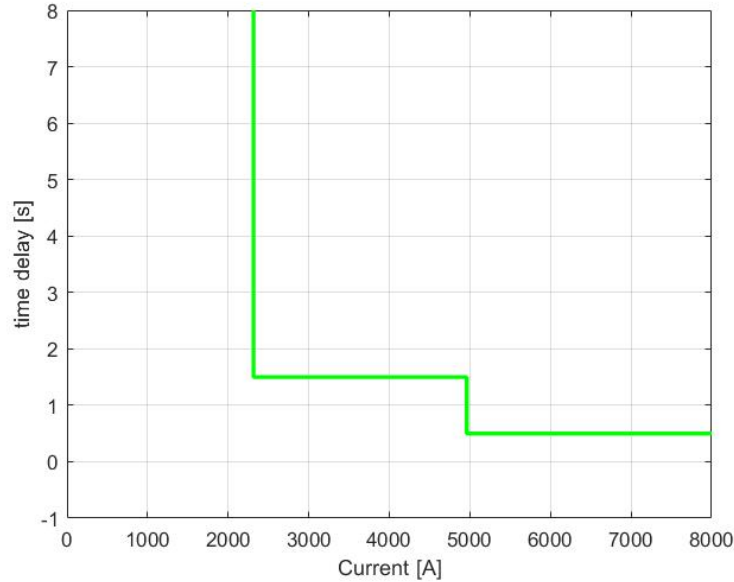


Figure 4.3: Time-Current 51T MV relay characteristic

Overvoltage protection on MV busbars

For the MV circuit breaker, an overvoltage protection on MV busbars with two independent time tripping thresholds is required. The relay 59 operates this protection function with two delayed thresholds. However, in the digital twin only the second one was implemented because the OLTC of Magra-Brenta Transformer is not simulated. Relay settings are provided in Tab.4.3.

Table 4.3: 59 MV relay setting

Threshold	Voltage [kV]	Delay [s]	Tripping
59.S1	$1.15V_{2n,ph} = 14.6$	10	OLTC block
59.S2	$1.2V_{2n,ph} = 15.2$	60	MV breaker

Homopolar overvoltage protection on MV busbars

For the MV circuit breaker, a homopolar overvoltage protection on MV busbars with one independent time tripping threshold is required. It is against earth faults on both the MV side of the transformers and the MV busbars. Moreover, it works as backup protection in case of the earth-directional relays in the MV feeders fail. The relay 59N operates this protection function with one delayed threshold. Relay settings are provided in Tab.4.4.

Table 4.4: 59N MV relay setting

Threshold	Voltage [kV]	Delay [s]	Tripping
59N	$8\% \cdot 3V_0 = 3$	40	HV & MV breaker

4.1.3 Magra and Brenta breaker

These are the circuit breakers before the two MV feeders of the same name. Each one must be equipped with the following protections [34]:

- Overcurrent protection: **50/51**;
- Earth-directional protection: **67N**.

The relays used are described in the following sections.

Overcurrent protection

For the MV feeders circuit breaker, an overcurrent protection with three independent time tripping thresholds is required. It is against overloads and multiphase short circuits on the MV line. As it can be seen in Fig.4.4, relays 50/51 operates this protection function with three thresholds: the first two are delayed while the last one is instantaneous. The settings are better specified in Tab.4.5.

Table 4.5: 50/51 MV relay settings [34]

Threshold	Current [A]	Delay [s]	Tripping
51.S1	400	2	MV feeder breaker
51.S2	1200	0.4	MV feeder breaker
50	2000	0	MV feeder breaker

As it can be seen in Fig.4.5, the selectivity between the HV and MV transformer circuit breakers and MV feeders ones is guaranteed, by time and current grading, up to a high value of current.

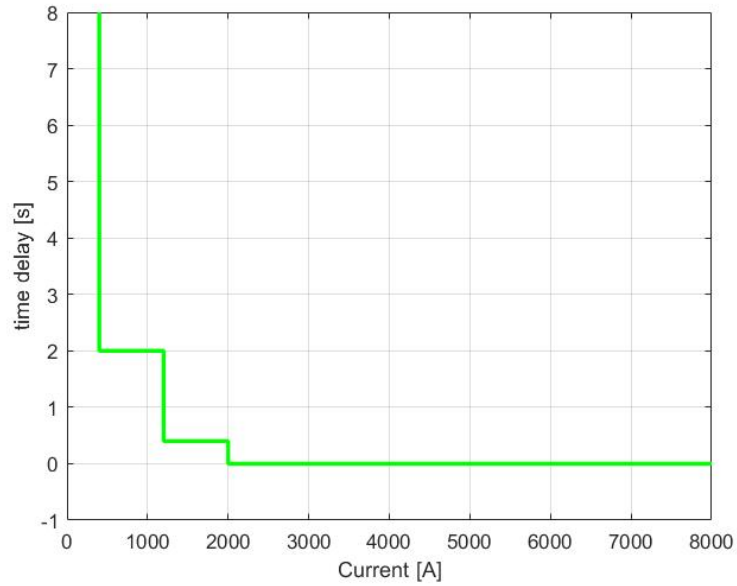


Figure 4.4: Time-Current 50/51 MV relay characteristic

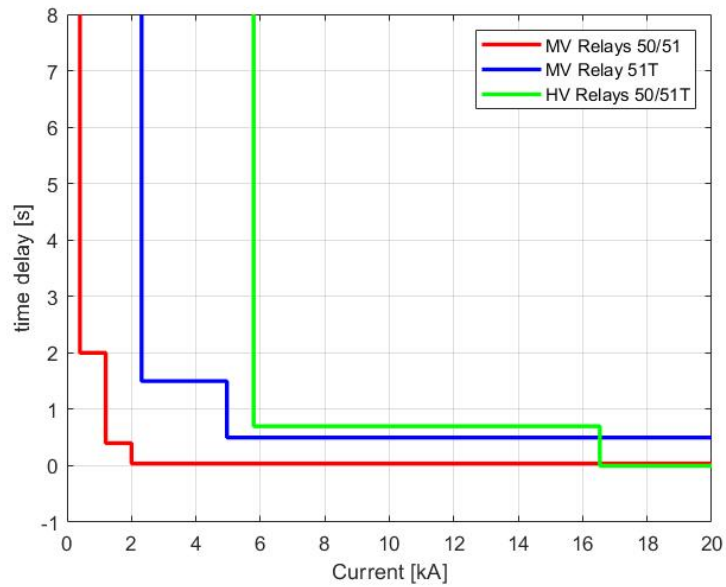


Figure 4.5: Time-Current characteristics of 51T and 50/51 MV relays and 50/51T HV relays

Earth-directional protection

For the MV feeders circuit breaker, an earth-directional protection, reactive power sensitive, with five independent time thresholds is required. It is against phase-to-earth fault and detects what feeder, among the ones connected to the same MV busbar, is faulty. The relay $67N$ operates this protection function by avoiding the tripping of the relay $59N$ installed in MV busbar that operates on HV and MV breakers and whose potential action would determine the lack of supply for all the MV feeders connected to the MV busbar, also for the healthy ones, due to the opening of the transformer circuit breakers [34]. Relay settings are provided in Tab.4.6. As it can be seen in the table below, the measured parameters useful for relay functionalities are:

- I_0 : homopolar current amplitude at the beginning of the MV feeder;
- V_0 : homopolar voltage amplitude of the MV busbar at which the MV feeder is connected;
- $\widehat{V_0 I_0}$: phase angle difference between the phasors of the two above-mentioned parameters.

Table 4.6: $67N$ MV relay settings [34]

Threshold	I_0 [A]	V_0 [V]	$\widehat{V_0 I_0}$ [°]	Delay [s]	Tripping
$67N.S1$	2.5	1143	$61 \div 157$	2	MV feeder breaker
$67N.S2a$	2.5	315	$60 \div 120$	0.4	MV feeder breaker
$67N.S2b$	200	1143	$10 \div 190$	0.6	MV feeder breaker
$67N.S3$	200	1143	$190 \div 370$	0.4	MV feeder breaker
$67N.S4$	-	1143	-	22	MV feeder breaker
$67N.S5$	-	1143	-	43.5	MV feeder breaker

The threshold $67N.S1$ is against single-phase-to-earth faults when the MV neutral point in primary substation is compensated, while the thresholds $67N.S2a$ and $67N.S2b$ are, respectively, against single-phase-to-earth faults and two-phase-to-earth ones when the MV neutral point in primary substation is insulated [35]. The last two threshold are a backup protection for avoiding the opening of the HV and MV transformer circuit breakers tripped by relay $59N$ [34]. Obviously, the settings in Tab.4.6 are effective for the grid configuration in [34]. Probably the DSO could have modified the thresholds according to the network reconfiguration and changes.

4.2 Secondary substation protection systems

In the digital twin implemented, only two secondary substations were simulated. They are managed by DSO and connected to *Node 5* (Substation 203845) and *Node 6* (Substation 203844). In each substation there is one MV/LV transformer. In this case, the protection of the transformer is carried out with a switch disconnecter equipped with fuses. Per each feeder departing from the LV busbar a circuit breaker equipped with an electronic relay is implemented. They are against any type of fault on LV feeders. The protection equipment simulated was implemented only for secondary substation 203845 and it is shown in Fig.4.6.

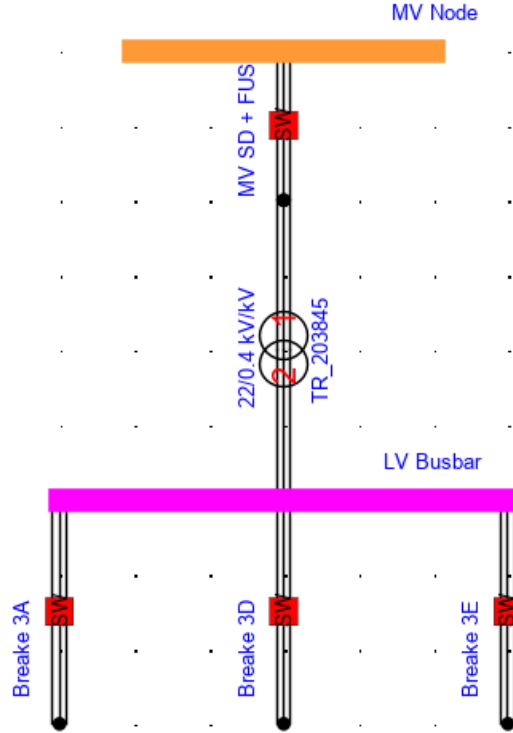


Figure 4.6: Protection devices implemented in secondary substation 203845

In order to set the protections, the following MV/LV transformers parameters were first computed:

- Primary winding nominal current:

$$I_{1n} = \frac{S_n}{\sqrt{3} \cdot V_{1n}} = \frac{400 \cdot 10^3}{\sqrt{3} \cdot 22000} = 10.5A; \quad (4.5)$$

- Secondary winding nominal current:

$$I_{2n} = \frac{S_n}{\sqrt{3} \cdot V_{2n}} = \frac{400 \cdot 10^3}{\sqrt{3} \cdot 400} = 577A; \quad (4.6)$$

In the following sections, the relay installed in the circuit breakers and the fuses will be described.

4.2.1 MV Switch Disconnecter and Fuses

For the protection of the transformer, a switch disconnecter and fuses are required. Basing on the primary winding nominal current of the transformer, the nominal current of the fuses was set to 10A. The component chosen is shown in Chap.4.4.2. The total time required by the fuses to interrupt the fault current can be computed basing on the time-current characteristic shown in Fig.4.7.

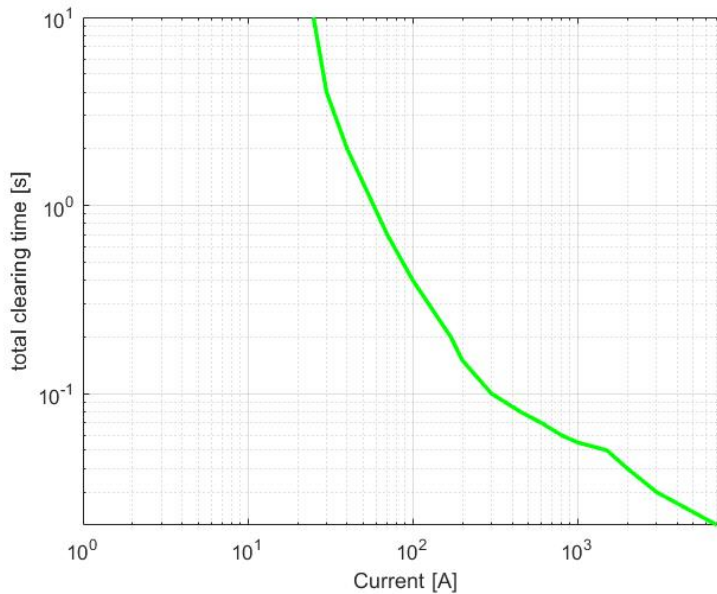


Figure 4.7: Total clearing time-current characteristic of the MV fuses with $I_n = 10A$

In Fig.4.8, the time-current characteristics of both relays 50/51 of MV breaker and MV fuses are plotted on the same logarithmic axes graph in order to prove that selectivity is guaranteed.

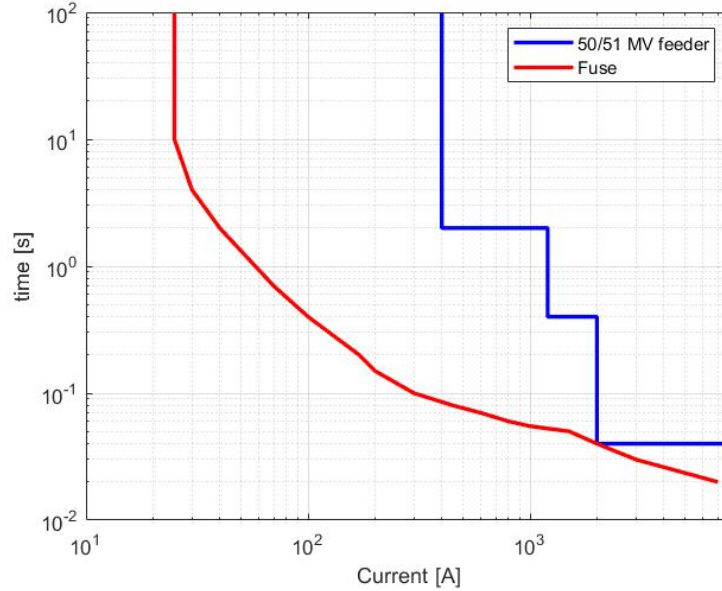


Figure 4.8: Selectivity among secondary substation protections and MV feeders breakers

Finally, when three-phase MV/LV transformers are put into service the initial value of the magnetic flux is very high. As a consequence, the initial magnetizing current, called *Inrush* current, is much higher than the nominal one [24]:

$$\hat{I}_{inrush} = (8 \div 15) \cdot I_{1n} \quad (4.7)$$

For this reason, the MV protection device, fuses in this case, must sustain the inrush current phenomenon without tripping. In order to compute the values of the primary winding current during the electromagnetic transient, the following equation was used [36]:

$$i_{inrush}(t) = \frac{k_i \cdot I_{1n}}{\sqrt{2}} \cdot e^{\left(-\frac{t}{\tau_{inrush}}\right)} \quad (4.8)$$

The parameters to be replaced in the equation above, relating oil transformers with nominal power equal to $400kVA$ like the ones installed in the secondary substations simulated, are provided in Tab.4.7.

Table 4.7: Parameters for inrush current computation [36]

Parameter	Value
k_i	12
τ_{inrush}	0.25s

In Fig.4.9, the inrush current is plotted together with MV fuse time-current characteristic. As it can be seen, the MV protection of the transformer allows the start-up of the machine without tripping.

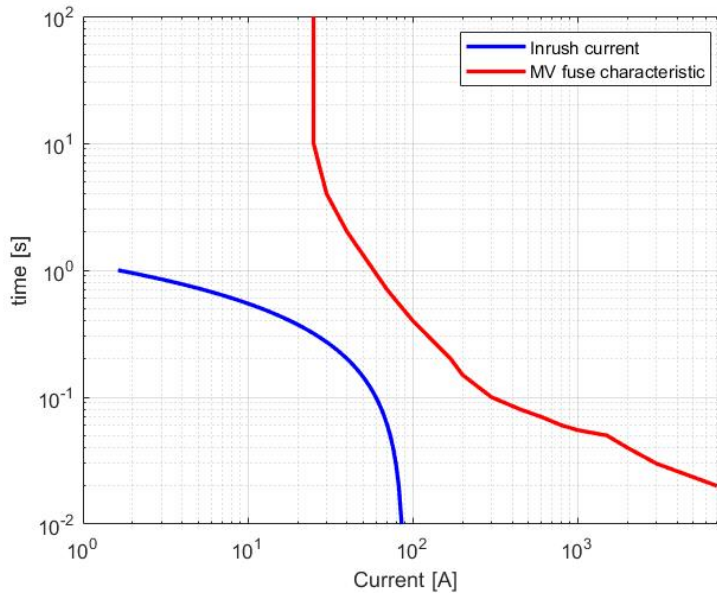


Figure 4.9: Inrush current phenomenon of MV/LV transformer

4.2.2 Breaker 3A, 3D and 3E

These are the LV feeders circuit breakers and they are against overloads and short circuits on LV lines. They are equipped with an electronic relay with three thresholds for overcurrent protection. For the implementation of the model and the settings, the selection of *Ekip Touch* relays in [37], suitable for distribution grid, were taken as reference. The LV lines are made up of copper underground in pipe cables. In Tab.4.8, the current carrying capacity of each LV lines after secondary substation 203845 are provided, basing on the catalogue [38].

Table 4.8: Cross-sectional area and current carrying capacity of LV lines after secondary substation 203845, data from [38]

Line	Cross-sect. area [mm²]	Curr. carrying cap. [A]
203845_3A_1	$3 \times 150 + 95N$	311
203845_3D_1	$3 \times 95 + 50N$	249
203845_3E_1	$3 \times 150 + 95N$	311

Basing on both the data in table above and standard CEI 64-8, in Tab.4.9 the sizing of the LV feeders circuit breakers are provided.

Table 4.9: Nominal current of LV feeders circuit breakers

Circuit breaker	Nominal current [A]
Breaker 3A	250
Breaker 3D	160
Breaker 3E	250

Once known the nominal current, the thresholds of the relay can be set basing on the formalism in Tab.4.10. Moreover, the upper and lower limit characteristic are shown in Fig.4.10.

According to the formalism in Tab.4.10, the settings chosen for the LV feeders relays are specified in Tab.4.11 and 4.12. The relay signal produce the tripping of the circuit breaker on which it is installed.

Table 4.10: Formalism for *Ekip Touch* relay settings [37]

Threshold	Current [A]	Time [s]	Delay [s]
49	$I_1 = (0.4 \div 1)I_n$	$t_1 = 3 \div 144$	$t_d = \frac{9t_1}{(1.2I_n/I_1)^2}$
50TD	$I_2 = (0.6 \div 10)I_n$	$t_2 = 0.05 \div 0.8$	$t_d = t_2$
50	$I_3 = (1.3 \div 15)I_n$	-	$t_d \leq 0.03$

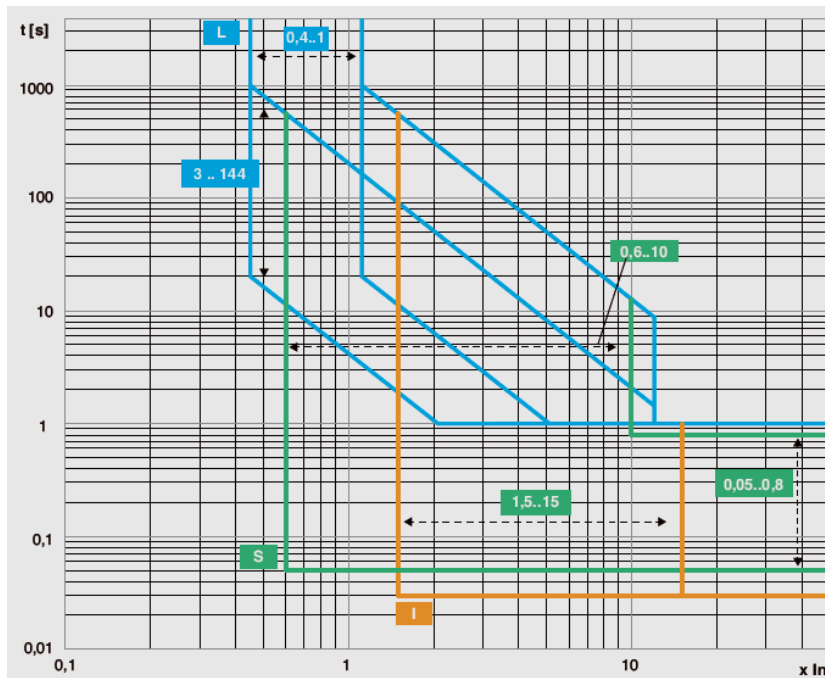


Figure 4.10: *Ekip Touch* relay set up ranges [37]

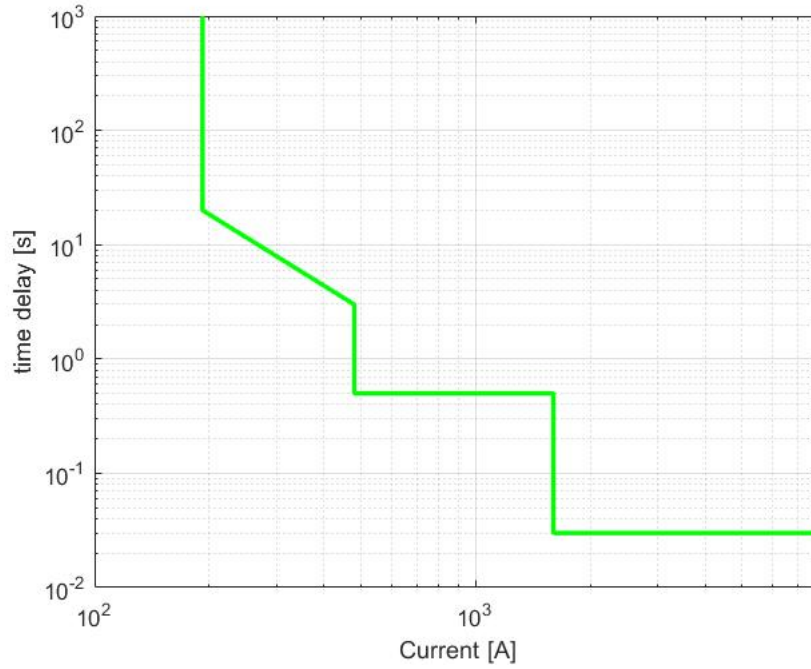
Table 4.11: Settings of 49/50/51 LV relays with $I_n = 160A$

Threshold	Current [A]	Delay [s]
49	$I_1 = I_n = 160$	$t_1 = 3$
50TD	$I_2 = 3I_n = 480$	$t_2 = 0.5$
50	$I_3 = 10I_n = 1600$	-

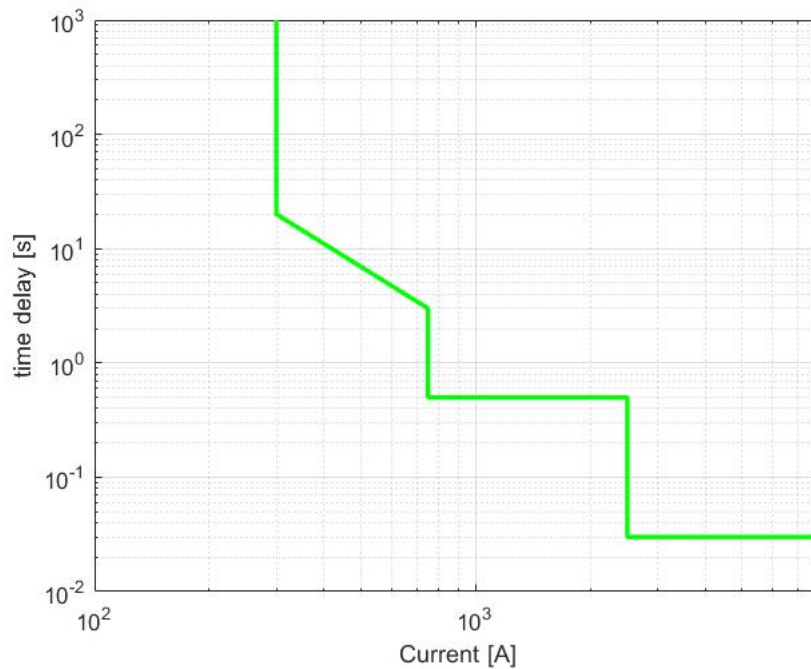
Table 4.12: Settings of 49/50/51 LV relays with $I_n = 250A$

Threshold	Current [A]	Delay [s]
49	$I_1 = I_n = 250$	$t_1 = 3$
50TD	$I_2 = 3I_n = 750$	$t_2 = 0.5$
50	$I_3 = 10I_n = 2500$	-

With the above-mentioned settings, the consequent time-current characteristics of the LV relays are shown in Fig.4.11.



(a) LV relay with $I_n = 160A$.



(b) LV relay with $I_n = 250A$.

Figure 4.11: Time-current characteristic of LV feeders relays

4.3 Low voltage cable protection system

In Tab.4.8, the cross-sectional areas of the first feeder segments after the secondary substation 203845 are provided. However, along the LV lines these cross-sectional area of the cables change. In particular, the data provided by the Turin DSO for the second segment of the LV lines are shown in Tab.4.13 together with the related current capacity [38].

Table 4.13: Cross-sectional area and current carrying capacity of the second segment of LV lines after secondary substation 203845, data from [38]

Line	Cross-sect. area [mm^2]	Curr. carrying cap. [A]
203845_3A_2	$3 \times 95 + 50N$	249
203845_3E_2	$3 \times 95 + 50N$	249

Due to the change of cross-sectional area, the cables in the table above can not be always protected with the circuit breaker at the beginning of the LV feeder. For this reason, LV fuses were implemented in the digital twin. In compliance with the standard CEI 64-8, fuses with a nominal current of $I_n = 200A$ were chosen. In particular, the fuse *NH2GG40V200-1* in [39] is a gG fuse suitable for cables protection. In Fig.4.12, the time-current characteristic of this fuse is shown.

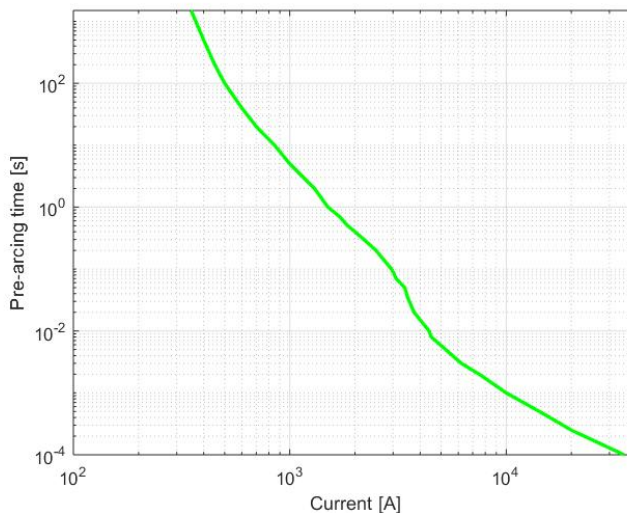


Figure 4.12: *NH2GG40V200-1* time-current characteristic

4.4 Protection devices models

In the following sections, the model of the components used to implement circuit breakers, switch disconnectors and fuses and the control logics used to simulate time-current characteristics will be described.

4.4.1 Circuit breaker, switch disconnector and LV fuses

Circuit breaker is a mechanical switching device capable of establishing, carrying and interrupting currents both in normal operating circuit conditions and in fault ones. Switch disconnector is a mechanical switching device capable of establishing, carrying and interrupting currents in normal operating circuit conditions. For this reason, switch disconnectors must be protected against short circuit currents, for example by means of fuses, but they can sustain fault effects without getting damaged [40]. Fuse is a protection device that interrupts overcurrents that melt the thin conductor wire inside the chassis of the component.

Unfortunately, RSCAD[®] library does not include the model for LV fuses. So in the digital twin circuit breakers, switch disconnectors and LV fuses are implemented by using the same component shown in Fig.4.13.

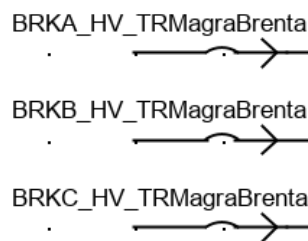


Figure 4.13: Circuit breakers, switch disconnectors and LV fuses component

The difference among circuit breakers, switch disconnectors and fuses models is in their control: the first and the last one are automated, in other words their trip is controlled by a control logic that simulates the real behaviour. The second one, instead, is manually controlled by means of *Switch* in *Runtime* environment in RSCAD[®]. The main parameters of the components are provided in Tab.4.14.

Table 4.14: Parameters circuit breakers, switch disconnectors and LV fuses component

Parameter	Value	Meas. unit
Phase closed resistance	10^{-9}	Ω
Extinguish Arc for $\text{abs}(I)$ at or below	0	A

The last parameter is a current value. This is compared with the absolute value of the current that is flowing in the component when an open command is given. If the absolute value is below this threshold, current will be interrupted. Since the grid is an inductive circuit, this threshold was set to 0 [20].

4.4.2 MV Fuses

The component already included in RSCAD[®] library is suitable for MV level and it is shown in Fig.4.14.



Figure 4.14: MV fuses component

The *Power System* library includes fuses with five different rated currents. The total clearing time-current characteristics of the fuse, on varying of rated current, are provided in Fig.4.15. The main parameters, required by RSCAD[®], are provided in Tab.4.15.

Table 4.15: Parameters of MV fuses for MV/LV transformer protection

Parameter	Value	Meas. unit
Rated Current	10	A
Base frequency	50	Hz
Fuse ON resistance	0.001	Ω

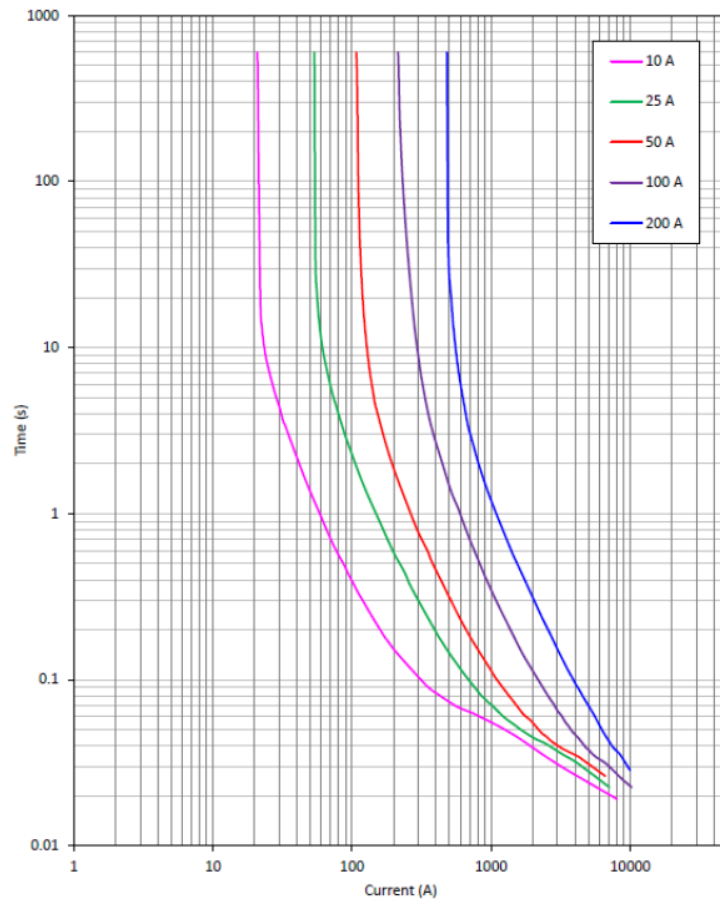


Figure 4.15: Total clearing time-current characteristics of the MV fuses models

4.5 Control logic of the relays

In this section, the control logics implemented for relays modeling is described by using flow charts. While, the block schemes built in RSCAD[®] for controlling circuit breakers are shown in the Appendix A.

4.5.1 HV breaker relays

In the HV breaker in Fig.4.1 relays 50/51T are installed. In order to simulate the time-current characteristic of these relays, a block scheme based on the flow chart shown in Fig.4.16 was implemented and repeated three times (one per each phase). The initialized variables are:

- **Ia_rms**: rms value of *a-phase* current of the circuit breaker;
- **t_d=0**: the delay time of the relay is initially set to 0;
- **50/51T_A**: it is the relay signal that commands the tripping of the phase a of the circuit breaker.

At any given time, Ia_rms is compared with the thresholds set (see Tab.4.1). So there are two options:

- **threshold values are exceeded**: according to the the fault current value I_f , there are two cases which both involve the tripping of HV and MV breakers in Fig.4.1:
 - $579A < I_f < 1653A$ (threshold 51): the output of the *If-Else* block in the green square is *YES*. At the beginning, $t_d = 0$ and the output of the *If-Else* block in the red square is *NO*. Until the fault goes on, t_d is increased of $150\mu s$ per each simulation time-step. Once $t_d > 0.7s$, the output of the *If-Else* block in the red square changes to *YES*. A 0 signal is sent to the *AND* gate and, consequently, its output is equal to 0. In this way, the output of the *If-Else* block in the yellow square is *YES* and the variable $50/51T_A = 0$. It entails the tripping of the above-mentioned breakers after $\approx 0.7s$
 - $I_f > 1653A$ (threshold 50): the output of the *If-Else* block in the blue square is *YES*. A 0 signal is sent to the *AND* gate and, consequently, its output is equal to 0. In this way, the output of the *If-Else* block in the yellow square is *YES* and the variable $50/51T_A = 0$. It entails the tripping of the above-mentioned breakers almost instantaneously;

- threshold values **are not exceeded**: there is not fault, so the two input signals of the *AND* gate are both 1. It means that the output of the same gate is 1 and, consequently, the output of the *If-Else* block in the yellow square is *NO*. In this case, the variable $50/51T_A = 1$ and HV and MV breakers remain closed.

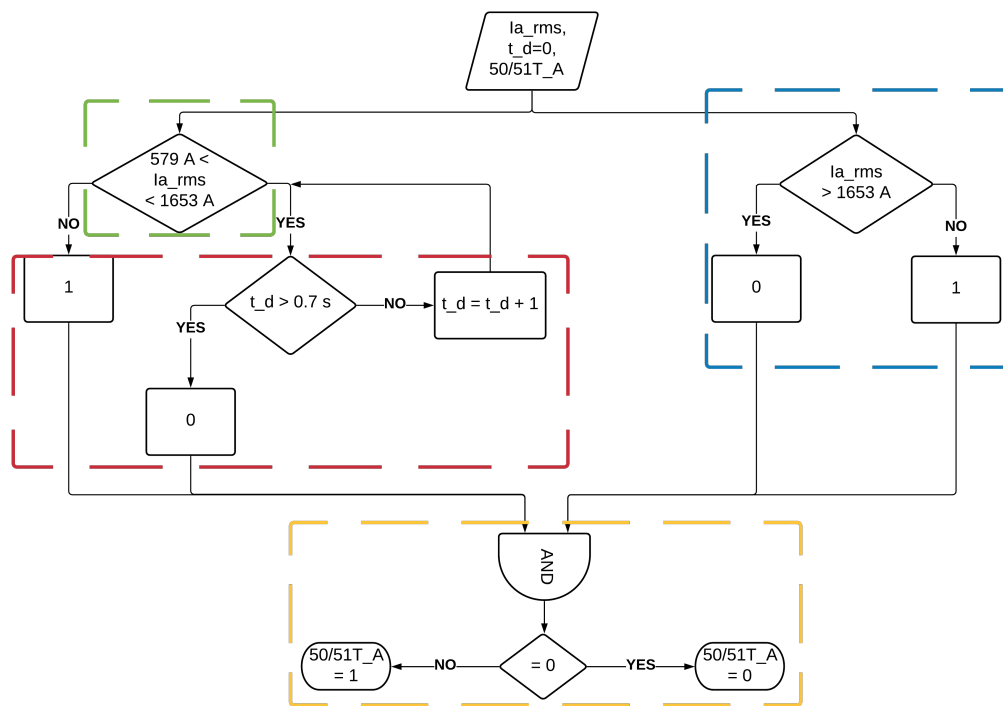


Figure 4.16: Flow chart of the *a-phase* control logic of relays 50/51T

Due to the circuit breaker is triple polar, the possible trip of one phase will also cause the trip of the other two, without time delay. This function is implemented by using another *AND* gate whose inputs are the three variables $50/51T_A$, $50/51T_B$ and $50/51T_C$ (one per each phase) and whose output is the signal that control the trip of the circuit breaker. If at least one of the input signal is equal to 0, the output will be 0 as well and the three poles of the breaker will be tripped at the same time. For conciseness, this last *AND* gate is not represented.

In Fig.4.17, the block scheme implemented in RSCAD[®] for simulating the control logic explained before is shown. The painted square are used to indicate the logic function executed by the block with respect to the flow chart in Fig.4.16.

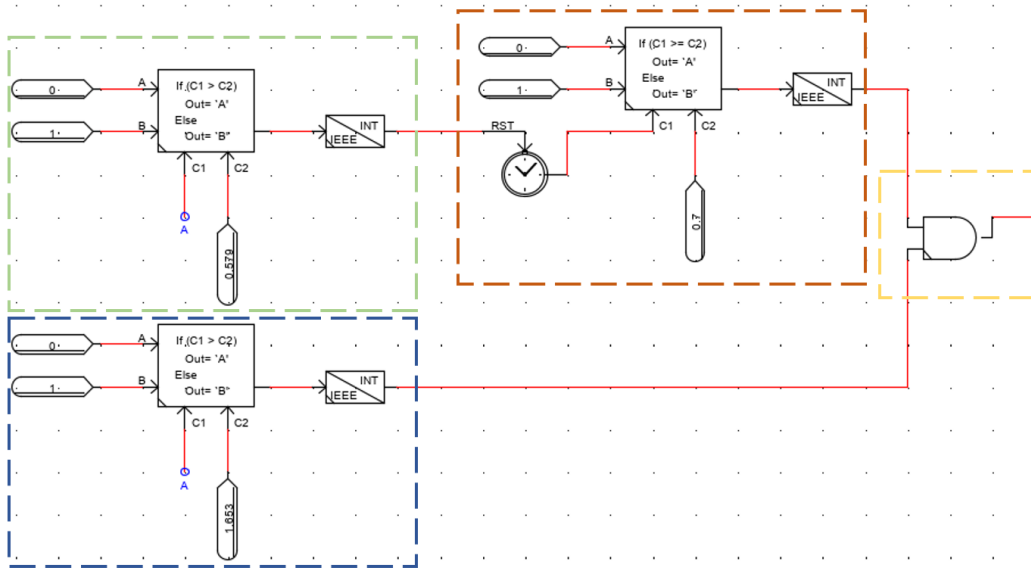


Figure 4.17: Block scheme implemented of the *a-phase* control logic of relays 50/51T

4.5.2 MV breaker relays

The MV breaker in Fig.4.1 is equipped with relays 51T, 59 and 59N.

In the next sections the control logic of these relays will be described by using flow charts. The signal of one of these relays, involves the tripping of the HV and MV circuit breakers shown in Fig.4.1.

Relay 51T

The flow chart of this relay relating to one phase of the circuit breaker is almost equal to the one shown in Fig.4.16 and it is shown in Fig.4.18. The variables initialized are of the same type, the differences lie in both threshold values and time delay. Again, due to the triple polarity of the breaker, the contemporary opening of the three phases is obtained by implementing another *AND* gate whose inputs are the three variables *51T_A*, *51T_B* and *51T_C* (one per each phase) and whose output is the signal that control the trip of the circuit breaker.

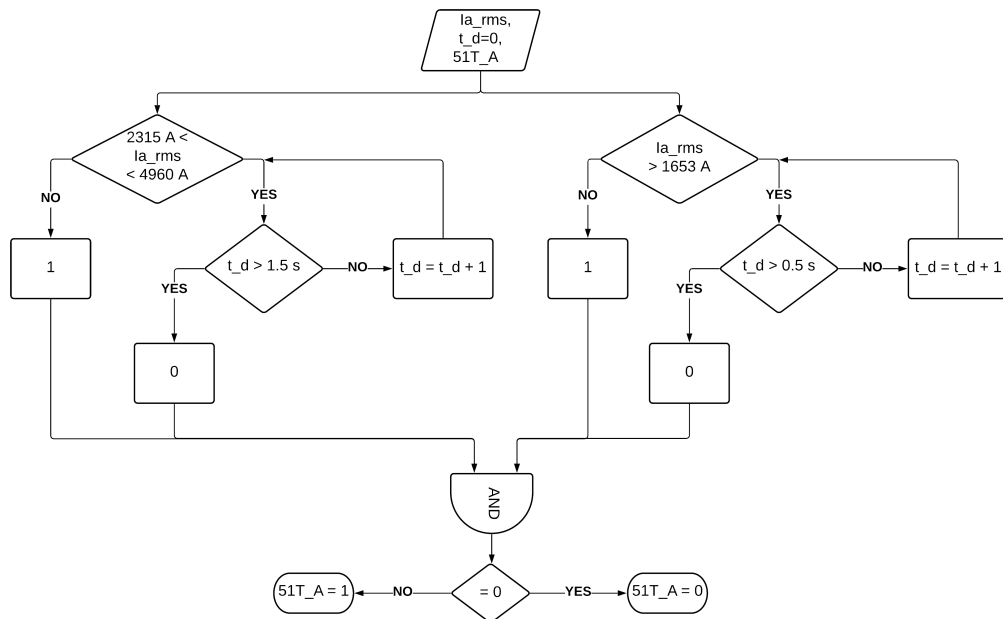


Figure 4.18: Flow chart of the *a-phase* control logic of relays 51T

Relay 59

For this relay, only the threshold 59.S2 was simulated (see Tab.4.3). As a consequence, the flow chart of *a-phase* is simpler than the previous ones because, per each rms value of the phase voltage of MV busbar, an *If-Else* condition was implemented with a time delay of 60s. The principle of operation is the same of the one described in Chap.4.5.1. Now, the variable measured **Va_rms** is the rms value of the *a-phase* voltage of the circuit breaker. Same as before, due to the triple polarity of the breaker, the contemporary opening of the three phases is obtained by implementing another *AND* gate whose inputs are the three variables *59_A*, *59_B* and *59_C* (one per each phase) and whose output is the signal that control the trip of the circuit breaker.

Relay 59N

The flow chart of this relay is the simplest one (shown in Fig.4.20), as well as its block scheme, because it has only one threshold and it is based on the measure of **3V0_rms** that is three times the rms value of the homopolar component of the MV busbar voltage.

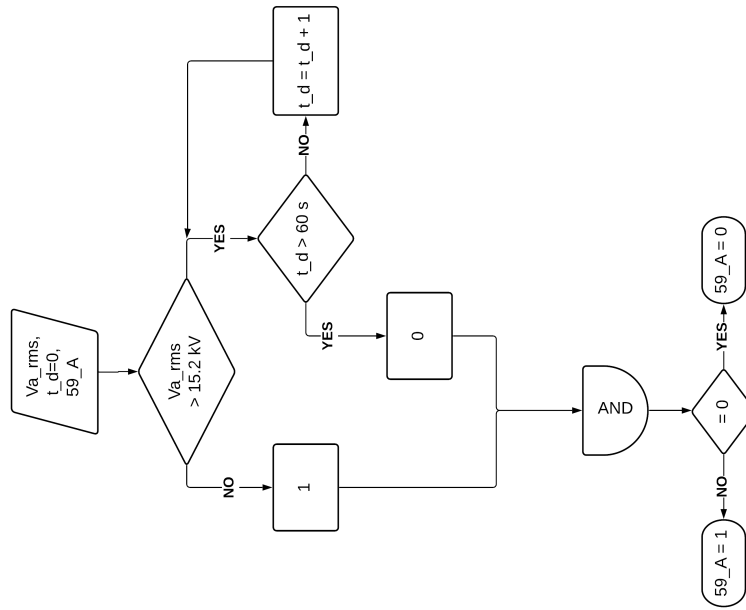


Figure 4.19: Flow chart of the *a*-phase control logic of relays 59

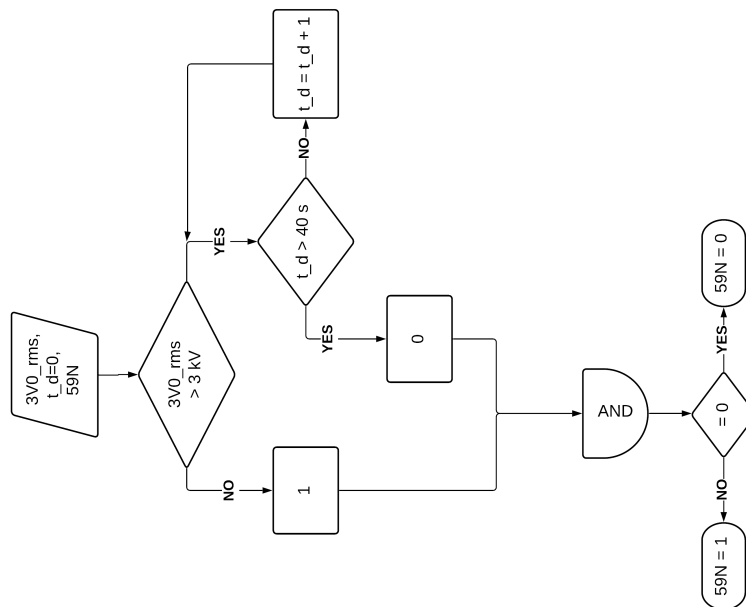


Figure 4.20: Flow chart of the control logic of relays 59N

4.5.3 Magra and Brenta breaker relays

The MV feeders circuit breakers are equipped with the relays 50/51 and 67N. In the following sections, the flow charts of the control logic of the above-mentioned relays will be provided.

Relays 50/51

The control logic implemented for these relays is equal to the other over-current relays simulated for the other circuit breakers of the grid as well as the principle of operation of the block scheme. In this case, there are three thresholds: two of which are time delayed and the last one is instantaneous (see Tab.4.5). The flow chart of the *a-phase* is shown in Fig.4.21. Once again, due to the triple polarity of the breaker, the contemporary opening of the three phases is obtained by implementing another *AND* gate whose inputs are the three variables *50/51_A*, *50/51_B* and *50/51_C* (one per each phase) and whose output is the signal that control the trip of the circuit breaker.

Relay 67N

This relay is quite different from the other ones analysed before because it requires many variables to be measured. The flow chart of the first threshold (see Tab.4.6) is shown in Fig.4.22. The variables initialized are

- **|I0|**: homopolar current amplitude at the beginning of the MV feeder;
- **|V0|**: homopolar voltage amplitude of the MV busbar at which the MV feeder is connected;
- **ang(V0,I0)**: phase angle difference between the phasors of the two above-mentioned variables;
- **FAULT**: simulation variable that indicates if there is a fault or not;
- **t_d=0**: the delay time of the relay is initially set to 0;
- **67N.S1**: relay signal for first threshold alarm.

As it can be seen in Fig.4.22, there are four conditions to be satisfied in order to have a circuit breaker opening. From left to right:

1. the first *If-Else* block verifies the condition relating to the amplitude of the homopolar current;
2. the second *If-Else* block verifies the condition relating to the amplitude of the homopolar voltage;
3. the third *If-Else* block verifies the condition relating to the phase angle between homopolar current and homopolar voltage phasors;
4. the fourth *If-Else* block is used in order to enable the check of the first three above-mentioned conditions only when there is a fault.

When these conditions are satisfied all at the same time, the inputs of the *OR* gate are all equal to 0, as well as its output. Once $t_d > 2s$, the variable $67N.S1 = 0$ and the MV feeder circuit breaker is opened. As it can be seen in Tab.4.6, there are six thresholds to be simulated. However, the flow chart of the first four thresholds are equal to the one shown in Fig.4.22. The control logic of the last two ones, instead, is shown in Fig.4.23. In this case, only one condition, the one regarding the homopolar voltage, must be verified, so the flow chart is simpler.

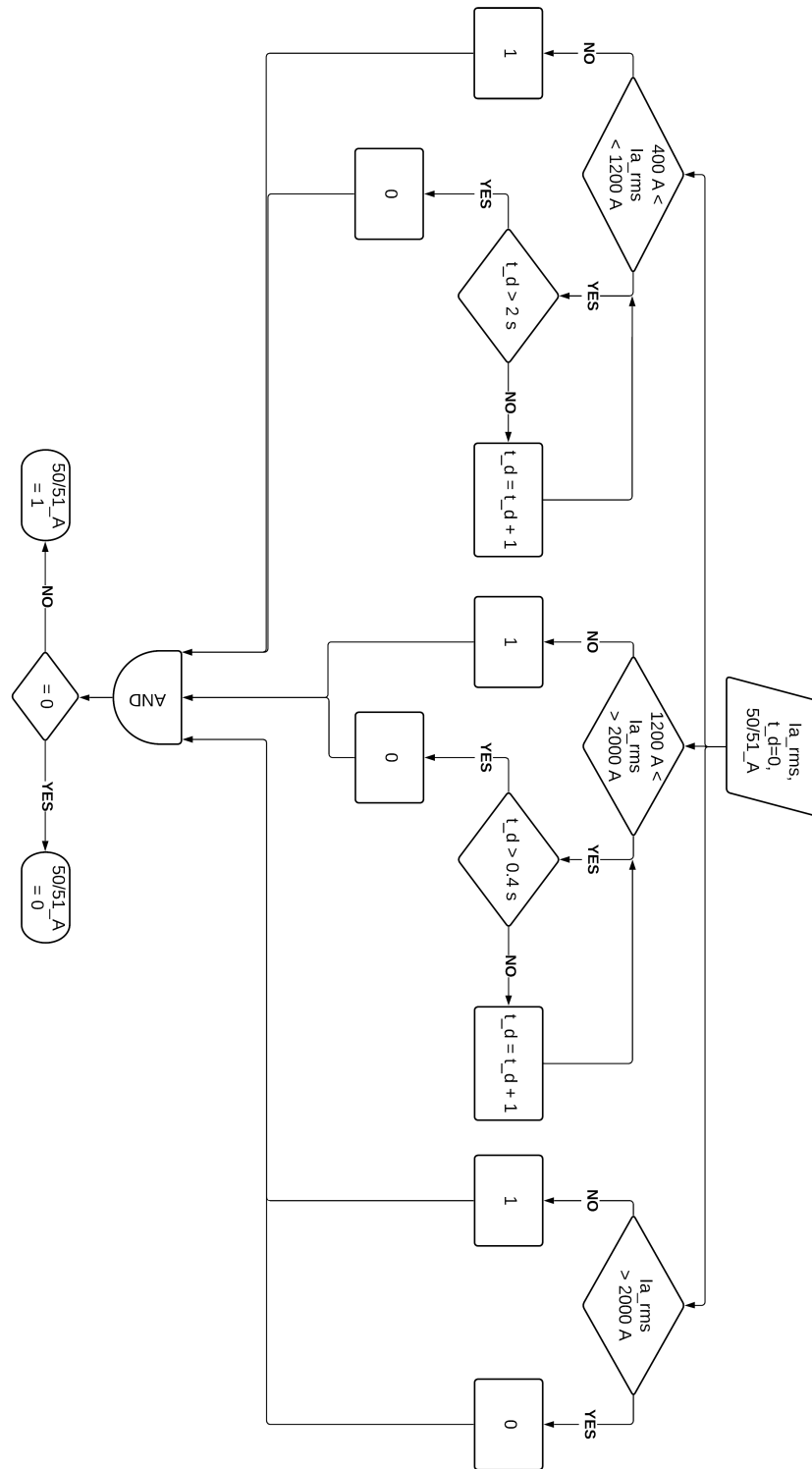


Figure 4.21: Flow chart of the *a-phase* control logic of relays 50/51

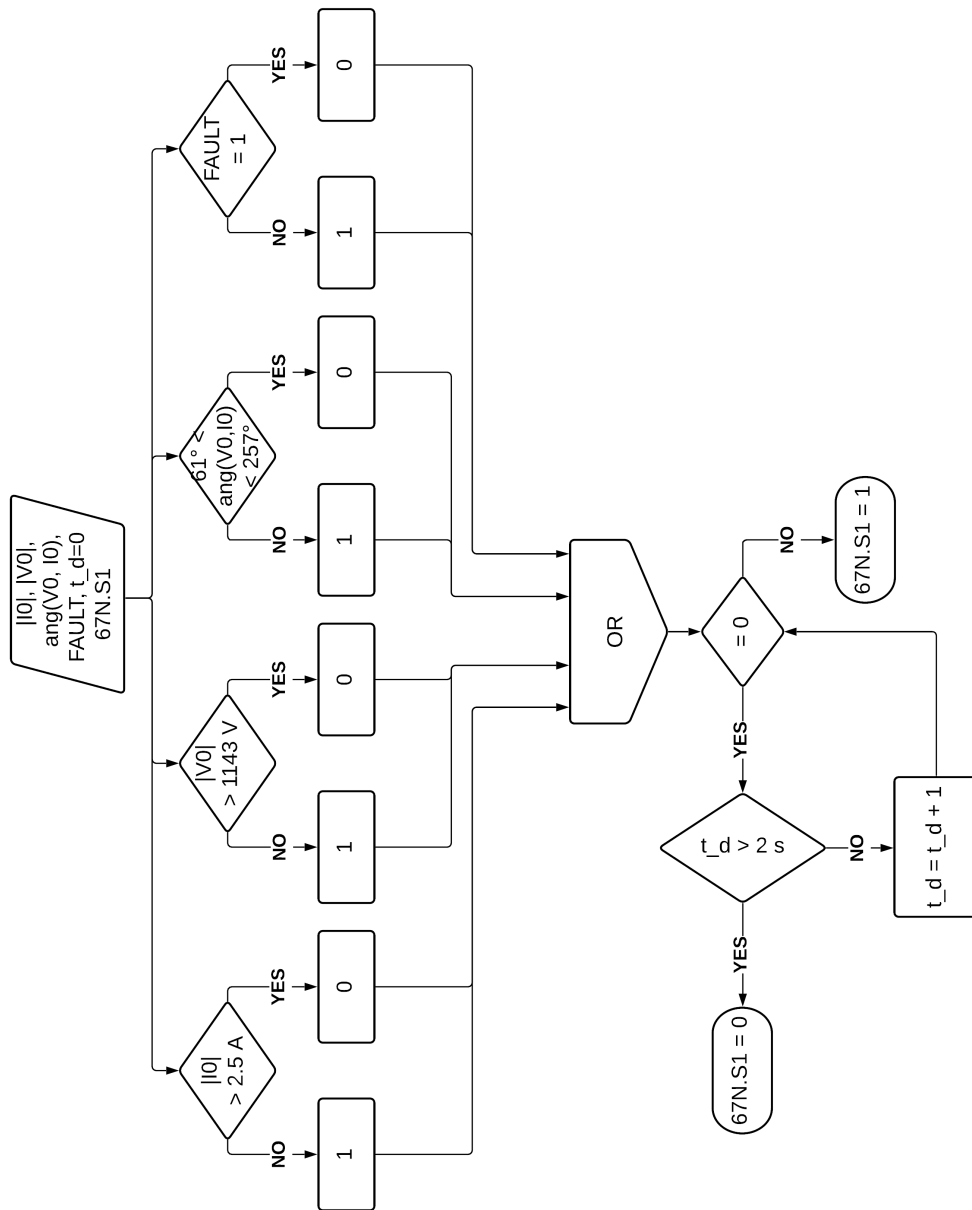


Figure 4.22: Flow chart of the first threshold control logic of relays 67N

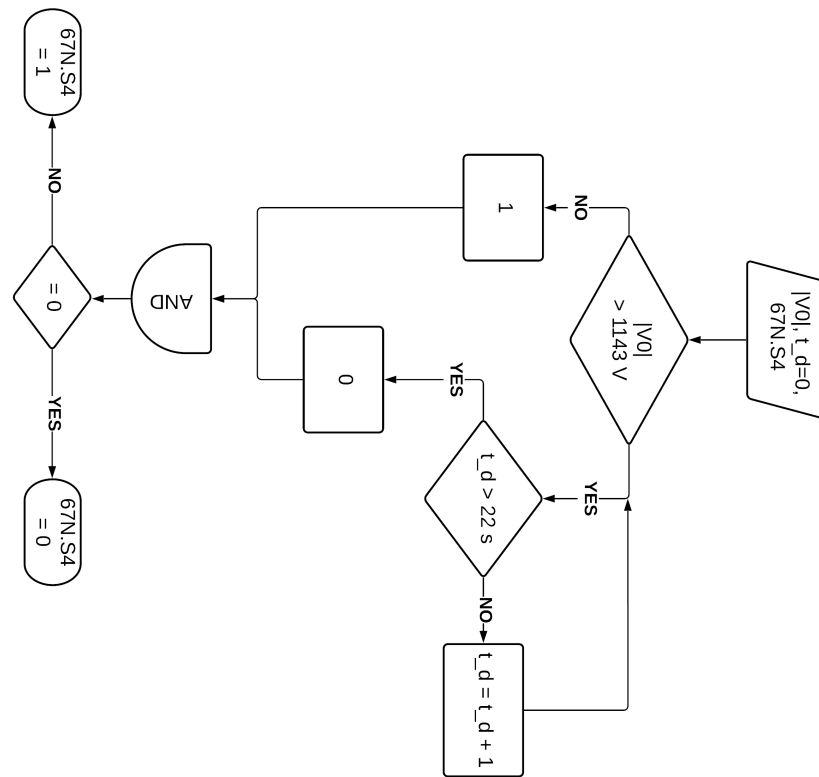


Figure 4.23: Flow chart of the fifth threshold control logic of relays 67N

4.5.4 Breaker 3A, 3D and 3E

The circuit breakers for LV feeders protection are equipped with an electronic relay with three threshold, the first one is time-dependent while the last two ones are not. The control logic is the same of the other overcurrent relays. The flow chart of *a-phase* is shown in Fig.4.24. The triple polarity of the circuit breaker and the contemporary opening of the three phases is obtained by implementing another *AND* gate whose inputs are the variables *LV_A*, *LV_B* and *LV_C* (one per each phase) and whose output is the signal that control the trip of the circuit breaker.

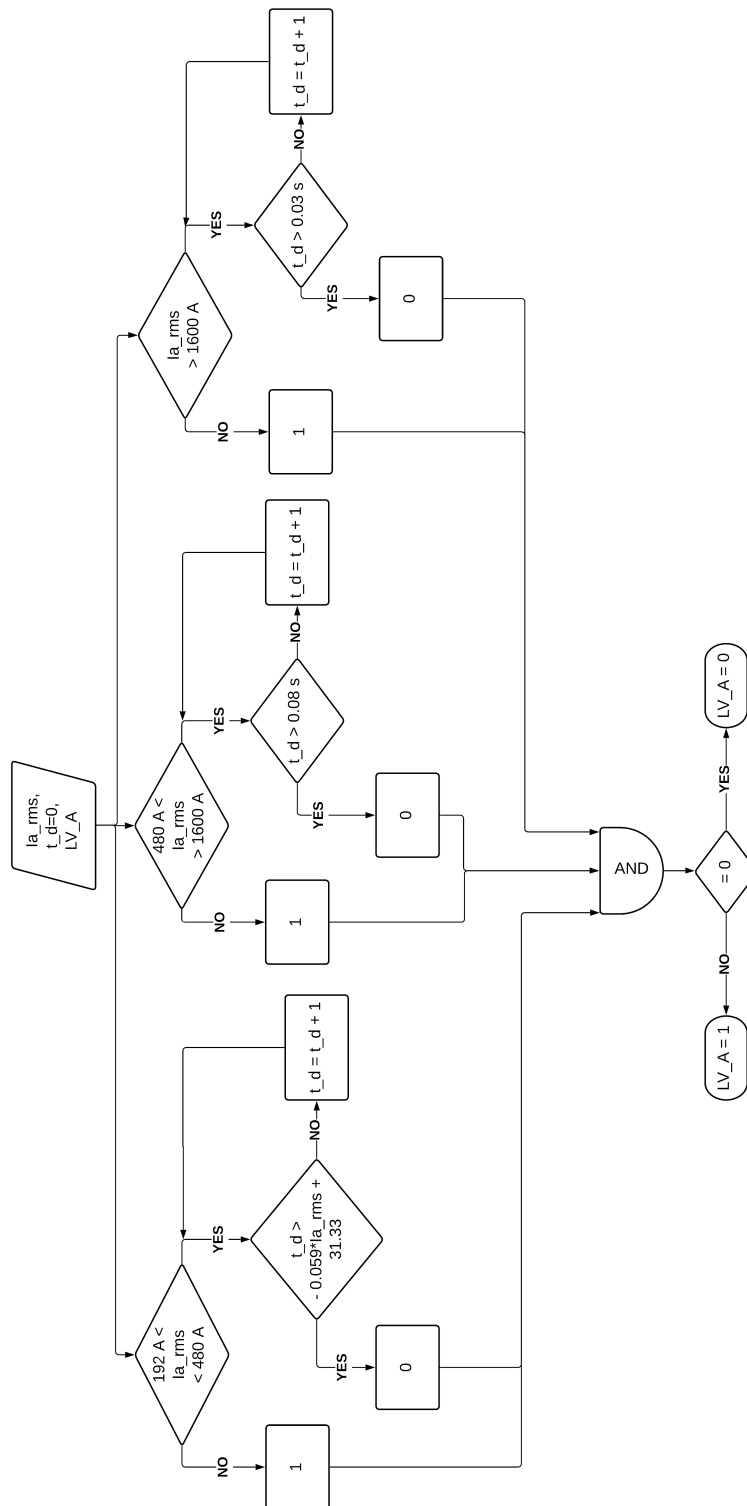


Figure 4.24: Flow chart of the *a*-phase control logic of LV electronic relay

4.5.5 LV fuses

As can be read in Chap.4.4.1, unfortunately in RSCAD[®] libraries there is any component for LV fuses modeling. For this reason, in the digital twin these fuses are implemented by using both the component in Fig.4.14 and the control logic whose flow chart is shown in Fig.4.25.

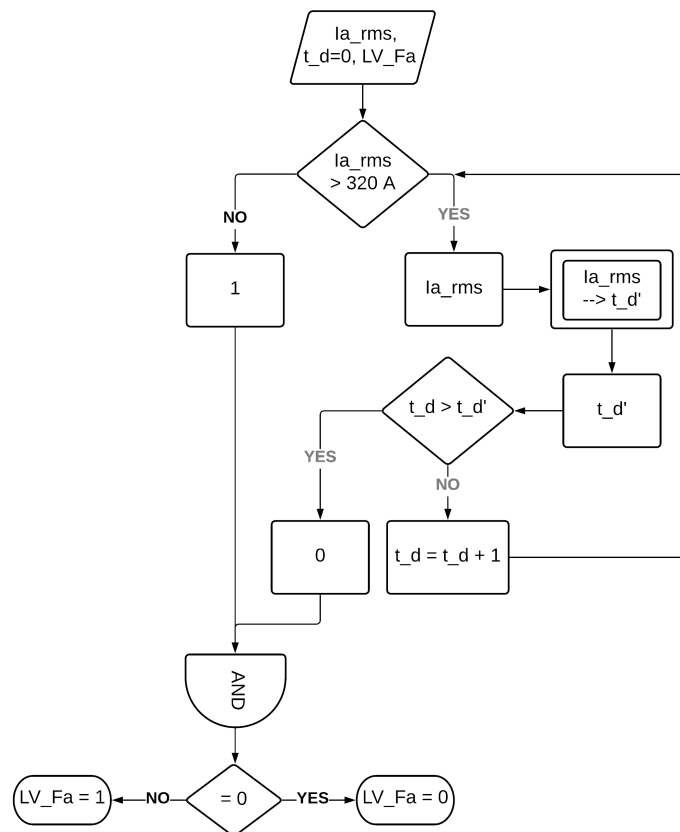


Figure 4.25: Flow chart of the control logic of the LV fuse

The double square block is a *Lookup table*. In fact, the time-current characteristic in Fig.4.12 was defined in the digital twin through a piecewise function that is implemented by means of a table whose input is the rms value of the fuse current, while the output is the pre-arcing time concerning the input current. The values used for the *Lookup table* are provided in Tab.4.16. For current values between two discretized inputs, the RSCAD[®] block retrieves the operating time by means of linear interpolation.

Table 4.16: *Lookup table* for simulating LV fuses time-current characteristic

Current [A]	Time [s]
350	1500
450	500
450	200
500	100
600	40
700	20
850	10
1000	5
1300	2
1500	1
1700	0.7
1850	0.5
2000	0.4
2200	0.3
2500	0.2
2950	0.1
3000	0.09
3100	0.07
3400	0.05
3500	0.035
3750	0.02
4400	0.01
4500	0.008
4950	0.006
6200	0.003
7500	0.002
10000	0.001
15000	0.00045
20000	0.00025
35000	0.0001

4.6 Manual control of the circuit breakers

Per each circuit breaker simulated in the digital twin, also a manual control is implemented. As an example, the logic implemented for controlling manually the Magra feeder breaker is shown in Fig.4.26.

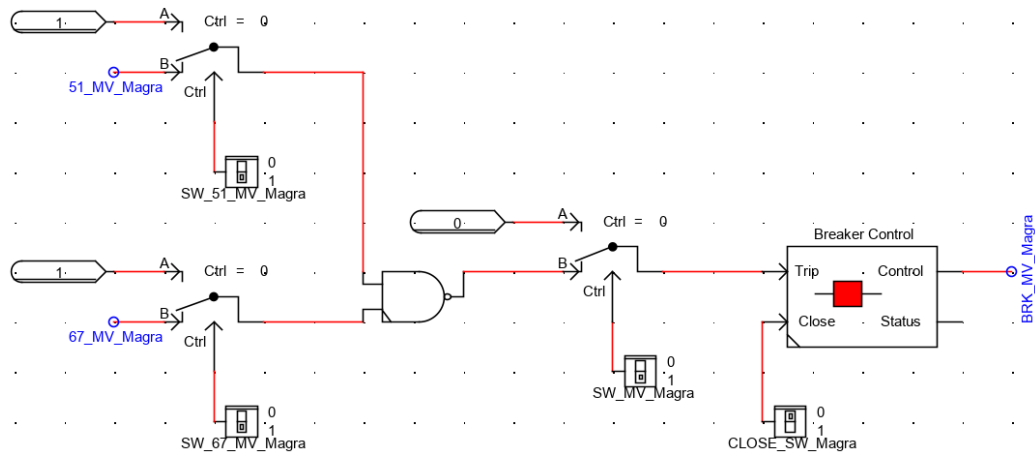


Figure 4.26: Control logic for both relays deactivation and manual reclosing of circuit breakers

As it can be seen in the figure above, there are four switches:

- **SW_51_MV_Magra:** when it is equal to 1, the relay 50/51 is enabled to trip the circuit breaker; while when it is equal to 0, the relay is disabled;
- **SW_67_MV_Magra:** same as above, but this switch control enabling/disabling of relay 67N;
- **SW_MV_Magra:** with this switch all the relays installed can be disabled at the same time. In this way, the circuit breaker will not be tripped in case of fault;
- **CLOSE_SW_Magra:** after a tripping event occurs and the circuit breaker was opened, with this switch the user can reclose it. If the fault is not extinguished yet, the circuit breaker will be automatically reopened by the activation of the relays. While, if the fault is extinguished the breaker will remain closed.

More generally, as it can be seen in Fig.4.26, the manual control implemented can be used for both deactivating one or more relays and reclosing the circuit breaker after its trip.

Chapter 5

Simulation results

In this chapter, various types of faults were simulated at MV level in *Node 6*, at the end of MV feeder Magra (see Fig.2.1), in order to test the functionalities of the relays control logics described in Chap.4. Specifically, the operating time of the circuit breakers will be computed in *Runtime* environment by considering the time instant in which the fault occurs and the time instant in which a relay commands the trip of the circuit breaker on which it is installed. The time diagrams will be provided. In these diagrams, the variable *FLT* can be equal to:

- **0**: there is no fault;
- **1**: there is a fault in the above-mentioned node. The type of fault will be specified in the section title.

In the same diagrams, together with *FLT*, other variables, that will be specified step by step, will be plotted.

In this way, the selectivity among the components of the protection equipment implemented in the digital twin can be tested. Finally, thanks to the manual control in Fig.4.26, one or more relays can be deactivated at the same time in order both to simulate the failure of one or more protections and to verify the operating time of the upstream protection. For clarity, there is no time delay between relay activation and circuit breaker trip. However, thanks to the *Breaker Control* block (shown in Fig.4.26), mechanical time delay can be implemented.

5.1 Multiphase faults

In case of multiphase faults, the fault current value is very high. For this reason, circuit breakers trip must be as fast as possible in order to limit

the damages on the power system equipment. As it can be seen in Fig.5.1, the overcurrent relay 50/51 commands the trip of Magra breaker almost instantaneously. Basing on the settings provided in Tab.4.5, can be deduced that threshold 50 was exceeded.

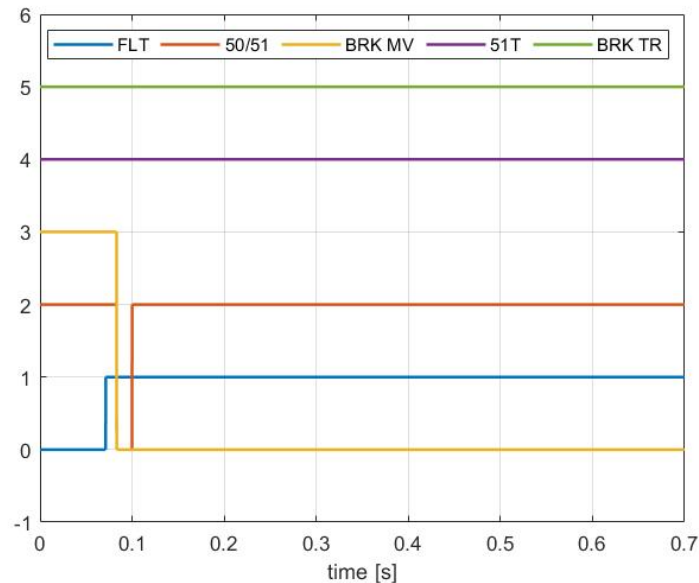


Figure 5.1: Operating time of MV feeder circuit breaker for multiphase faults at MV level

In the event that Magra breaker fails, the HV and MV breaker (see Fig.4.1) will trip for interrupting the fault current. In this case, the trip of the transformer circuit breakers will be commanded by overcurrent relay 51T, installed in MV breaker, whose operations are time delayed with respect to the relay of the same type installed in MV feeder circuit breaker, precisely for selectivity reason (see Fig.4.5). In fact, in this situation the *BUS 2* (see Fig.2.1) would be unsupplied and the outage caused by the fault on Magra feeder, the faulty feeder, would impact also on Brenta feeder, the healthy one, resulting in an increasing of both *Power Not Supplied (PNS)* and, consequently, *Energy Not Supplied (ENS)* due to the higher number of not served MV and LV users. Despite the drawback, this procedure is indispensable in case of MV feeder circuit breaker fails due to electronic relay failure or because breaker connections remain attached due to the thermal effect of the fault current.

By disabling the relay 50/51 in Magra breaker, in Fig.5.2 can be observed that this breaker remain closed (despite relay signal is activated), while HV

and MV transformer breakers were opened after $\approx 0.5s$ from the fault time instant, tripped by relay $51T.S2$ (see Tab.4.2 and Fig.4.5).

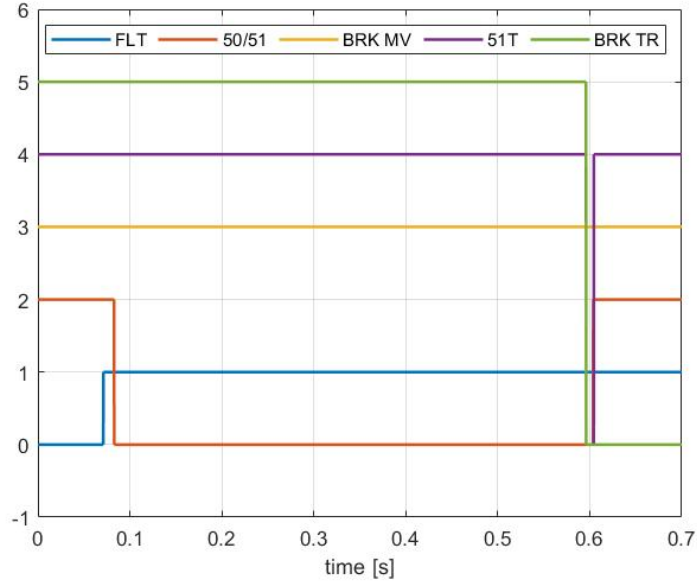


Figure 5.2: Operating time of transformer circuit breakers for multiphase faults at MV level with failure of MV feeder breaker

5.2 Phase-to-earth faults with compensated neutral

In case of phase-to-earth faults, the fault current is much lower than in multiphase cases and overcurrent relays are not able to detect the fault. For this reason, MV feeder circuit breakers, like Magra one (see Fig.4.1), are equipped with earth-directional protection relay $67N$. As it can be seen in Fig.5.3, relay $67N.S1$ trips the MV feeder breaker after 2s (see Tab.4.6). For this test, the neutral points of the secondary windings of HV/MV transformers is compensated. It means that the the neutral point are connected to ground through an RRL impedance. However, DSO did not provide data about compensation impedance so the values of both the compensation resistances and the compensation inductance are set up basing on the parameters of the MV lines.

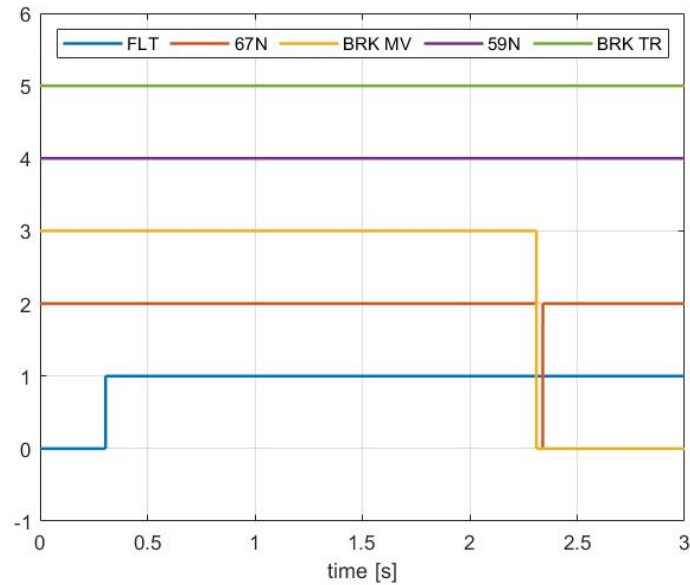


Figure 5.3: Operating time of circuit breakers for phase-to-earth faults at MV level

As before, in case of failure of the above-mentioned breaker, the tripping of the HV and MV circuit breakers must be commanded. In this case, the backup protection that trip the transformer breakers is the maximum homopolar voltage relay $59N$ installed in MV breaker (see Fig.4.1). For testing the accuracy of the selectivity, the relay $67N$ of MV feeder was disabled and, only for simulation burden reason, the time delay of relay $59N$ in Tab.4.4

was reduced. As can be seen in Fig.5.4, the MV breaker remain closed while the HV and MV transformer breakers were opened by the signal of relay 59N after 2.5s that is the value set up as time delay for this test.

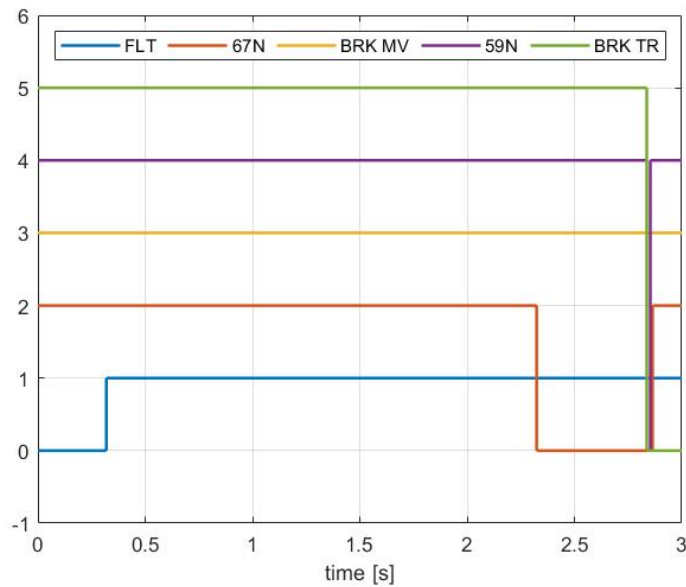


Figure 5.4: Operating time of circuit breakers for phase-to-earth faults at MV level with failure of MV feeder breaker

5.3 Conclusion

As it can be seen in Chapter 5, the relays control logics implemented are effective and the protection devices interrupt any type of fault in compliance with the guidelines provided by the TSO and the DSO. The digital twin implemented works properly and can be used both to add RES components for analysing technical issues and to study other types of electromagnetic transients concerning the power system. Moreover, thanks to real-time simulation, both Power and Control Hardware-In-the-Loop (PHIL and CHIL) simulation can be done by using the digital twin implemented as the electricity grid with which to interface a real component without the risk that it can be damaged during the tests.

Appendix A

Block schemes of the relays

In this appendix, the block schemes implemented in RSCAD[®] and based on the logic represented by the relating flow chart in Chapter 4.5 are shown.

A.1 HV breaker

Relays 50/51T

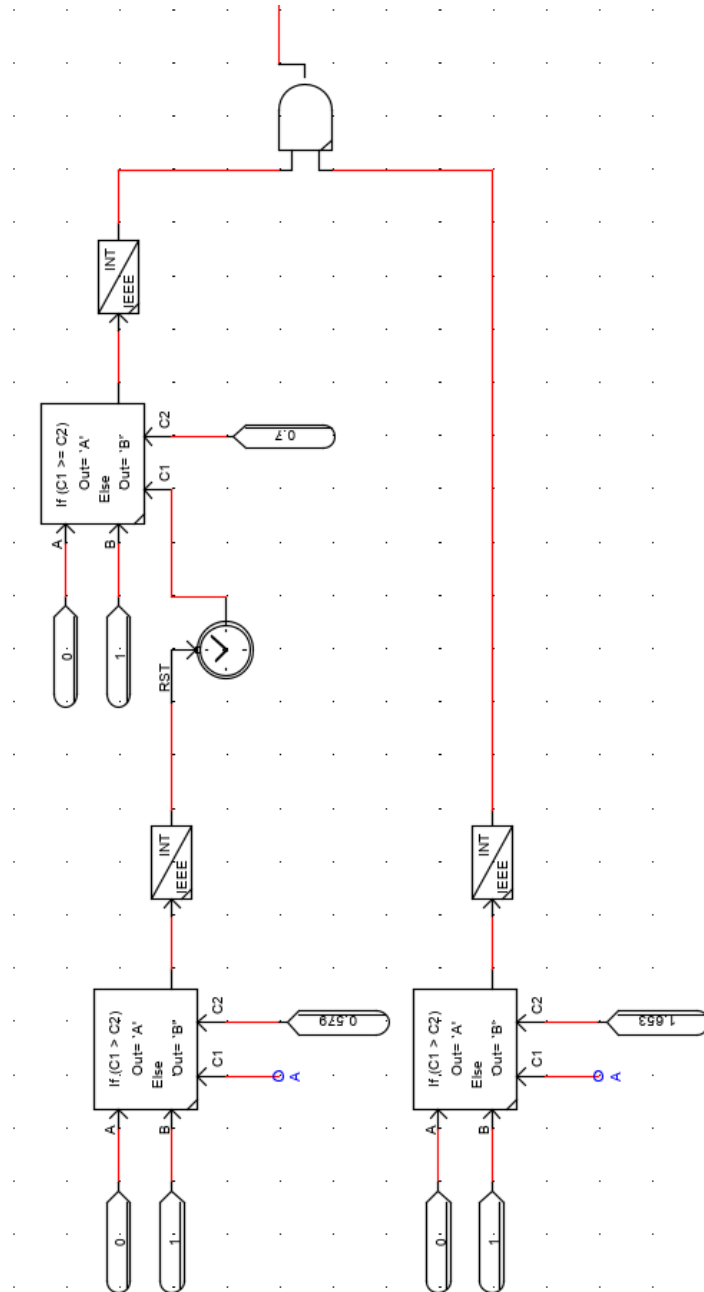


Figure A.1: Block scheme of the *a-phase* control logic of relays 50/51T in HV breaker

A.2 MV breaker

Relay 51T

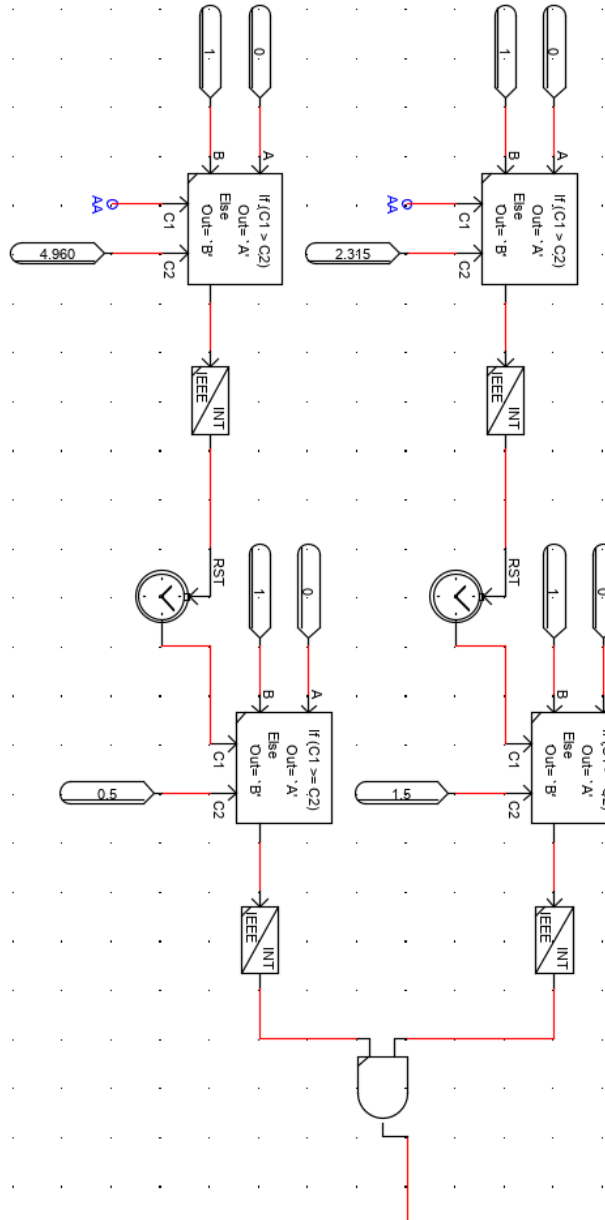


Figure A.2: Block scheme of the *a-phase* control logic of relays 51T in MV breaker

Relay 59N

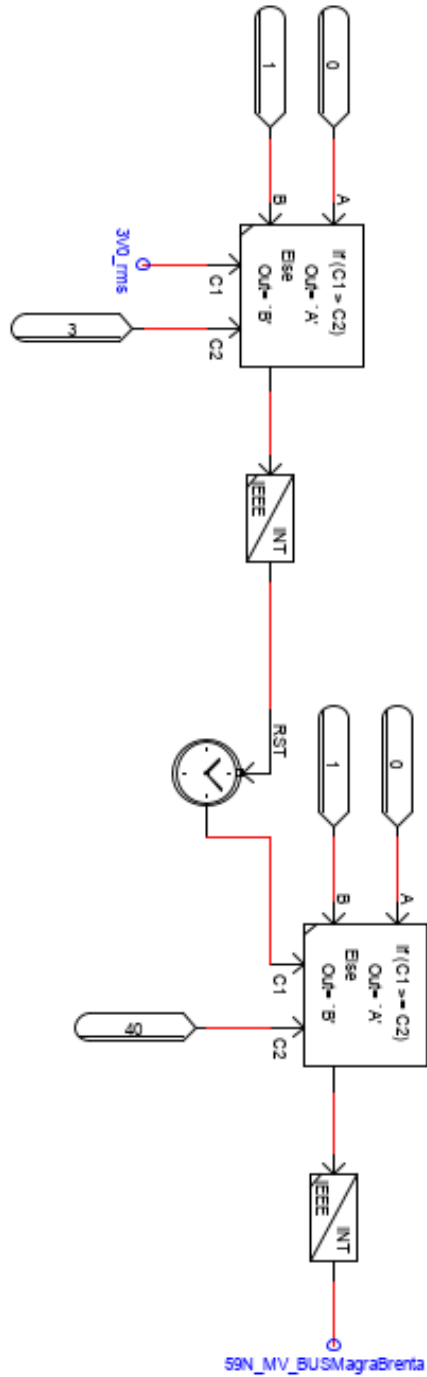


Figure A.4: Block scheme of the *a-phase* control logic of relays 59N in MV breaker

A.3 Magra and Brenta breaker relays

Relays 50/51

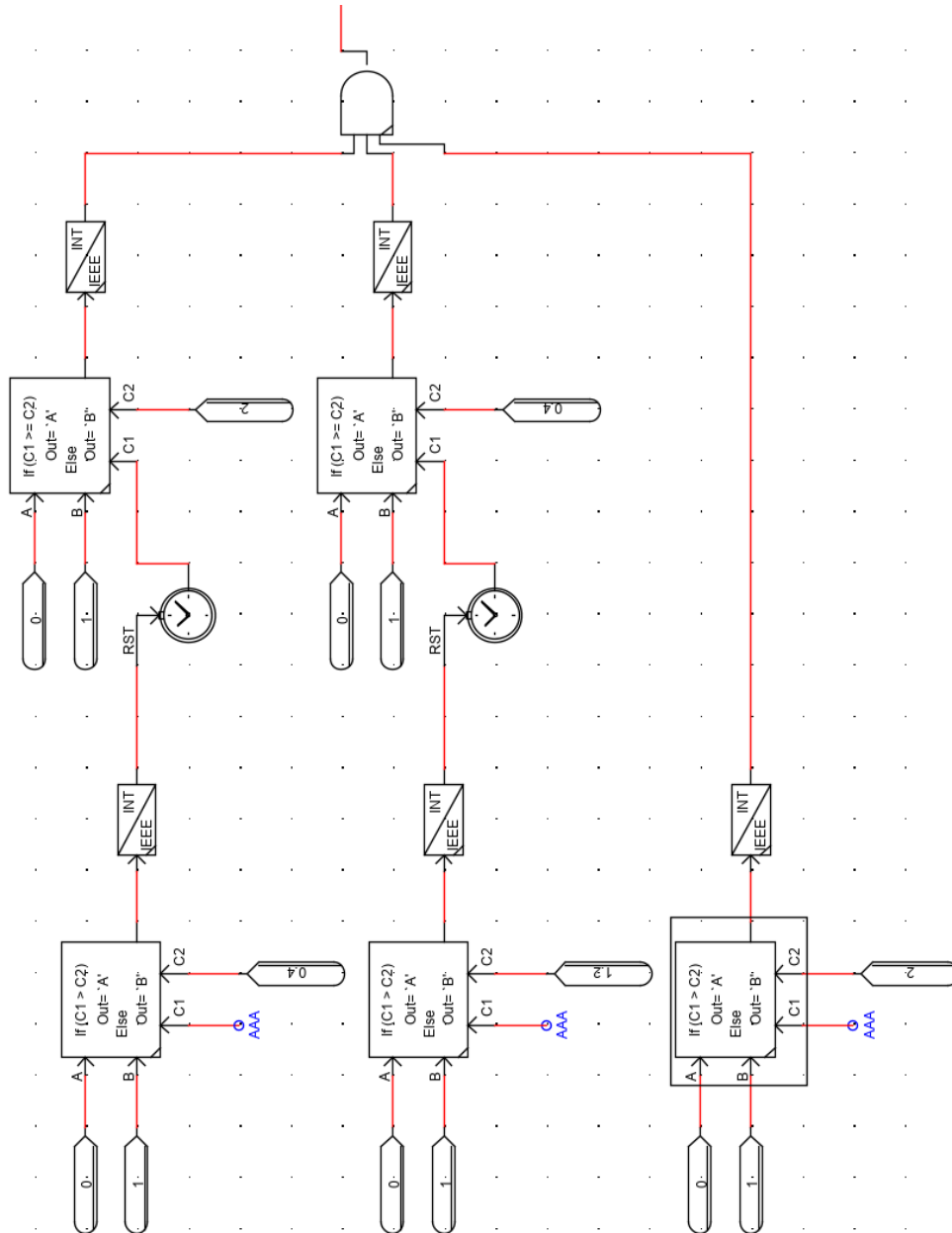


Figure A.5: Block scheme of the *a-phase* control logic of relays 50/51 in MV feeder breaker

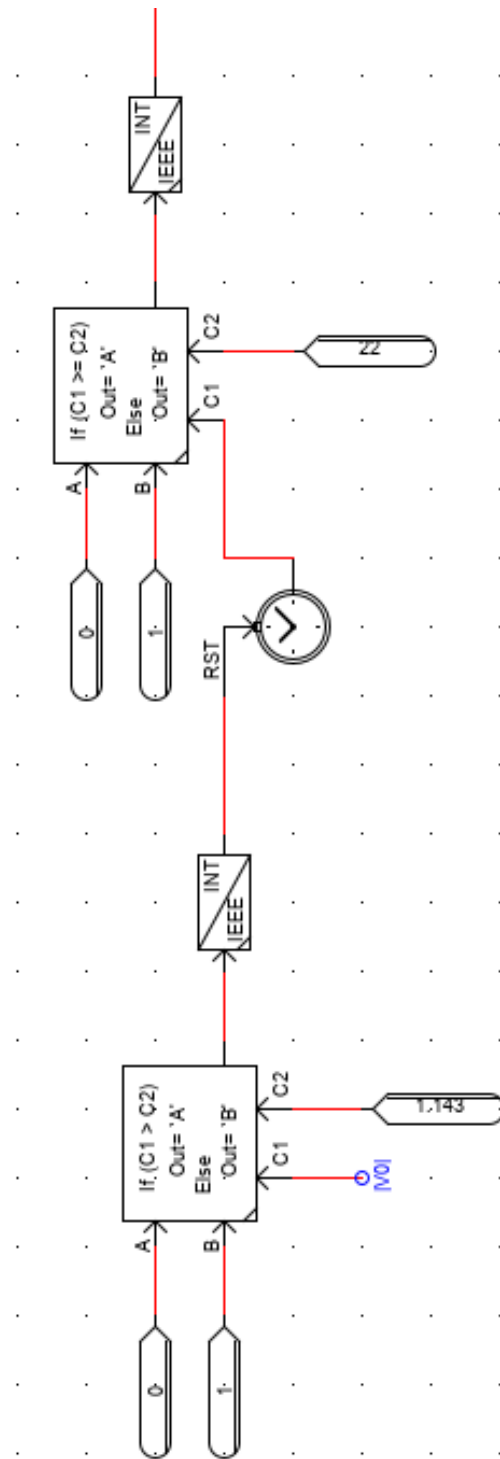


Figure A.7: Block scheme of the *a-phase* control logic of relays 67N.S4 in MV feeder breaker

A.4 Breaker 3A, 3D and 3E

Relays 49/50/51

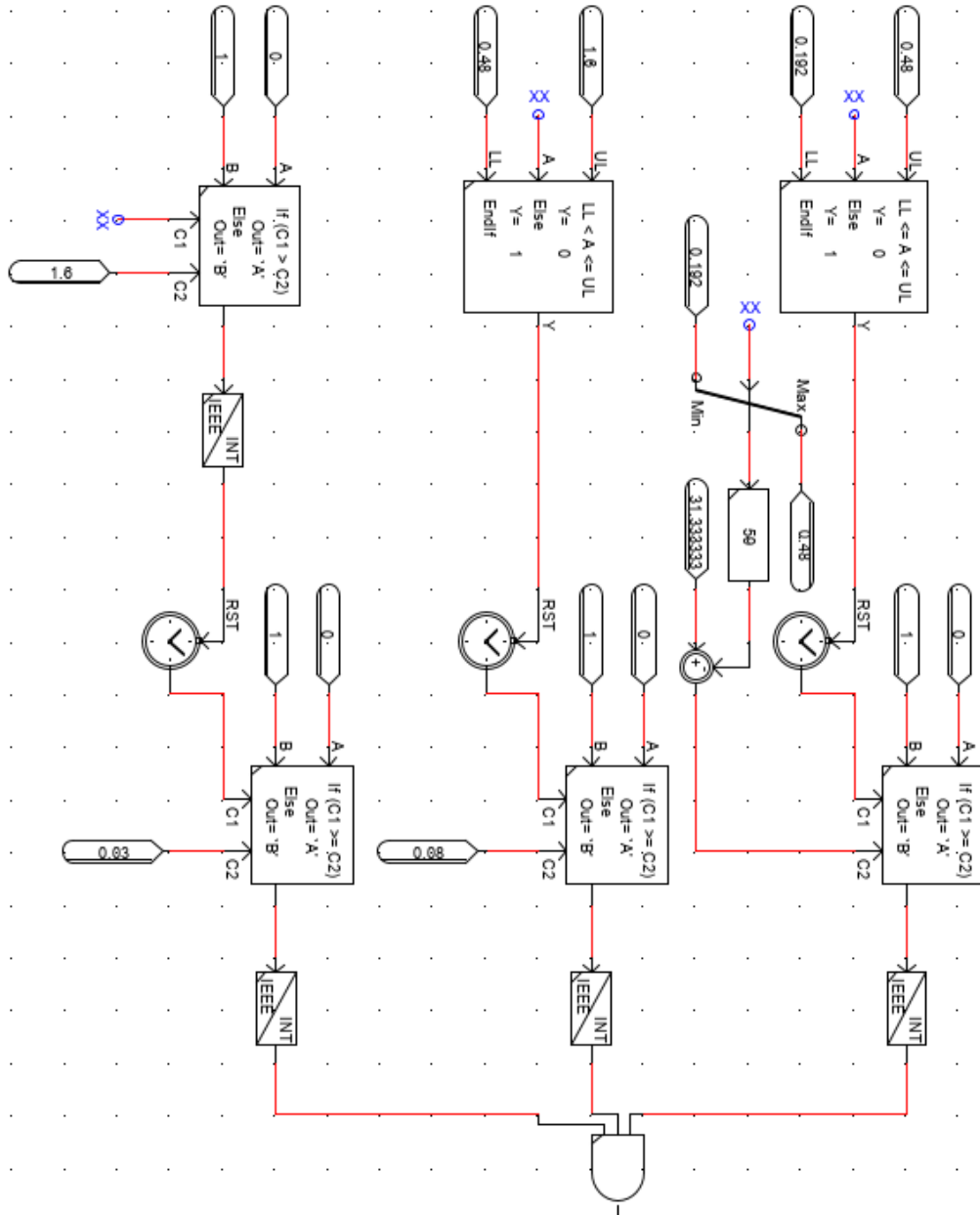


Figure A.8: Block scheme of the *a-phase* control logic of relays 49/50/51 with $I_n = 160A$ in LV feeder breaker

References

- [1] IRENA. *Global Renewables Outlook: Energy transformation 2050*. Report. Renewable Energy Agency, Abu Dhabi, 2020.
- [2] IRENA. *A summary of Reaching zero with renewables: Eliminating CO₂ emissions from industry and transport in line with the 1.5 °C climate goal*. Report. Renewable Energy Agency, Abu Dhabi, 2020.
- [3] MIP Energy Strategy Group. *Renewable Energy Report. La ripartenza del mercato e le sfide della crescita*. Report. Politecnico di Milano, School of Management, 2020.
- [4] MIP Energy Strategy Group. *Smart Mobility Report. La sostenibilità nei trasporti: opportunità e sfide per la filiera e gli end user*. Report. Politecnico di Milano, School of Management, 2020.
- [5] Ministry of Economic Development et al. *Integrated National Energy and Climate Plan*. Version English. Italy, Dec. 2019.
- [6] Morteza Shabanzadeh and Mohsen Moghaddam. “What is the Smart Grid? Definitions, Perspectives, and Ultimate Goals”. In: Nov. 2013. DOI: 10.13140/2.1.2826.7525.
- [7] K. Vu, M. M. Begouic, and D. Novosel. “Grids get smart protection and control”. In: *IEEE Computer Applications in Power* 10.4 (1997), pp. 40–44. DOI: 10.1109/67.625373.
- [8] S. Parhizi et al. “State of the Art in Research on Microgrids: A Review”. In: *IEEE Access* 3 (2015), pp. 890–925. DOI: 10.1109/ACCESS.2015.2443119.
- [9] ESMAP. *Mini Grids for Half a Billion People: Market Outlook and Handbook for Decision Makers. Executive Summary*. ESMAP Technical Report. World Bank, Washington DC, 2019.
- [10] IRENA. *Innovation Outlook: Renewable Mini-grids*. Report. Renewable Energy Agency, Abu Dhabi, 2016.

-
- [11] MIP Energy Strategy Group. *Smart Grid Report. Le prospettive di sviluppo delle Energy Community in Italia*. Report. Politecnico di Milano, School of Management, 2014.
- [12] MIP Energy Strategy Group. *Electricity Market Report. Decentralizzazione, Elettrificazione, Digitalizzazione: quali prospettive per comunità energetiche ed aggregazioni virtuali?* Report. Politecnico di Milano, School of Management, 2020.
- [13] Autorità per l'energia elettrica e il gas. *Relazione annuale sullo stato dei servizi e sull'attività svolta*. Presentazione del Presidente dell'Autorità. 2001.
- [14] Helena Gerard, Enrique Rivero, and Daan Six. "Basic schemes for TSO-DSO coordination and ancillary services provision". In: (2016).
- [15] Cesar Diaz-Londono et al. "Experimental modeling and aggregation strategy for thermoelectric refrigeration units as flexible loads". In: *Applied Energy* 272 (2020), p. 115065. ISSN: 0306-2619. DOI: <https://doi.org/10.1016/j.apenergy.2020.115065>. URL: <http://www.sciencedirect.com/science/article/pii/S0306261920305778>.
- [16] Gianfranco Chicco. "Class notes of the course Smart Electricity Systems". 2019.
- [17] Radu Bojoi. "Class notes of the course Smart Electricity Systems". 2019.
- [18] Stefano Frittoli. "Remote interconnection of real-time simulators: performance analysis and case studies". Tesi di Laurea Magistrale in Ingegneria Elettrica. Politecnico di Torino, 2021.
- [19] RTDS Technologies Inc. *RSCAD Controls Library Manual*. 2019.
- [20] RTDS Technologies Inc. *RSCAD Power System Components Manual*. 2019.
- [21] Vladimiro Medved and Raffaele Schinco. *Le correnti di corto circuito negli impianti elettrici AT, MT e BT*. Ed. by UTET. 2001.
- [22] H. Hizarci and B. E. Turkay. "Impact of distributed generation on radial distribution network with various load models". In: *2017 52nd International Universities Power Engineering Conference (UPEC)*. 2017, pp. 1–5. DOI: 10.1109/UPEC.2017.8231905.

- [23] Joseph Kangombe Makasa. “Real-time simulator studies and model development for time-domain voltage stability analysis”. Master of Science in Engineering, in the School of Electrical, Electronic and Computer Engineering. University of KwaZulu-Natal, Durban, South Africa, 2006.
- [24] Vincenzo Cataliotti. *Impianti elettrici*. Ed. by Flaccovio Editore. Vol. 1. 2005.
- [25] *RSCAD: Real-Time Simulation Software Package*. URL: <https://knowledge.rtds.com/hc/en-us/articles/360046352893-RSCAD-Real-Time-Simulation-Software-Package>.
- [26] *Critical decisions demand precision*. URL: <https://www.rtds.com/technology/>.
- [27] *Scalability and flexibility without performance loss*. URL: <https://www.rtds.com/technology/simulation-hardware/>.
- [28] *GTIO Cards*. URL: <https://knowledge.rtds.com/hc/en-us/articles/360034281234-GTIO-Cards>.
- [29] RTDS Technologies Inc. *Power Hardware In the Loop Simulation (PHIL)*. Report. 2018.
- [30] *Our proprietary software does it all – no add-ons required*. URL: <https://www.rtds.com/technology/graphical-user-interface/>.
- [31] RTDS Technologies Inc. *DISTRIBUTION MODE: User Manual*. 2019.
- [32] TERNA S.p.a. *Criteri generali per la taratura delle reti a tensione uguale o superiore a 110 kV*. Allegato A.11. Guida tecnica. Version 01. 2018.
- [33] Vincenzo Cataliotti. *Impianti elettrici*. Ed. by Flaccovio Editore. Vol. 2. 2008.
- [34] Elisa Fallini. “Modellazione ed analisi di sistemi interconnessi di distribuzione di alta e media tensione”. Tesi di Laurea Magistrale in Ingegneria Elettrica. Politecnico di Torino, 2017.
- [35] Davide Caliandro. “Ottimizzazione degli algoritmi di riconoscimento dei guasti a terra intermittenti nella rete di distribuzione”. Tesi di Laurea Magistrale in Ingegneria Elettrica. Politecnico di Torino, 2019.
- [36] ABB. *MV/LV transformer substations: theory and examples of short-circuit calculation*. 1SDC007101G0202. Technical Application Papers. 2008.

-
- [37] ABB. *SACE Emax 2*. 1SDH001330R0001 - ECN000086018. Istruzioni di esercizio per il progettista. Version B. 2018.
 - [38] Baldassari Cavi. *RG7RX*. Catalogo cavi Bassa Tensione. 2020.
 - [39] Mersen. *NH fuse-links gG 400VAC*. Low voltage IEC fuses.
 - [40] Gianfranco Chicco. "Class notes of the course Distribuzione ed utilizzazione dell'energia elettrica". 2016.